Australian Government
Geoscience Australia

pmd*CRC

New Perspectives: The foundations and future of Australian exploration.

Abstracts for the June 2008 pmd*CRC Conference

R.J. Korsch & A.C. Barnicoat (editors)

Record
2008/09
Part 1

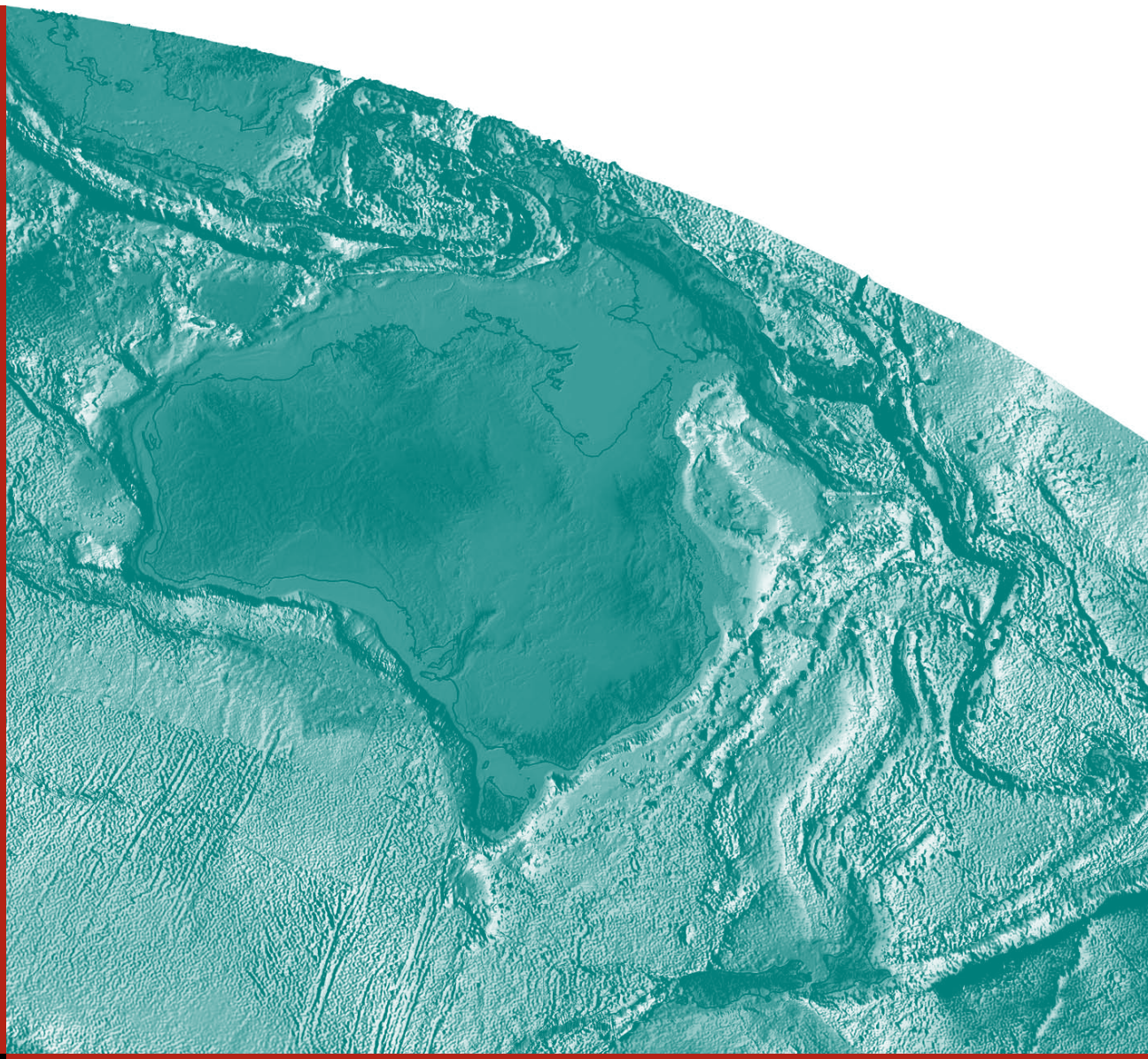

New perspectives: The foundations and future of Australian exploration

Abstracts for the June 2008 *pmd**CRC* Conference

GEOSCIENCE AUSTRALIA

RECORD 2008/09

EDITED BY R. J. KORSCH AND A. C. BARNICOAT

*pmd**CRC*, Geoscience Australia, GPO Box 378, Canberra, ACT 2601

Department of Resources, Energy and Tourism
Minister for Resources and Energy: The Hon. Martin Ferguson, AM MP
Secretary: Dr Peter Boxall

Geoscience Australia
Chief Executive Officer: Dr Neil Williams PSM

ISSN 1448-2177
ISBN 978-1-921236-88-4

GeoCat No. 65830

Bibliographic reference: Korsch, R.J. and Barnicoat, A. C., editors, 2008. New perspectives: The foundations and future of Australian exploration. Abstracts for the June 2008 *pmd*CRC* Conference. Geoscience Australia, Record 2008/09.

Abstracts were solicited by the Organising Committee of the 2008 *pmd*CRC* Conference and were peer reviewed for this volume. Nevertheless, any analyses or scientific opinions expressed in this volume are the sole responsibility of the authors.

CONTENTS - Part 1

Foreword

Seven years ago the predictive mineral discovery*Cooperative Research Centre (***pmd****CRC*) was created to apply the collective knowledge and expertise, from government agencies, education institutions and industry, to the problems surrounding mineral exploration in Australia.

These seven years have marked a significant break-through in the science surrounding mineral exploration. This, the ***pmd****CRC*'s final conference, will showcase the culmination of the research developed during the life of the CRC to the wider exploration industry. The conference presents an energetic program with emphasis on the enabling technologies and unique work practices developed through the unique approach of the CRC's Integrated Research Programs: Terrains and Architecture, History, Fluids, Modelling and IT and Delivery. These developments in technology and practice have been achieved through a linking of science with industry by developing a clear understanding of the relationships between fundamental physical and chemical processes, observable features and exploration applications and embedding the relationship between industry and science. This has been achieved by placing researchers into industry situations to feed data and observations into the research programs and help industry apply the newly developed concepts to the exploration process.

The focus of the presentations, at this conference, fall into two main areas within the framework of the CRC's 'Five Questions' approach to mineral systems. The main areas are Architecture and Deposition, with a common thread of explaining how the technologies and techniques developed by the CRC facilitate the exploration process. Case studies are presented in each instance highlighting the positive impact the technology has had on industry practice. The presentations also demonstrate the methods used to enmesh the technologies, techniques and practices with system-based concepts and specific research areas by integrating across disciplines and scales to produce a multilayered understanding of key terrains.

The science presented at this conference presents a new way of looking at and of thinking about the issues surrounding exploration. It also presents a change to the work practices and relationship between science and the exploration industry in Australia to ensure future success and economic development.

Dr Bob Haydon
CEO
predictive mineral discovery* Cooperative Research Centre

The Mineral Systems approach of the *pmd**CRC

ANDY BARNICOAT

*pmd***CRC*, Geoscience Australia, GPO Box 378, Canberra, ACT 2601 Andrew.Barnicoat@ga.gov.au

Introduction

Ore deposits are economic accumulations of metals one to three or more orders of magnitude more concentrated than average crustal levels. These accumulations develop either as a result of the transport of ore-forming elements, followed by their preferential deposition in a restricted volume, or by the selective dissolution of non-ore-forming elements and their transport away from the site of dissolution. A range of processes control the development of these concentrations, and the expression of these processes has been codified into the concept of *Mineral Systems* by Wyborn et al. (1994). These authors defined a mineral system as 'all geological factors that control the generation and preservation of mineral deposits', and based the concept on that of Petroleum Systems as formalised by Magoon and Dow (1991). The system perspectives of Wyborn et al. (1994) and Magoon and Dow (1991) are both based around a three-fold focus on sources, transport and traps.

The conceptual framework of source-transport-trap is misleading, at least in its simplistic application. No matter what the original composition of a fluid is it will rapidly interact, both physically and chemically, with the rocks it passes through, and components dissolved in the fluid reflect differing parts of the flow path, depending on their concentrations in country rocks and solid/fluid partition coefficients (Ridley & Diamond, 2000). It is normal that the fluid originates from one source and metals and complexing anions are sourced from several other sources. The concept of a trap, paralleling the usage in petroleum systems, is also unhelpful as it implies that fluid flow ceases at the depositional site. Important aspects of the formation of ore bodies, not explicitly described by a source-transport-trap framework, include tectonic setting, which controls the source term, and the architecture, which controls the transport paths. It has been recognised increasingly that such factors are critical to understanding the siting of ore bodies.

Mineral Systems and the Five Questions

More recently, the mineral systems framework has developed to explicitly consider the critical geological features necessary for the development of concentrations of material. An approach known as the 'Five Questions' was developed in the Australian Geodynamics Cooperative Research Centre (AGCRC), and summarised in Walshe et al. (2005). The five questions are:

1. What are the geodynamic and P-T histories of the system?
2. What is the architecture of the system?
3. What are the fluid reservoirs?
4. What are the fluid flow drivers and pathways?
5. What are the metal and sulphur transport and depositional processes?

By answering these questions a about a mineral system, the definition of Wyborn et al. (1994) is fulfilled and the system and its context can be fully described. The full context is extremely important, as it provides information on the drivers of the processes that lead to the development of mineral deposits. An example of this approach to understanding ore formation is give in Ord et al. (2002), who investigated the origins of the Century Zn-Pb orebody in northern Queensland. The five questions make explicit the range of features than should be considered to understand the development of mineralisation, and they reveal the necessity to think across scales from that of the geodynamic setting to that of the depositional environment. This is not intended to suggest that consideration of the geodynamic setting of mineralisation is new: links between nature of mineral systems and their global setting have been discussed since soon after the time that plate tectonics became established (e.g. Sillitoe, 1972a, 1972b; Spooner & Fyfe, 1973; see also Sawkins, 1984; Russell, 1992) and work continues on this topic (Groves & Bierlein, 2007). In addition, the five questions lead to consideration of the *chemical architecture,* covered in questions 3, 4 and 5, concerning fluid reservoirs, fluid flow pathways and transport and depositional processes, at scales ranging from depositional sites upwards.

Experience has revealed that using the five questions does ensure that all aspects of the context of a mineral system are considered. But are the questions sufficient to fully evaluate the processes responsible for ore formation? In the next section, the controls on the development of concentrations of ore elements are analysed.

Fundamental controls on ore formation

As noted in the Introduction, the concentration of ore elements in a deposit arises either by transporting the appropriate material in to a site or by removing diluents. A simple expression can be written that considers the rate of deposition:

rate of deposition = mass flux of transport medium × gradient in carrying capacity

as it is changes in the carrying capacity of the transport medium that lead to deposition (Walsh et al., 1984; Rimstidt, 1997). Without a decrease in carrying capacity, all of the element in question will continue to be carried by the fluid. In cases where material removal is the critical process, the deposition rate will be negative. Over time, the quantity of deposited material builds up, with the amount of material deposited given by the integral of the deposition rate with respect to time. For example:

- The rate of heavy mineral deposition is given by the water flow rate multiplied by the change (gradient) in entrainment capacity. Entrainment capacity is proportional to velocity^2 (Bagnold, 1966; Allen; 1997).
- The rate of ore formation in magmatic systems is specified by the rate of magma supply and changes in the solubility of the elements of interest due to changing temperature, composition, etc.
- In hydrothermal systems, the fluid flow rate and changes in solubility due to changes in P, T and chemistry are responsible for deposition.

A specific expression for this relationship in hydrothermal systems can be created by combining an equation given by Phillips (1990, 1991; see also Cathles & Adams, 2005), together with Darcy's Law for fluid flow in a porous medium. This allows the fundamental controls on hydrothermal ore formation to be clearly identified. The basic relationship is:

$$\int -\Phi \frac{\kappa \rho g}{\mu} \nabla P \bullet \left(\frac{\partial c_e}{\partial T} \nabla T + \frac{\partial c_e}{\partial p} \nabla p + \sum_r \frac{\partial c_e}{\partial c_r} \nabla c_r \right) .dt \qquad \textit{Equation I}$$

where Φ is the porosity, κ is the permeability of the medium, ρ the fluid density, g the acceleration due to gravity, μ the fluid's viscosity, P the pressure in Pa, c_e the equilibrium concentration in the fluid of the

element of interest in mol m^{-3}, T the temperature in K, c_r the concentration of other elements (species) that influence c_e in mol m^{-3}, and t the duration of the fluid flow event. ∇ is the gradient operator such that $\nabla T = \partial T/\partial x + \partial T/\partial y + \partial T/\partial z$, and the • between the fluid flow velocity and the bracketed terms signifies the scalar product of vector quantities, the velocity and the gradients. This is critical as the rate of deposition is maximised when the flow is perpendicular to the gradient(s). Equation (1) is merely the mathematical expression of the relationship noted at the beginning of this section, and states that deposition rate is given by the fluid flow rate and sum of the products of solubility sensitivities with respect to T, P and the concentration of other species multiplied by the spatial gradients in P, T and concentration respectively. The minus sign is required as the rate of solid production is the opposite of the change in fluid composition yielded by the solubility sensitivity terms. Equation (1) has been used by Hanor (1994) and Hobbs and Ord (1997) to explore processes in sedimentary basins and mineral systems respectively.

A central assumption in this analysis is that local equilibrium is attained. Observations from sedimentary basins, where fluids in general are rock buffered (e.g Hanor, 1994; 2001) support the general applicability of this assumption; analysis of waters produced from a North Sea oilfield at ~120°C have been shown to equilibrate on time scales of <1-2 years (Houston et al., 2007). Major element composition in geothermal waters is also controlled by mineral equilibria at temperatures greater than about 100°C (Arnorsson et al., 2007), unless boiling and phases separation intervene (Simmons & Brown, 2000) and, even then, local equilibrium is attained. The assumption of local equilibrium is thus quite adequate to be useful in identifying critical parameters controlling ore deposition.

Equation (1) shows that there is a suite of factors that control the amount of material deposited. Several of these are intrinsic features of the system and the fluid involved – fluid density and viscosity, and the acceleration due to gravity. Other factors are controlled by the nature of the system itself, and hence are independent controls on the amount of material (ore) formed:

1. Permeability
2. Porosity
3. Gradient in hydraulic potential
4. Solubility sensitivity of the element of interest with respect to *P, T* and c_r
5. Spatial gradients of *P, T* and c_r
6. Time (duration of the system).

Translation into the real world

In order to utilise the expression and factors described above, it is necessary to translate the terms into something more tangible. A look at the factors reveals that they can be evaluated if the Five Questions are answered in an appropriate manner (see the left-hand two columns in Figure 1).

For example, the permeability factor will be explored if the question about architecture is answered with a view to outlining where permeable structures and lithologies are distributed. Gradients in P,T and c_r will be examined in answering the question on metal transport and deposition.

Thus, it is possible to link the underlying factors responsible for ore formation and the mineral system via the Five Questions. It is further possible to link the answers to the five questions to the exploration process, with the information drawn from the Five Questions analysis depending on the nature of the exploration issue at hand (Figure 1). When seeking to make large-scale exploration decisions (terrain/province selection), information concerning the geodynamic setting is most appropriate, whereas when evaluating drill targets, information about controls on ore deposition is relevant. In other words, the information taken from a mineral systems analysis depends on the scale at which exploration decisions are required.

Some of these parameters translate readily to mappable features that have concerned exploration geologists for many years. Permeability is related to the distribution of structures and of permeable sedimentary facies, for example. A preliminary examination of the parameters and what controls them yields the following three sets of geological inputs:

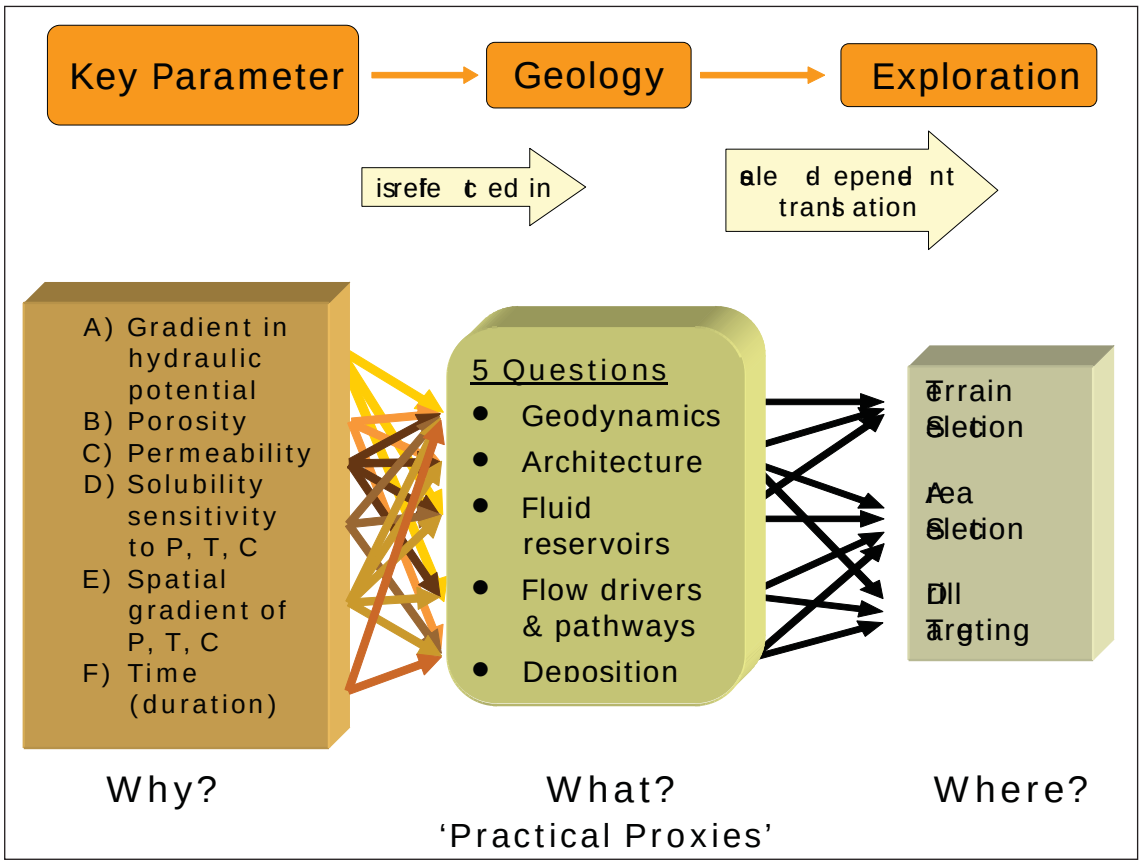

Figure 1. Linkages within a Mineral Systems framework between the key factors (derived from the basic relationship described in the text), the Five Questions and exploration.

Palaeogeography feeds into most of the critical factors:

- Describes distribution of (emergent) topography and hydrocarbon generation potential, both potential sources of hydraulic gradient (factor A in Figure 1).
- Controls distribution of facies and diagenesis that control porosity and permeability distribution in sedimentary sequences (factors B and C).
- Describes potential source regions for meteoric fluids (emergence again) and brines in marginal marine areas: key controls on solubility sensitivity (factor D).
- Allows identification of stable areas where P and T gradients could have been stable for long periods (factors E and F).

Magmatism also plays a major role in many critical factors:

- Source of fluids and temperature distributions that may create hydraulic gradients (factor A).
- Driver for fracture generation and hence a control on permeability (factor C).
- Act as a fluid source, the nature of which will depend on the origin of the magma: key control on solubility sensitivity (factor D).

- Creates spatial gradients in temperature and potentially chemistry (factor E).
- Repetitive magmatism will lead to long-lived hydrothermal systems (factor F).

(Structural) Architecture dominates several of the critical factors:

- Controls the distribution of dilation sites that play an important role in developing steep hydraulic gradients (factor A).
- Defines most of the high-permeability domains in the crust (factor C) and sites of elevated porosity (factor B).
- Defines locally steep pressure gradients, and plays a role in facilitating fluid mixing (factor E).
- Repeated failure on structures (including reactivation of deeper faults and other structures) allows prolonged fluid movement and/or multiple deposition/mixing/etc. events (factor F).

This list is clearly not complete, but shows how links can be a made between the fundamental parameters and detectable (hence practical/usable) features.

One group of parameters, the solubility sensitivities ($\partial c_e/\partial T$, $\partial c_e/\partial P$ and $\partial c_e/\partial c_r$) explicitly have not been considered in the past. These will all vanish to zero if the hydrothermal fluid is unsaturated in the element of interest, although this is complicated in cases where fluid mixing occurs. In such sites, large gradients in solubility will occur, which is why mixing is such an effective process of ore formation. They are controlled at the most fundamental level by the geodynamic setting, which controls c_e.

Conclusions

It is possible to link between fundamental physical and chemical parameters and the exploration process by means of the geological expression of the fundamental processes and the application of a scale-dependent mapping of these into exploration decision making. The most important step in the process is translating the understanding of process and the key parameters controlling process into factors that can be determined spatially. It is this that allows the conceptual framework of Mineral Systems to be ported practically into the domain of the mineral explorationist. One of the legacies of the ***pmd****CRC* is that it has not only made progress in facilitating the understanding of the exploration industry of critical scientific progress, but also that it has lead to researchers developing a much firmer understanding of the exploration process and how new ideas are applied to the process of targeting in exploration.

Acknowledgements

I am grateful to many people in the ***pmd****CRC* for discussions and sharing ideas. In particular, conversations with Bruce Hobbs, John Walshe, Heather Sheldon, Jon Hronsky, Greg Hall and Cam McCuaig have been of great help to me.

References

Allen, P.A., 1997. Earth surface processes. Blackwell Science, 404pp..

Arnorsson, S., Stefánsson, S. & Bjarnason, J.O., 2007. Fluid-fluid interactions in geothermal systems. Reviews in Mineralogy and Geochemistry, 65, 259-312.

Bagnold, R.A., 1966. An approach to the sediment transport problem from general physics. United States Geological Survey Professional Paper, 422-I, 37pp.

Cathles, L.M. & Adams, J.J., 2005. Fluid flow and petroleum and mineral resources in the upper (<20-km) continental crust. Economic Geology 100th Anniversary Volume, 77-110.

Groves, D.I. & Bierlein, F.P., 2007. Geodynamic settings of mineral systems. Journal of the Geological Society, London, 164, 19-30.

Hanor, J.S., 1994. Physical and chemical controls on the composition of waters in sedimentary basins. Marine and Petroleum Geology, 11, 31-45.

Hanor, J.S., 2001. Reactive transport involving rock-buffered fluids of varying salinity. Geochimica Cosmochimica Acta, 65, 3721-3732.

Hobbs, B.E. & Ord, A., 1997. Plumbing systems responsible for the formation of giant ore deposits. Geofluids II '97 Extended Abstracts; Queen's University Belfast, 100-102.

Houston, S.J., Yardley, B.W.D., Smalley, P.C. & Collins, I., 2007. Rapid fluid-rock interaction in oilfield reservoirs. Geology, 35, 1143-1146.

Magoon, L. B. & Dow, W.G., 1991. The petroleum system – from source to trap. American Association of Petroleum Geologists Bulletin, 75, 627.

Ord, A, Hobbs, B..E, Zhang, Y., Broadbent, G.C., Brown, M., Willets, G., Sorjonen-Ward, P, Walshe, J.L. & Zhao, C., 2002. Geodynamic modelling of the Century deposit, Mt Isa Province, Queensland. Australian Journal of Earth Sciences, 49, 1011–1039

Phillips, O.M. 1990. Flow controlled reactions in rock fabrics. Journal of Fluid Mechanics, 212, 263-278.

Phillips, O.M. 1991. Flow and reactions in permeable rocks. Cambridge University Press, 285pp.

Russell, M.J., 1992. Plate tectonics and hydrothermal ore deposits. In: Brown, G.C., Hawkesworth, C.J. & Wilson, R.C.L., eds, Understanding the Earth, 2nd edition. Cambridge University Press, 204-221.

Ridley, J.R. & Diamond, .LW., 2000. Fluid chemistry of orogenic lode gold deposits and implications for genetic models. Reviews in Economic Geology, 13, 141-162

Rimstidt, J.D., 1997. Gangue mineral transport and deposition. In: Barnes, H.L., ed., Geochemistry of hydrothermal ore deposit,, 3rd edition, Wiley & Sons, New York, 487-515.

Sawkins, F.J., 1984. Metal deposits in relation to Plate Tectonics. Springer-Verlag, Berlin, pp325.

Sillitoe, R.H., 1972a. Formation of certain massive sulphide deposits at sites of sea-floor spreading. Transactions of the Institution of Mining and Metallurgy, B81, B141-148.

Sillitoe, R.H., 1972b. A plate tectonic model for the origin of porphyry copper deposits. Economic Geology, 67, 184-197

Simmons, S.F. & Brown, K.L., 2000. Hydrothermal Minerals and Precious Metals in the Broadlands-Ohaaki GeothermalSystem: Implications for Understanding Low-Sulfidation Epithermal Environments. Economic Geology, 95, 971-999.

Spooner, E.T.C. & Fyfe, W.S., 1973. Sub-Sea-Floor Metamorphism, Heat and Mass Transfer. Contributions to Mineralogy and Petrology, 42, 287-304.

Walsh, M.P., Bryant, S.L., Schechter, R.S. & Lake, L.W., 1984. Precipitation and dissolution of solids attending flow through porous media. American Institute of Chemical Engineers Journal, 30, 317-327.

Walshe, J.L., Cooke, D.R. & Neumayr, P., 2005. Five questions for fun and profit: A mineral systems perspective on metallogenic epochs, provinces and magmatic hydrothermal Cu and Au deposits. In: Mao, J. & Bierlein, F.P., eds, Mineral Deposit Research: Meeting the Global Challenge, Vol. 1, Springer, Berlin, 477-480.

Wyborn, L.A.I, Heinrich, C.A. & Jaques, A.L., 1994. Australian Proterozoic Mineral Systems: Essential Ingredients and Mappable Criteria. Australasian Institute of Mining and Metallurgy Publication Series, 5/94, 109-115.

Geodynamics: Using geochemistry and isotopic signatures of granites to aid mineral systems studies: an example from the Yilgarn Craton

D.C. CHAMPION AND K.F. CASSIDY

*PMD**CRC*, GEOSCIENCE AUSTRALIA, GPO BOX 378, CANBERRA ACT 2601
David.Champion@ga.gov.au

Introduction

The mineral systems approach adopted by the *pmd**CRC* recognises that mineral deposits, although geographically small in extent, are the result of geodynamic processes that occur, and can be mapped at, a variety of scales, up to craton-scale. Accordingly, understanding the four-dimensional evolution of any geological terrane is important. Better understanding of the space-time evolution of geological terranes, and their components, provides important constraints on the geodynamics and architecture of mineral systems. It also has the potential to explain the often heterogeneous distribution of mineralisation within these regions.

One approach to constraining the crustal evolution of any region is by using the geochemical, isotopic and geochronological characteristics of granites and other felsic rocks. The integrated information these rocks convey provide direct constraints on the timing, extent and nature of crustal growth (lateral versus vertical). They also provide important, but less precise, indirect constraints on the nature and age of the crustal domains the granites occur within, through the combined use of geochemistry and isotopic tracers, such as Sm-Nd.

Granites

Granites (used in the broadest sense, i.e., diorites to true granites) have diverse and potentially complex origins. Two broad end-members can be recognised, namely: 1) differentiates of mantle melts (± crustal interaction) through to 2) purely crustal melts (± interaction with mantle-derived melts, other crustal melts/material). A third mechanism, strictly a variant of 2), namely partial melting of oceanic crust (± sediment) in subducting slabs (± crustal interaction) is also recognised. This is commonly thought, though not universally accepted, to have been the dominant mechanism for production of the voluminous Archean tonalite-trondhjemite-granodiorite suite (TTGs). Regardless of the mechanism of formation, granites are generally a complex mix of components. This complexity means that granites often carry a variety of crustal and/or mantle signatures. It means that deciphering these signals can be difficult, though this can be ameliorated by the study of selected granite groups, that is, dominantly crustal- or dominantly

mantle-derived types. In addition, the Archean is somewhat simpler, as granites of this age are dominated by two major granite groups: TTGs and potassic granites, with generally simpler mechanisms of formation: basalt → TTG → potassic granites (e.g., Champion & Smithies, 2001). Petrogenetic complexity can be further ameliorated by the use of tracers such as radiogenic isotopes. These have long been used in geological studies to provide constraints on geological processes and source components for a wide variety of geological situations (e.g., magmatism, mineral deposits). Individual isotope systems (e.g., U-Pb, Sm-Nd, Rb-Sr) provide different constraints - largely a function of the physio-chemical behaviour of the parent-daughter isotopes in question, their half life, and the geological environment they are in. One important isotopic tracer frequently used in granite studies is Sm-Nd – ^{147}Sm breaks down to ^{144}Nd by alpha decay with a half life of ~106 billion years. Sm and Nd are both lanthanides, that is, members of the rare earth series of elements (REE), and as such have very similar behaviour in felsic systems such as granites. As documented by de Paolo (1982), Sm-Nd can, therefore, be used to effectively 'see' through crustal processes, that is, provide an 'average' (model-dependant) crustal age for the source of the rocks in question. For voluminous rocks such as granites, which often have a significant crustal component; this provides a potentially powerful proxy into determining the bulk age of the crustal block the granites that occur within, that is, in effect broadly mapping crustal growth, as well demonstrated by Bennett and DePaolo (1987). This approach is even more powerful when combined with granite geochemistry and geochronology (including that for inherited components).

Conversely, radiogenic isotope studies of granites also provide constraints on the role of, and contribution from, the mantle. In particular, enriched (elevated LILE, LREE) geochemical signatures with unsupported isotopic signatures, especially in mafic and intermediate igneous rocks, often indicate the role of recent mantle enrichment processes (such as in subduction zones) and provide strong evidence for mantle connectivity. The Sm-Nd system, with the long half life of ^{147}Sm, is ideal for such studies, although other isotope systems (e.g., Rb-Sr, U-Pb, Lu-Hf) are often used.

Yilgarn Craton

The Archean Yilgarn Craton of Western Australia is not only one of the largest extant fragments of Archean crust in the world, but is also one of the most richly-mineralised regions in the world. The craton is dominated by granitic rocks - over 70% by surface area and at least similar amounts by volume, based on seismic refraction studies (Drummond, 1988). Around 80% of these granites are either sodic granites (members of the TTG suite) or potassic granites derived from them (Champion & Sheraton, 1997). Other granites, although minor, include enriched intermediate to felsic intrusive such as syenites and high-Mg diorites (sanukitoids) which suggest mantle-enrichment processes (see below). As such the geochemical, isotopic and geochronological characteristics of all these granites can be used to provide information on the four-dimensional evolution of the craton and the relative roles of crust and mantle in crustal growth. This paper presents the results of granite studies undertaken within the Yilgarn Craton by Geoscience Australia and collaborating partners over the last ten years. In particular, it draws on the results of two AMIRA projects, P482 (Cassidy et al., 2002) and P624 (Barley et al., 2003). The data are used to show that the Yilgarn Craton consists of distinct crustal terranes with differing crustal histories. More importantly, pre-existing continental crust has played a major role in younger orogenic events and appears to have exerted a significant, but poorly understood, spatial control on the distribution of mineral systems, such as gold, komatiite-associated nickel sulphide and volcanic-hosted massive sulphide (VHMS) base metal systems. The granites also record strong evidence for subduction-like processes that may have played a significant role in gold mineralisation.

Yilgarn Craton geology - new subdivisions

The Yilgarn Craton dominantly consists of typical Archean granite-greenstone terranes that formed between ca. 3.10 and 2.60 Ga (Fig. 1). Minor older rocks (back to 3.7 Ga) occur within the Narryer Terrane. Greenstone successions, typically dominated by mafic (and ultramafic) volcanism, but including

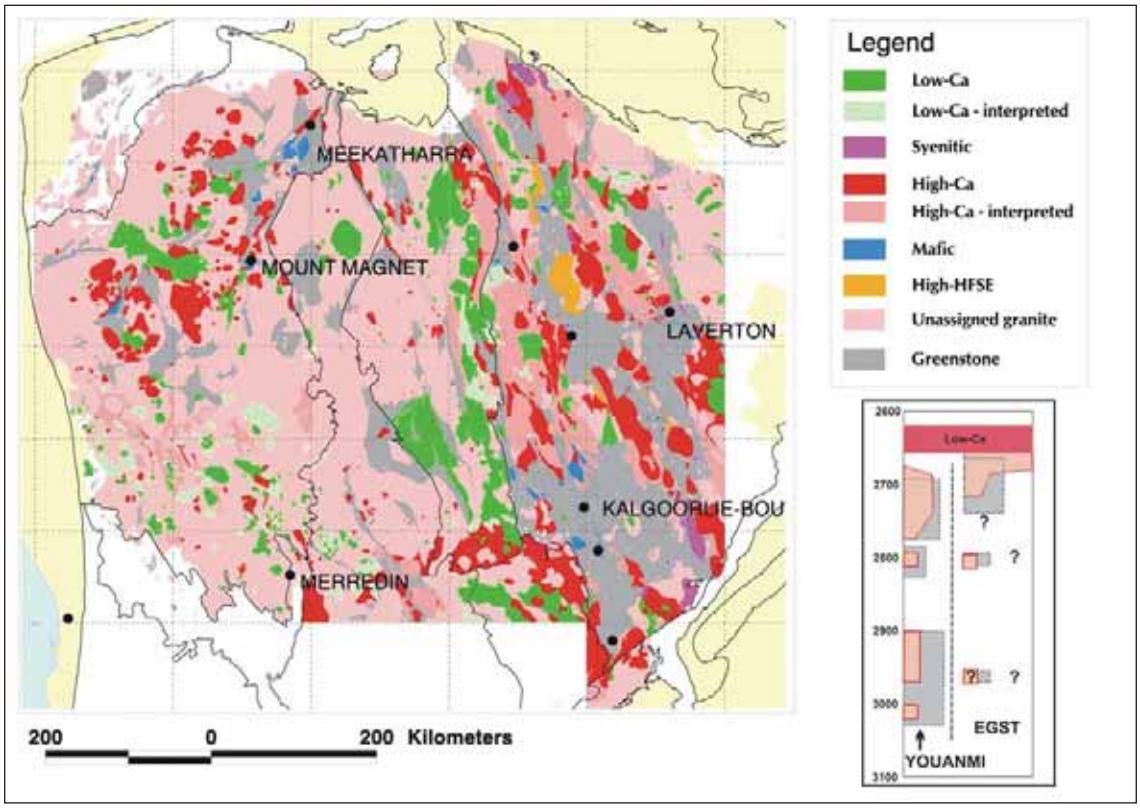

Figure 1. Distribution of granite groups within the Youanmi Terrane and Eastern Goldfields Superterrane of the Yilgarn Craton (from Cassidy et al., 2002). Granite groups are as outlined in Table 1. Inset shows the relative age distributions of greenstone rocks and granites.

felsic metavolcanic rocks and metasedimentary rocks, form less than 30% by area of the craton. These greenstone successionss formed episodically from ca. 3.0-2.9 Ga in the western Yilgarn to 2.72-2.655 Ga in the east (Figure 1). Episodic (intermediate to) felsic magmatism occupies a similar time frame, and was largely synchronous with greenstone formation. The only exception to this is the late (ca. 2.655 to 2.63 Ga) craton-wide granite event, that effectively marks cratonisation (Figure 1). The great majority of the felsic magmatic record in the Yilgarn Craton is ca. 2.76 to 2.63 Ga in age. Felsic plutonism older than this is poorly preserved, largely as isolated, often gneissic, remnants.

Previous subdivisions of the Yilgarn Craton were based on greenstone morphology (Gee et al., 1981), fault-bounded tectonostratigraphy (Myers, 1995), or both (e.g., Swager, 1997; Barley et al., 1998, 2002, 2003), which did not take into account the felsic magmatic rocks that form the bulk of the craton. Geochemistry, geochronology and Sm-Nd isotopic data from the Yilgarn granites (Figures 1, 2; Cassidy et al., 2006; Champion et al., 2006), in conjunction with detailed greenstone studies in the eastern Yilgarn (Barley et al., 2002, 2003), indicate that the bulk of the craton can be subdivided into two major provinces (see Cassidy et al., 2006) – an older craton nucleus, the Youanmi Terrane (YT; formerly Southern Cross and Murchison Provinces), and a collage of terranes in the east – the Eastern Goldfields Superterrane (EGST; formerly Eastern Goldfields Province).

Granite groups

The bulk of granites of the Yilgarn Craton are mineralogically very similar, with >80% being biotite-bearing monzogranites or granodiorites (Table 1). Accordingly, geochemistry and geochronology is required to help characterise and discriminate specific granite groups.

Group Area %	Lithologies	Geochemistry	Isotopic signature	Youanmi Terrane	Kalgoorlie Superterrane	Comments
High-Ca >60%	granodiorite, granite, . trondhjemite. Distributed both within and external to greenstone belts	high Na_2O, Na_2O/K_2O, low Th, LREE, Zr; mostly Y-depleted, Sr-undepleted. Range of LILE, LREE and Th contents; younger rocks extend to more LILE-enriched compositons.	ε_{Nd} varies between +3.6 and -6.4, mostly between +2.5 and -2.0. Isotopic signature strongly terrane-specific (Fig. 2).	>3.0 Ga-2.9? Ga, ca. 2.81 Ga, ca. 2.76 to 2.68 Ga; mostly 2.73-2.68 Ga.	ca. 2.8 Ga (minor remnants); 2.74-2.65 Ga; majority 2.685 to 2.655 Ga. Youngest members appear to occur within Kalgoorlie Terrane.	
Low-Ca >20%	granodiorite, granite Mostly external to greenstone belts	high K_2O, low Na_2O, high Rb, Th, LREE, Zr; moderately fractionated end-members.	ε_{Nd} varies between +2.0 and -5.1. Like the High-Ca granites, the isotopic signature is terrane specific.	2.65-2.6 Ga; mostly 2.65 to 2.63 Ga. Possibly also 2.685 Ga.	2.655 to 2.63 Ga.	
High-HFSE up to 5+%	granite, minor granodiorite Mostly internal or marginal to greenstone belts.	distinctive combination of high FeO*, MgO, TiO_2, Y, Zr with low Rb, Pb, Sr, Al_2O_3	ε_{Nd} varies between +2.0 and -4.7. Strongly terrane specific, where measured.	3.01 to 2.92 Ga?, ca. 2.81 Ga, 2.76 Ga to 2.45 & younger?; also 2.655-2.62 Ga	>2.72 Ga to 2.665 Ga; 2.7 to 2.68 Ga most common. Mostly geographically restricted to Kurnalpi Terrane & northeast Kalgoorlie Terrane.	spatial association with VHMS mineral systems
Mafic up to 5+%	diorite, granodiorite, granite, tonalite & trondhjemite	low SiO_2 (55-70+%), moderate to high Ni, V, MgO. Range of LILE, LREE and Th; subdivided into high - and low-LILE	Mostly ε_{Nd} of +2.8 to +1.0. Values of -1.7 and -2.8 for 2 samples in the western Youanmi Terrane. No correlation between geochemistry and isotopic signature.	3.01 to 2.92 Ga?, ca. 2.81 Ga, 2.76 Ga to 2.10 Ga	>2.72 Ga to 2.65 Ga; possibly younger? LILE-enriched members tend to be ca. 2.665 Ga and younger.	common spatial association with gold mineralisation, especially high-LILE members
Syenitic <5%	syenite, quartz syenite, monzonite, quartz monzonite	high total alkalis (Na_2O + K_2O) 10-12%; commonly low MgO, FeO*, TiO_2.	all very similar, ε_{Nd} of +0.8 to +2.3, mostly all within error of each other: +1.5 to +2.0.	none recorded	ca. 2.65 Ga, and 2.655-2.645 Ga	some spatial association with gold mineralisation

Table 1. Characteristics of the five granite groups in the Yilgarn Craton.

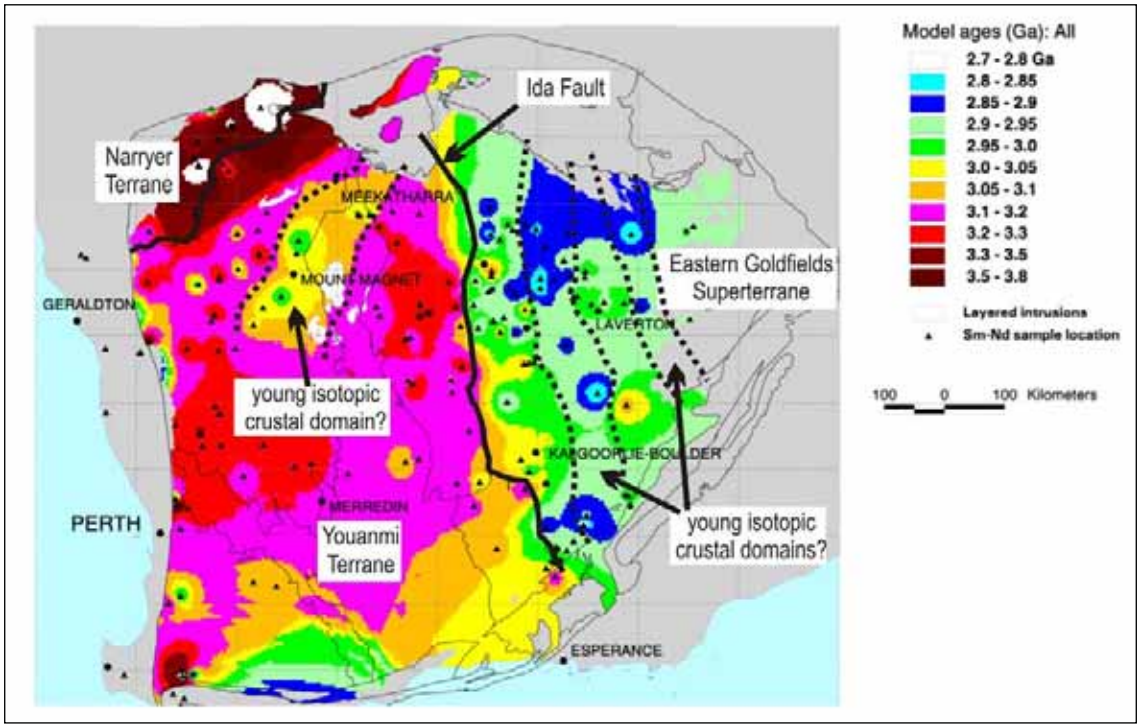

Figure 2. Nd depleted-mantle model age map of the Yilgarn Craton. Image produced by gridding Nd depleted-mantle model ages calculated from Sm-Nd point data (from Champion & Cassidy, in prep.).

Champion and Sheraton (1997) recognized five main granite groups, largely on the basis of petrological and geochemical characteristics. More recent work has confirmed and extended this general subdivision for granites across the Yilgarn Craton (Table 1). The granites can be divided into two major geochemical groups: High-Ca (TTGs) and Low-Ca (potassic granites), consisting of over 60% and 20% respectively, of the total granites, and three minor (High-HFSE, Syenitic and Mafic) geochemical groups (Table 1; Figure 1). All groups, except the syenites, occur within both the YT and EGST; the syenites are localised within the latter. The three minor groups appear to be strongly localised within, or marginal to, greenstone belts.

The High-Ca granites (2.72-2.66 Ga) are felsic (68-77% SiO_2), dominantly sodic rocks (Table 1), that form a LILE-rich end-member to the ubiquitous TTG group of granites that occur in all Archean cratons. Like TTGs elsewhere, the High-Ca granites are (mostly) characterized by Sr-undepleted, Y-depleted signatures, indicating they were largely produced at high pressures, by partial melting of dominantly basaltic source rocks, either within thickened mafic crust or by melting of subducting oceanic crust. Unlike many TTGs, however, the High-Ca granites have chemical, isotopic and inherited zircon compositions consistent with a significant crustal component, requiring either a wholly crustal protolith, or significant crustal interaction if derived via melting of subducting slabs.

The younger Low-Ca group is chemically distinct from the High-Ca granites. The former are characterised by high-LILE, strong enrichments in LREE and some of the HFSE, and have compositions consistent with crystal fractionation. They were derived by partial melting of crust of broadly tonalitic composition, that is, they represent reworking of older (High-Ca) felsic crust.

Other granite types in the EGST are volumetrically minor, but include both crustal- and mantle-derived rocks. Importantly, the latter have geochemical and isotopic signatures suggesting mantle metasomatism, and provide the best evidence for a subduction environment. Minor granite groups include: a) the high SiO_2

(>74% SiO_2), crustal-derived, High-HFSE group (2.685-2.66 Ga) with distinctive A-type characteristics but low LILE contents, especially Rb and Pb; b) a geochemically diverse but isotopically similar group of mostly mantle-derived, commonly more mafic (<60 to >70% SiO_2) granites (2.69-2.65 Ga) that exhibit large between-suite variations in LILE and LREE (i.e., variably enriched); and c) isotopically similar, peralkaline rocks such as syenites (and monzonites) (2.665-2.64 Ga).

Age distribution

U-Pb zircon geochronology of the granites (Nelson, 1997; Fletcher et al., 2001; Cassidy et al., 2002; Dunphy et al., 2003; Geological Survey of Western Australia, 2006; Sircombe et al., 2007) indicates that granite magmatism spans from ca. 3.0 to 2.63 Ga, with an apparent continuum in magmatism between 2.72 and 2.63 Ga across the craton. Oldest rocks belong to the High-Ca, High-HFSE and Mafic groups. Importantly, the geochronological database clearly confirms distinct episodes of specific granite magmatism (Figure 1). This is best illustrated by the High-Ca granites, which display a peak between 2.72 and 2.68 Ga in the YT and a younger pronounced peak between 2.68 and 2.655 Ga in the EGST. Notably, while voluminous High-Ca magmatism was occurring in the EGST (2.68-2.655 Ga), at this time the YT was the site of minimal magmatism of any type. The period ca. 2.68 Ga is important, therefore, as it not only marks the cessation of significant plutonism in the YT, but also the switch from localised Mafic and High-HFSE granites in the EGST to widespread High-Ca granites. The other significant feature confirmed by the geochronology is the switch from High-Ca to Low-Ca magmatism at ca. 2.655 Ga (Fig. 1). Low-Ca granites are late in the magmatic sequence, with ages between 2.655 and 2.63 Ga. These ages are found across the Yilgarn Craton and record what must have been a voluminous, craton-wide event of some significance.

Sm-Nd isotopes and crustal development

Two diverging patterns are evident in the Sm-Nd isotopic data for Yilgarn granites. Firstly, those granites which show geochemical, isotopic and zircon inheritance evidence for a significant or wholly crustal component (Low-Ca, High-Ca, High-HFSE) record a range of ε_{Nd} and model age signatures (Table 1). Given the crustal component in these rocks, these isotopic data can be used to constrain the crustal prehistory of the Yilgarn Craton. Champion and Cassidy (in prep.) used 2-stage Nd depleted-mantle model ages (T_{2DM}), to produce a gridded map showing relative crustal ages (not absolute age) for the Yilgarn Craton (Figure 2). Results of this work, from the widespread High-Ca and Low-Ca granites in particular, clearly identify a major isotopic break between the YT and the EGST (Figure 2). The simplest interpretation for such an isotopic break is that it represents a major change in average crustal age. The fact that the isotopic break, for the most part, closely corresponds with the ground position of the Ida Fault, supports this. The isotopic data, therefore, effectively subdivide the craton into a larger older crustal block (YT) that is bounded to the east by the significantly younger, more economically-important, EGST. The isotopic data also delineate two isotopically 'younger' domains that broadly correspond to geological domains; one in the central part of the YT, co-incident with layered mafic intrusives, and one within the EGST (Figure 2). The range in ages and types of granites within these two 'younger' domains suggest that the latter simply reflect zones of younger crust, though they could also, in part, reflect palaeo-crustal thickness, that is, simply less crustal interaction. This may be particularly so for the High-Ca granites, which dominate these 'young' zones. Importantly, these domains are either characterised by isotopic signatures with young residence times (i.e., Nd T_{2DM} ages close to crystallisation ages), and/or contain evidence for arc-related juvenile magmatism (e.g., calc-alkaline andesites).

The second isotopic pattern is best illustrated by the Mafic group granites. These rocks show a range of geochemical compositions independent of their isotopic signature, i.e., variable degrees of LILE- and LREE-enrichment, that is not matched by changing Sm-Nd isotopic signature. This suggests that the geochemical enrichment recorded in these granites was either introduced by crustal interaction after

partial melting, or that enrichment occurred in the source not long before partial melting. The former is considered unlikely because: 1) the enriched geochemical signature is most evident in the more mafic end-members; and 2) the isotopic variation in the crust, mapped by the High-Ca and Low-Ca granites, in not evident in the Mafic granites. The simplest way to explain the isotopic and geochemical signatures is via mantle enrichment processes (metasomatism), similar to those observed in modern subduction environments, by introduction of a (dehydrated or partial melt) slab component to the mantle wedge (e.g., Tatsumi & Eggins, 1995). Such a subduction environment is also favoured by the presence of syenites with a calc-alkaline signature (e.g., Smithies & Champion, 1999), by calc-alkaline lamprophyric rocks, and by the calc-alkaline volcanics that dominate the Kurnalpi Terrane (Barley et al., 2003).

Constraints from felsic magmatism on tectonic models for the EGST

Champion and Cassidy (in Barley et al., 2003), proposed preferred tectonic environments for the formation of each granite group. Although tectonic models based on granite data alone are equivocal, they can be used in conjunction with the points raised above to provide important constraints for tectonic models of the Yilgarn Craton, particularly the EGST. Favoured tectonic models indicate a variety of arc environments (largely pre-existing continental crust - not island arc-like) with or without various rifting regimes, pre ca. 2.655 Ga.

Granite magmatism pre-2.68 Ga appears to be largely syn-volcanic, with clear match-ups between intrusive and extrusive units. It is not surprising, therefore, that tectonic models interpreted from these granites (e.g., Cassidy et al., 2002), closely match those suggested for the volcanic and sedimentary successions of this age (Barley et al., 2002, 2003). Overall, there is a dominance of continental margin signatures as well as evidence of magmatic recycling of older arc-related crust.

The two most significant changes in magmatic style in the EGST occur at ca. 2.675 and 2.655 Ga. The earlier changes in style of magmatism are interpreted to represent variations within an overall subduction-related environment. The change at 2.675 Ga, from localised Mafic and High-HFSE granites to widespread dominantly High-Ca granites (within all terranes of the EGST), coupled with the first significant appearance of LILE-enriched magmatism around this time (high-LILE subgroups of the High-Ca and Mafic groups), suggests that significant recycling of crustal material commenced during this period. This was possibly either as a consequence of a subducted crustal component, and/or, more likely, crustal thickening (e.g., Hildreth and Moorbath, 1988), and/or, speculatively, perhaps a significant change (shallowing) in the angle of slab subduction, with commensurate associated crustal shortening and deformation (e.g., Gutscher, 2002). The appearance of High-Ca magmatism at much the same time across all terranes within the EGST, suggests that this process was similarly occurring across all terranes. Importantly, this period also corresponds to the timing of cessation of High-Ca magmatism in the YT. That is, widespread High-Ca magmatism ceased in the YT at about the same time as it commenced in the EGST (Fig. 1). These two events are most likely related and, together with the crustal thickening hypothesis, may indicate some form of terrane accretion at this time. The appearance of widely distributed enriched Mafic granites, with sanukitoid affinities, shortly after the widespread appearance of the High-Ca granites, is consistent with petrogenetic models for sanukitoid magmas, that is, melting of a slab-melt metasomatised mantle wedge (e.g., Smithies & Champion, 2000).

The 2.655 Ga change from High-Ca dominated- to Low-Ca dominated-magmatism reflects a significant change in switch in magmatic style, and presumably represents some fundamental reordering of the tectonic environment at that time, interpreted by Champion and Cassidy (in Barley et al., 2003) to be the cessation of subduction. Mafic granite emplacement continued for a short period after this switch, best documented in the Kalgoorlie Terrane, and may have included younger lamprophyric magmatism. The continuation of such magmatism does not necessarily reflect subduction, but may be due to reworking of subduction-modified mantle (e.g., Smithies & Champion, 2000) and/or slab break-off processes

(e.g., Beakhouse, 2007). From around post-2.648 Ga, there is no preserved (or recognised) record of subduction-related Archean magmatism within the Yilgarn Craton. In this regard, the cessation of Low-Ca magmatism (ca. 2.62-2.63 Ga) marks the timing of effective cratonisation of the Yilgarn Craton as a whole.

Crustal isotopic domains and mineral systems

Consideration of the relationship between crustal age (based on Sm-Nd model ages) and the distribution of mineral deposits shows that there is a close spatial association between komatiite-associated nickel sulphide, VHMS base-metal and gold mineralisation with specific crustal domains, with this best expressed in the EGST. These associations are:

1. komatiite-associated nickel-sulphide deposits are concentrated in terranes with pre-existing crust; that is, Youanmi, Kalgoorlie, and an 'old' domain of the Kurnalpi Terrane.
2. VHMS base-metal systems appear spatially associated with terranes with juvenile crust, for example, the 'young' domains in the central Youanmi and Kurnalpi Terranes (Figure 2). The Golden Grove deposits in the central YT and the Teutonic Bore and Jaguar deposits in the Kurnalpi Terrane are all associated with juvenile crust.
3. although gold mineralisation occurs in all terranes across the Yilgarn Craton, the majority of the gold endowment is spatially restricted to areas underlain by crust of intermediate age (Nd T_{2DM} ages of 2.95-3.1 Ga in Fig. 2); specifically the Kalgoorlie Terrane and an 'old' domain of the Kurnalpi Terrane. In the EGST, at least, there is little significant gold mineralisation in domains with more juvenile signatures.

Huston et al. (2005) suggested that the high heat flow and extensional structures, that are characteristics of juvenile crustal domains, encourage formation of VHMS deposits in such an environment. This relationship of metal endowment and specific crustal domains effectively explains why the Abitibi Subprovince in Canada is more endowed in VHMS mineralisation than the Yilgarn Craton; that is, the crust is not juvenile enough in the Yilgarn.

Why these apparent relationships hold for komatiite-associated nickel-sulphide and gold mineral systems is not entirely clear, and it is noted that the relationship for gold does not appear to hold for the extremely well (gold) endowed Abitibi Subprovince. Using empirical relationships it is possible that, unlike VHMS systems, gold endowment in specific terranes is not related to the nature of the underlying lithosphere, but perhaps to the favourable sequences of geological events, for example, the superposition of plume-related and subsequent subduction-derived 'enriched' magmatism on a pre-existing lithospheric architecture. The development of specific mineral systems, therefore, possibly reflects the interaction of specific geotectonic processes, such as later lithospheric-scale orogeny, with pre-existing crustal and mantle reservoirs. Gold potential is likely enhanced where accretionary fluid events, such as introduction of the Mafic granites using lithospheric-scale plumbing systems, are able to interact with gold-rich lithospheric source rocks and/or other (gold-carrying) fluids. This association is best developed in the Kalgoorlie and eastern Kurnalpi terranes in the EGST, and the young crustal domain in the YT, where there is evidence for both plume-related and subduction-derived magmatism. It is possible that the absence of a critical feature (such as plume-related komatiites in the 'young' crustal belt, or significant mantle-derived Mafic granites) potentially decreases the metal inventory and/or the ability to extract fertile material during orogeny, making these crustal domains less prospective.

Acknowledgements

The authors wish to acknowledge that many of the results presented here were made possible through a number of industry-funded AMIRA projects, especially P482 and P624. The authors would also like to acknowledge co-workers from the University of Western Australia: Mark Barley, Stuart Brown, Ian

Fletcher, Stephen Gardoll, David Groves, Bryan Krapez, Neal McNaughton, Jan Dunphy; Geoscience Australia: Richard Blewett, Anthony Budd, Karol Czarnota, Paul Henson, Tanya Fomin, Natalie Kositcin, Alan Whitaker; and, the Geological Survey of Western Australia: Bruce Groenewald, Hugh Smithies, Martin Van Kranendonk, Steve Wyche.

References

Barley, M.E., Krapež, B., Brown, S.J.A., Hand, J. & Cas, R.A.F., 1998. Mineralised volcanic and sedimentary successions in the Eastern Goldfields Province, Western Australia. Australian Mineral Industry Research Association, Project P437, Final Report, 282pp.

Barley, M.E., Brown, S.J.A., Krapež, B. & Cas, R.A.F., 2002. Tectonostratigraphic analysis of the Eastern Yilgarn Craton: an improved geological framework for exploration in Archaean Terranes. Australian Mineral Industry Research Association, Project P437A, Final Report, 257pp.

Barley, M.E., Brown, S.J.A., Cas, R.A.F., Cassidy, K.F., Champion, D.C., Gardoll, S.J. & Krapež, B., 2003. An integrated geological and metallogenic framework for the eastern Yilgarn Craton: developing geodynamic models of highly mineralised Archaean granite-greenstone terranes. Australian Mineral Industry Research Association, Project P624, Final Report 192, 188pp.

Beakhouse, G.P., 2007. Gold, granite and late Archean tectonics: a Superior Province perspective. In: Bielein, F.P. & Knox-Robinson, C.M., eds, Proceedings of Kalgoorlie '07 Conference. Geoscience Australia, Record, 2007/14, 191-196.

Bennett, V.C. & DePaolo, D.J., 1987. Proterozoic crustal history of the western United States as determined by Neodymium isotopic mapping. Geological Society of America, Bulletin, 99, 674-685.

Cassidy, K.F., Champion, D.C., McNaughton, N.J., Fletcher, I.R., Whitaker, A.J., Bastrakova, I.V. & Budd, A.R., 2002. Characterization and metallogenic significance of Archaean granitoids of the Yilgarn Craton, Western Australia. Australian Mineral Industry Research Association Project P482/MERIWA Project M281, Final Report, 514pp.

Cassidy, K.F., Champion, D.C., Krapež, B., Barley, M.E., Brown, S.J.A., Blewett, R.S., Groenewald, P.B. & Tyler, I.M., 2006. A revised geological framework for the Yilgarn Craton, Western Australia. Western Australia Geological Survey, Record, 2006/8.

Champion, D.C. & Sheraton, J.W., 1997. Geochemistry and Sm-Nd isotopic systematics of Archaean granitoids of the Eastern Goldfields Province, Yilgarn Craton, Australia: constraints on crustal growth. Precambrian Research, 83, 109-132.

Champion, D. C. & Smithies, R. H., 2001. Archaean granites of the Yilgarn and Pilbara cratons, Western Australia. In: 4th International Archaean Symposium 2001, Extended Abstracts. AGSO-Geoscience Australia, Record 2001/37, 134–136.

Champion, D.C., Cassidy, K.F. & Smithies, R.H., 2006. Sm-Nd isotope characteristics of the Pilbara and Yilgarn Cratons, Western Australia: implications for crustal growth in the Archean. Geochimica Cosmochimica Acta, 70(18), Supplement 1, A95.

DePaolo, D.J., 1982. Neodymium Isotope Geochemistry. Springer Verlag, Berlin.

Drummond, B.J., 1988. A review of crust/upper mantle structure in the Precambrian areas of Australia and implications for Precambrian crustal evolution. Precambrian Research, 40/41, 101–116.

Dunphy, J.M., Fletcher, I.R., Cassidy, K.F. & Champion, D.C., 2003. Compilation of SHRIMP U-Pb geochronology data, Yilgarn Craton, Western Australia, 2001-02. Geoscience Australia, Record, 2003/15, 139pp.

Fletcher, I.R., Dunphy, J.M., Cassidy, K.F. & Champion, D.C., 2001. Compilation of SHRIMP U-Pb geochronology data, Yilgarn Craton, Western Australia, 2000-01. Geoscience Australia Record, 2001/47, 110pp.

Gee, R.D., Baxter, J.L., Wilde, S.A. & Williams, I.R., 1981. Crustal development in the Archaean Yilgarn Block, Western Australia. In: Glover J.E. & Groves D.I., eds, Archaean Geology: Second International Symposium, Perth, 1980. Geological Society of Australia, Special Publication, 7, 43-56.

Geological Survey of Western Australia, 2006. Compilation of geochronology data, June 2006 update. Western Australia Geological Survey, Digital Data, ANZWA1220000726.

Gutscher, M-.A., 2002. Andean subduction styles and their effect on thermal structure and interplate coupling. Journal of South American Earth Sciences, 15, 3-10.

Hildreth, E.W. & Moorbath, S., 1988. Crustal contributions to arc magmatism in the Andes of Central Chile. Contributions to Mineralogy and Petrology, 98, 455-489.

Huston, D.L., Champion, D.C. & Cassidy, K.F., 2005. Tectonic controls on the endowment of Archean cratons in VHMS deposits: evidence from Pb and Nd isotopes. In: Mao, J. & Bierlein, F.P., eds, Mineral Deposit Research: Meeting the Global Challenge. Berlin/Heidelberg, Springer, 15-18.

Myers, J., 1995. The generation and assembly of an Archaean supercontinent: evidence from the Yilgarn craton, Western Australia. In: Coward, M.P. & Ries, A.C., eds, Early Precambrian Processes. Geological Society of London, Special Publication, 95, 143-154.

Nelson, D.R., 1997. Evolution of the Archaean granite-greenstone terrane of the Eastern Goldfields, Western Australia: SHRIMP zircon constraints. Precambrian Research, 83, 57-81.

Sircombe, K.N., Cassidy, K.F., Champion, D.C. & Tripp, G., 2007. Compilation of SHRIMP U-Pb geochronological data, Yilgarn Craton, Western Australia, 2004-2006. Geoscience Australia, Record, 2007/01, 182pp.

Smithies, R.H. & Champion, D. C., 1999. Geochemistry of felsic igneous alkaline rocks in the Eastern Goldfields, Yilgarn Craton, Western Australia: a result of lower crustal delamination? - implications for Late Archaean tectonic evolution. Journal of the Geological Society of London, 156, 561-576.

Smithies, R.H., & Champion, D. C., 2000. The Archaean high-Mg diorite suite: links to tonalite-trondhjemite-granodiorite magmatism and implications for early Archaean crustal growth. Journal of Petrology, 41, 1653-1671.

Swager, C.P., 1997. Tectono-stratigraphy of late Archaean greenstone terrains in the southern Eastern Goldfields, Western Australia. Precambrian Research, 83, 11-41.

Tatsumi, Y, & Eggins, G., 1995. Subduction Zone Magmatism. Frontiers in Earth Sciences, Blackwell Science, Massachusetts.

Architecture: Mapping the distribution of alteration: what different geophysical techniques can reveal

R. CHOPPING

*pmd**CRC*, Geoscience Australia, GPO Box 378, Canberra, ACT 2601
Richard.Chopping@ga.gov.au

Introduction

To understand the potential of geophysical techniques to map the distribution of chemical alteration, we must first look at the first principles of geophysical responses. Geophysical responses, observed by gravity, magnetic or seismic reflection surveys, arise from a contrast in physical properties, such as density, magnetic susceptibility or acoustic impedance (the product of density and seismic velocity).

Physical properties, such as density, magnetic susceptibility or seismic velocity, in crystalline basement, in which the majority of ore deposits occur, are controlled predominantly by the mineralogy of the rocks (Guéguen & Palciauskas, 1994). It is for this reason that, for example, we image granite bodies as lower gravity responses, and basalts as higher gravity responses (Telford et al., 1990). Note that the mineralogy of a rock does not depend just on the primary rock type; chemical alteration will also influence the mineralogy of a rock. Understanding the changes in physical properties produced by chemical alteration is paramount to understanding how geophysics can map alteration distribution.

The physical property changes that can be attributed to alteration have been examined at the St Ives Gold Mine and Sunrise Dam Mine, in the Eastern Goldfields, Yilgarn Craton, Western Australia. A summary of these findings is presented here; a more comprehensive discussion is in Chopping (2006b). A comparison between numerical modelling results (methodology after Chopping & Cleverley, this volume) and an hypothesis regarding the signature of fluid-flow and seismic reflection profiles in Laverton (Chopping, 2006a) will also be discussed below.

Physical properties at the St Ives Gold Mine

A study of the physical properties of a 1km deep drillhole at the St Ives Gold Mine shows that anomalous physical property changes can be attributed to chemical alteration. A method has been developed ('the alteration cone') to identify these zones from physical properties. The alteration cone represents a limited field on a scatter plot of two physical properties, within which the altered samples will plot. At the apex of the cone are the physical properties corresponding to the alteration assemblage; the open end of the cone covers a limited field, which contains the properties of unaltered samples or samples with a very low proportion of alteration. The concept of the alteration cone is described in Chopping (2006b).

Of particular note, a 1m thick zone from this drillhole, which contains a significant proportion of muscovite (as identified in a HyLogger study by Yang, 2006), shows physical properties which are consistent with

alteration to a muscovite-pyrrhotite assemblage. Samples logged by company geologists for alteration to either pyrite or pyrrhotite also consistently follow the trends suggested by the alteration cone methodology (Figure 1). Also, two narrow zones within the Devon Consols Basalt, intersected by this hole, show physical properties which are consistent with alteration to significant portions of pyrrhotite (Figure 2).

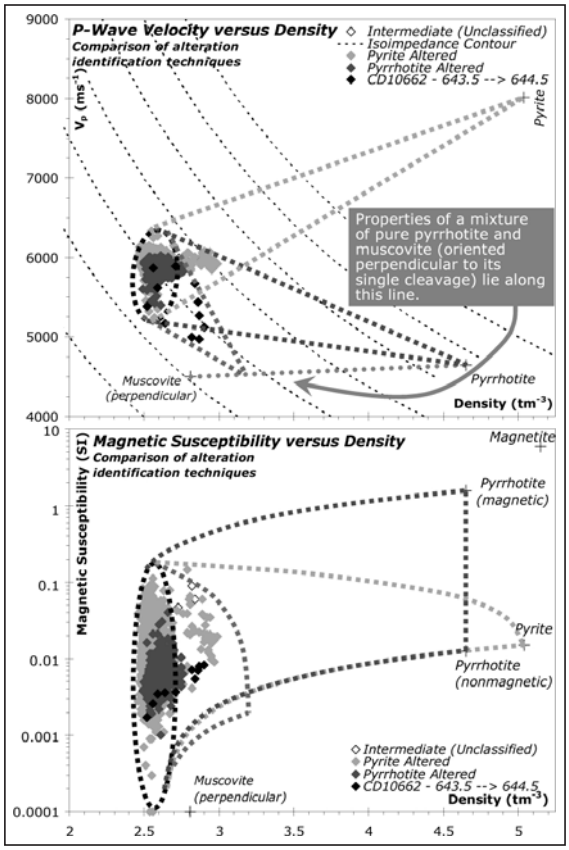

Figure 1: Seismic velocity-density and magnetic susceptibility-density plots for samples logged as an unclassified intermediate rock, in a deep drillhole at the St Ives Gold Mine. This intersection is most likely a basal volcaniclastic rock in the Black Flag beds. Two different symbols, light and dark grey diamonds, represent intervals logged to contain pyrite and pyrrhotite by Gold Fields exploration geologists. These samples follow the trends expected for pyrite and pyrrhotite alteration, denoted by light and grey dashed lines representing alteration cones for this unit. Black diamonds represent samples inferred from a HyLogger study (Yang, 2006) to contain a significant proportion of muscovite; these are most simply explained by alteration to an assemblage containing both pyrrhotite and muscovite.

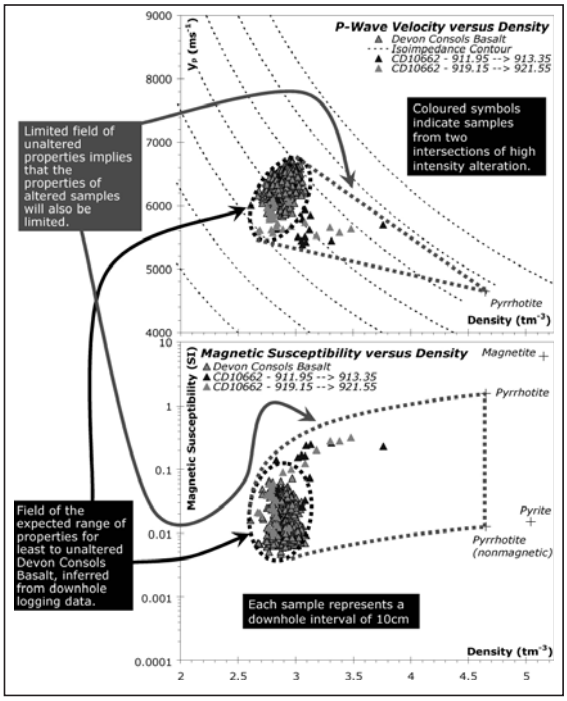

Figure 2: Seismic velocity-density and magnetic-susceptibility-density plots for samples logged as Devon Consols basalt, in a deep drillhole at the St Ives Gold Mine. Two symbols, light and dark grey diamonds, represent two intervals which show very anomalous physical properties – they plot significantly away from the restricted field of other samples (dashed oval, inferred to represent the properties of unaltered or least-altered Devon Consols basalt), and can be inferred, by the alteration cone methodology, to represent samples altered to pyrrhotite. This type of alteration can be inferred to be distal alteration to a mineralising system (Neumayr et al., 2005). The Victory-Defiance gold camp, which contains around 2 million ounces of gold, is located some 3 km west of this drillhole.

These results provide confidence that chemical alteration can and does produce significant physical property contrasts. The physical property contrasts are such that should the alteration be volumetrically significant, these zones of alteration can be detected in geophysical surveys. Neumayr et al. (2005) suggest that there may be between 5 and 10% sulphide (pyrite or pyrrhotite) alteration distal to gold systems of the Yilgarn Craton. This distal alteration would serve to slightly increase the gravity response with respect to the background (unaltered) response. This correlates with the increases in gravity response, with respect to the unaltered response, as observed from numerical models (Chopping and Cleverley, this volume).

The physical property results for St Ives also indicate that density-magnetic susceptibility relationships are very different for the following alteration minerals: magnetite, monoclinic (magnetic) pyrrhotite, and pyrite or hexagonal (non-magnetic) pyrrhotite. Other minerals which may be identified by their unique physical property signatures include hematite (very dense and approximately as magnetic as pyrite) and ilmenite (similar density to magnetic pyrrhotite, and slightly more magnetic). Note that density and magnetic susceptibility models can be produced for gravity and magnetic inversions respectively; hence potential field inversions could be used to target the relevant alteration minerals.

Alteration effects visible in regional seismic reflection profiles

Some reflections in regional seismic profiles are most likely due to chemical alteration along fluid-flow pathways (Drummond et al., 2004; Chopping, 2006a). An interpretation of a portion of the AGS-NY1 seismic line (Goleby et al., 2003), which passes through the Laverton township, suggests that these fluid-flow reflections are imaged as higher apparent frequency (Figure 3 – after Chopping, 2006a).

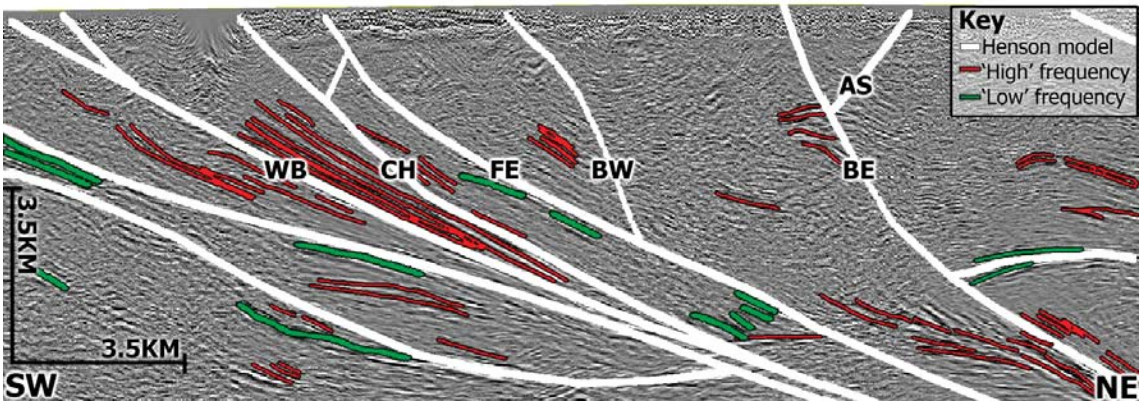

Figure 3: Interpretation of the AGS-NY1 seismic line. Faults and lithological contacts (white lines) are after Henson et al. (2006), and are abbreviated as follows: WB – base of Wallaby Basin; CH – Childe Harold Fault; FE – Far East Fault; BW – Barnicoat (West) Fault; BE – Barnicoat (East) Fault; AS – Apollo Shear. The Laverton township is located directly above the gap in reflectivity near the surface, just to the southwest of where the Childe Harold Fault meets the surface (top of figure). Black lines are interpreted 'high' frequency and relatively linear geometry reflections, which Chopping (2006a) interpreted to be most likely due to fluid flow in the region.

The probable seismic response of a numerical model of gold formation (Cleverley et al., 2006), using the methodology of Chopping and Cleverley (this volume), supports the hypothesis that these reflections are due to chemical alteration. The acoustic impedance section after the simulation of chemical alteration shows that there are distinct reflectors in the fault which have acted as fluid conduits. These reflectors do not appear for the unaltered model, and thus are due to chemical alteration. The reflectors are thin and would serve to change the seismic character around the fault, producing similar reflections as to those seen in the Laverton region.

Preliminary seismic velocity measurements on samples from Sunrise Dam indicate that the Sunrise Shear (an altered structure which has seen considerable fluid-flow) has the potential to be imaged using seismic methods (Figure 4). The seismic character of the Sunrise Shear depends heavily on its apparent thickness. In general, reflections will occur from the top and bottom of a thick zone, assuming the thickness is greater than ¼ of the seismic wavelength. In the case of regional seismic reflection profiles, the average crustal velocity is 6 km/s and the main frequency is ~50 Hz, yielding a wavelength of 120 m. Thus, if the Sunrise Shear is chemically altered over a thickness of less than 30 m, it would appear as a single reflection, which produces an apparent high-frequency reflection, like those observed in the regional Laverton seismic lines.

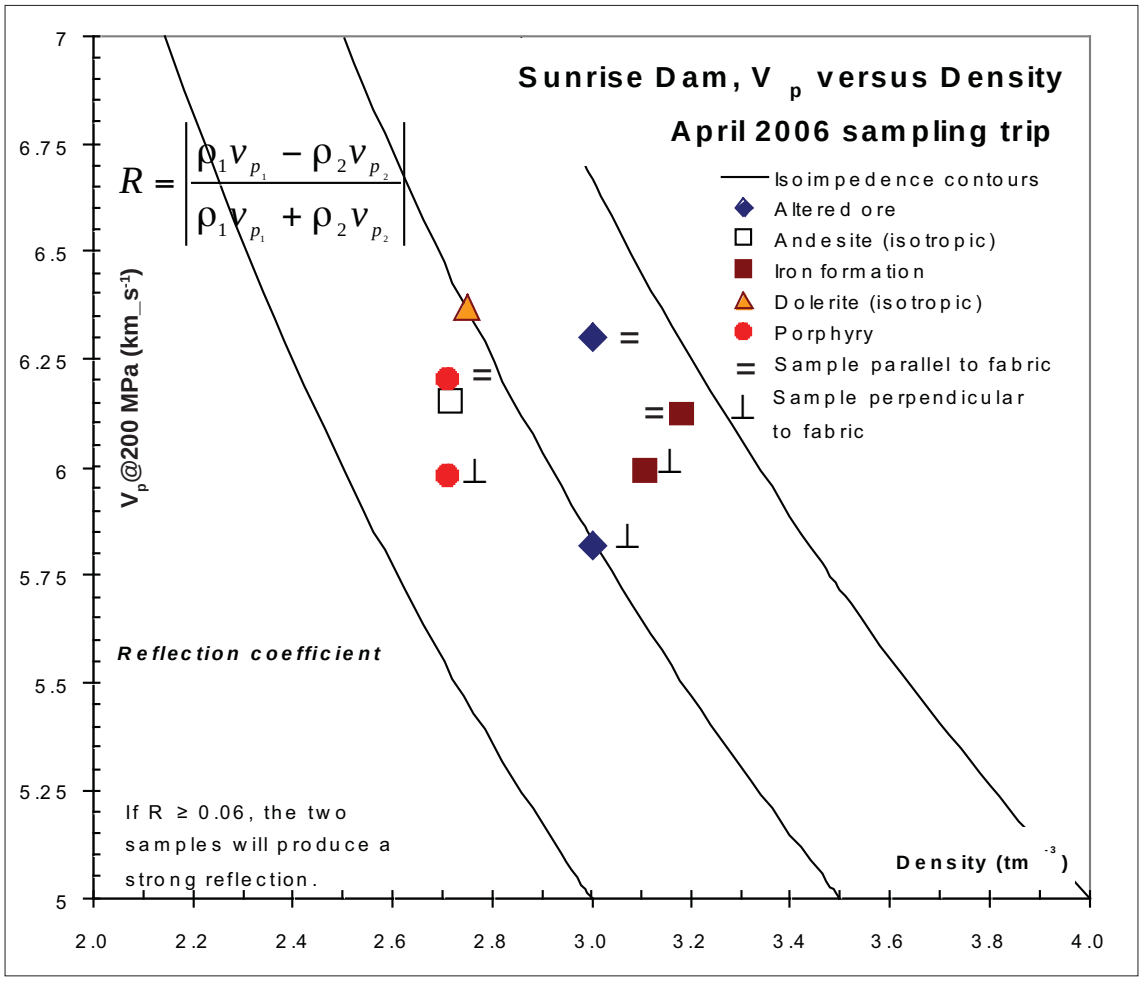

Figure 4: Preliminary seismic velocity-density results from the samples from Sunrise Dam, collected in April 2006. Samples plotting on adjacent isoimpedance contours have a reflection coefficient of 0.06, and will produce a strong reflection in seismic data (Salisbury et al., 2000); the formula for calculating the reflection coefficient (R) of two samples is also shown. There appears to be a moderate acoustic impedance contrast between unaltered rocks (circles, squares) and samples from within the Sunrise Shear (diamonds), suggesting structures such as the Sunrise Shear could be imaged in seismic data as moderate to strong reflections. Most samples are moderately anisotropic, that is, the velocity changes with orientation, and the samples from the Sunrise Shear are the most anisotropic of these samples. The anisotropy of the samples from the Sunrise Shear means that the reflectivity of the Sunrise Shear will vary with the angle of the structure to the incoming seismic energy.

Implications for alteration mapping using geophysics

Physical property studies performed in the Eastern Goldfields of the Yilgarn Craton, Western Australia, indicate that chemical alteration can produce physical property contrasts which are significant enough to be imaged using geophysical techniques. The detectability of zones of alteration will depend on the magnitude of the physical property changes, which themselves depend on the alteration assemblages and proportion of chemical alteration. Physical property studies support the known relationships between physical properties and alteration; methods to calculate the geophysical response from chemical models have been developed by Chopping and Cleverley (this volume). These geochemical models also support the possibility of imaging chemical alteration using geophysics.

There are several ways in which chemical alteration can be detected using geophysics:

- Physical property studies, such as downhole property logging or routine hand-specimen measurements of multiple properties, can be used to interpret alteration, and can be used as an adjunct to other studies such as HyLogger campaigns;
- Gravity surveys can detect distal alteration to sulphides, and numerical modelling results suggest they can also detect gravity changes due to carbonate or quartz alteration directly above a gold deposit (Chopping and Cleverley, this volume);
- Magnetic surveys can detect deposits, assuming appropriately non-magnetic hosts and magnetic alteration minerals (e.g. the Wallaby deposit; Coggon, 2004);
- Regional seismic reflection surveys can contain reflections which are likely to be the result of chemical alteration (supported by both numerical chemical models and hand-specimen measurements); and
- The combination of magnetic and gravity inversion results to produce a consistent subsurface density-magnetic susceptibility could be used to interpret some alteration minerals, as the results of these inversions are physical properties and thus can be interpreted as per other physical property studies.

Acknowledgements

The work contained in this abstract reflects a distillation of ideas from ***pmd****CRC* Project A3 with some chemical modelling from Project M9. Project A3 would not have been possible without strong industry support from the ***pmd****CRC* sponsors. Three sponsors in particular strongly supported the project, namely AngloGold Ashanti, Barrick Gold and Gold Fields International. N. Kositcin, R.J. Korsch and A. Schofield provided constructive reviews.

References

Chopping, R., 2006a. Seismic 'mapping' of fluid pathways for the world-class gold mineral system at Laverton. In: Barnicoat, A.C. & Korsch, R.J., eds., Predictive Mineral Discovery Cooperative Research Centre – Extended Abstracts from the April 2006 Conference. Geoscience Australia, Record 2006/07, 18-22.

Chopping, R., 2006b. Project A3 Report: The relationship between alteration and physical properties at the St Ives Gold Mine, Western Australia. Predictive Mineral Discovery Cooperative Research Centre (***pmd****CRC*), Melbourne, Australia, 61pp.

Cleverley, J.S., Hornby, P. & Poulet, T., (006. Pmd*RT: Combined fluid, heat and chemical modelling and its application to Yilgarn geology. In: Barnicoat, A.C. & Korsch, R.J., eds, Predictive Mineral Discovery Cooperative Research Centre – Extended Abstracts from the April 2006 Conference. Geoscience Australia, Record 2006/07, 23-29.

Coggon, J., 2004. Magnetism – the key to the Wallaby deposit. Exploration Geophysics, 35(1&2), 125-130.

Drummond, B.J., Hobbs, B.E. & Goleby, B.R., 2004. The role of crustal fluids in the tectonic evolution of the Eastern Goldfields Province of the Archaean Yilgarn Craton, Western Australia. Earth Planets Space, 56, 1163-1169.

Goleby, B.R., Blewett, R.S., Groenewald, P.B., Cassidy, K.F., Champion, D.C., Jones, L.E.A., Korsch, R.J., Shevchenko, S. & Apak, S. N., 2003. The 2001 Northeastern Yilgarn Deep Seismic Reflection Survey. Geoscience Australia Record 2003/28, 143pp.

Guéguen, Y. & Palciauskas, V., 1994. Introduction to the Physics of Rocks. Princeton University Press, 294pp.

Henson, P., Blewett, R.S., Champion, D.C., Goleby, B.R. & Czarnota, K., 2006. Towards a unified architecture of the Laverton Region, W.A. In: Barnicoat, A.C. & Korsch, R.J., eds, Predictive Mineral Discovery Cooperative Research Centre: extended abstracts from the April 2006 Conference. Geoscience Australia Record 2006/07, 47-51.

Neumayr, P., Walshe, J. L. & Hagemann, S., 2005. Camp- to Deposit-Scale Alteration Footprints in the Kalgoorlie-Kambalda Area. ***pmd****CRC* Project Y3 Final Report. http://www.pmdcrc.com.au/final_reports_projectY3.html.

Salisbury, M.H., Milkereit, B., Ascough, G., Adair, R., Matthews, L., Schmitt, D.R., Mwenifumbo, J., Eaton, D.W. & Wu, J., 2000. Physical properties and seismic imaging of massive sulfides. Geophysics, 65(6), 1882-1889.

Telford, W.M., Geldart, L.P. & Sheriff, R.E., 1990. Applied Geophysics (Second Edition). Cambridge University Press, Cambridge, 790 p.

Yang, K., 2006. Mineralogical Interpretation of HyLogging Data for Drill-holes from the Conqueror Deposit of the St Ives Goldfield, WA. CSIRO Exploration and Mining, Report P2005/463.

Flowpaths and Drivers: Creating forward geophysical models from reactive transport simulations

R. CHOPPING[1] AND J.S. CLEVERLEY[2]

[1]*pmd**CRC*, Geoscience Australia, GPO Box 378, Canberra, ACT 2601
[2]*pmd**CRC*, Computational Geoscience Group, CSIRO Exploration & Mining, PO Box 1130, Bentley, WA 6102
Richard.Chopping@ga.gov.au

Introduction

Geophysical responses, such as gravity, total magnetic intensity or seismic reflections, result from spatial variations in physical properties, such as density, magnetic susceptibility or acoustic impedance, of the present-day subsurface. The physical properties of the subsurface are a function of the prior geological history of the region. In basement terranes, where most mineral deposits are located, the physical properties are primarily controlled by the mineralogy of the rocks in the subsurface (Guéguen & Palciauskas, 1994). This mineralogy, in turn, is controlled by primary lithology as well as any chemical alteration overprint.

The pmd*RT reactive transport (RT) modelling code, through its simulations of heat and fluid flow, and chemical reactions, produces models of mineralogy that vary both spatially and temporally (Hornby & Poulet, 2008). These models of mineralogy can be used to produce physical property models and hence predict the geophysical response of the alteration system which has been simulated by the chosen reactive transport model.

This abstract describes a method which calculates potential geophysical responses of a reactive transport model, and provides a simple example of applying this method to a model simulating gold deposition (Cleverley et al., 2006). More detailed analysis of the possible geophysical signatures of this model are given by Chopping (2008). A comparison of these signatures with a known mineralised region is discussed by Chopping et al. (2008).

Creating physical property models from an RT model

A number of methods to calculate physical properties from mineralogy are in the published literature. We will discuss some of these methods for three key physical properties: density, magnetic susceptibility and seismic velocity. Further discussion and implementations of some of these methods are provided in Chopping (2008).

Density

Density, defined as the mass per unit volume of material, is the simplest physical property to calculate and thus is not discussed in the literature. Assuming the material does not contain any porosity then the calculated density is the bulk or material density (Emerson, 1990). For the purposes of using gravity surveys in the exploration of mineral deposits, the bulk density is the property required for calculating the gravity response.

Reactive transport models specify the mineralogy of the solid phases as the number of moles of each mineral per node. Defined in the chemical system specification of the model are the molar volume and molar mass for each mineral, which can be used to calculate the mass and volume of each mineral component of the mineralogy, for each node. The density of each node is simply specified by the total mass divided by the total volume of solid material at each node.

The gravity response depends also on the density contrast with respect to the entire crust. Most gravity maps are based on the Bouguer corrected gravity, which assumes a constant crustal density of 2670 kgm-3 (Telford et al., 1990). To produce a physical property model which would simulate the Bouguer response, the bulk density needs to be corrected to the Bouguer density:

Bouguer density contrast = bulk density – *2670* kgm^{-3}.

Magnetic susceptibility

Magnetic susceptibility is a dimensionless constant that relates the inducing magnetic field to the magnetic field produced by a magnetic material. Magnetic susceptibilities (generally denoted by the symbol k) are predominantly influenced by magnetite, ilmenite and/or pyrrhotite content, which are the three most ferromagnetic minerals. Some paramagnetic materials, such as quartz, have negligible to negative magnetic susceptibilities. For modelling magnetic response these are assumed to be particularly small, that is, $k_{quartz} \sim 10^{-7}$ to 10^{-9} in SI units (Telford et al., 1990).

The simplest method to calculate the magnetic susceptibility from mineralogy is to assume that it is a linear average, weighted by the volumetric proportion of the magnetic susceptibility of each mineral. This is an appropriate method for concentrations of magnetite up to ~ 20% by volume. Above this, the magnetic domains do not combine linearly (Shandley & Bacon, 1966; Fannin et al., 1990).

Other empirically derived formulae exist to calculate magnetic susceptibility based on magnetite content (e.g. Werner, 1945; Mooney & Bleifuss, 1953; Grant & West, 1965; Parasnis, 1973). These methods can be applied to the proportion of all magnetic minerals by using magnetite-equivalent volumes (Shandley & Bacon, 1966):

$$vol_{magnetite\ equivalent} = vol_{mineral} \times (k_{mineral}/k_{magnetite}).$$

This magnetite-equivalent volume may then be used in place of the magnetite volume in any method that is based on the volume proportion of magnetite.

Seismic Velocity

Similar to magnetic susceptibilities, the seismic velocity of an arbitrary mineralogy can be calculated using linear averaging, weighted by the volume of the minerals. Another method, generally named the time-averaged method (Wyllie et al., 1956), is to linearly average the slowness ($1/v$) of each of the minerals.

More elaborate schemes exist for calculating seismic velocity from mineralogy, such as Voigt-Reuss-Hill (in Berryman, 1995) or Hashin-Shtrikman (in Watt, 1988); these methods utilise the elastic moduli of the minerals. For minerals of mantle origin, the elastic moduli are well defined - they are required inputs to understand chemical compositions from regional and whole-earth seismic tomography results, but they are not well defined for crustal minerals. The linear and time-averaged methods produce similar results, with some subtle differences. Our preferred choice is to use the linear averaging of seismic velocities as it is slightly simpler than slowness-averaging to conceptualise.

Calculating the geophysical responses for the model

Calculating the gravity and magnetic response can be performed using the forward-modelling components

of the University of British Columbia, Geophysical Inversion Facility (UBC-GIF) potential field inversion codes *grav3d* (Li & Oldenburg, 1998) and *mag3d* (Li & Oldenburg, 1996). To calculate the gravity or magnetic response, the RT model must be sampled on a regular grid. A suitable interpolation method to best preserve the resolution and to limit the introduction of artefacts is the natural neighbour algorithm (Owen, 1992).

For 2D RT models, the regular grid must be extended into the third dimension to adequately calculate the gravity response. There may also be edge effects that result from mass changes off to the side; in this case, it is desirable to mirror the physical property model on either side.

The seismic response of the RT model is considerably more complex to forward-model than the gravity or magnetic responses. One simple method to image where reflections may arise from an arbitrary acoustic impedance model is to examine a vertical reflection profile. To calculate this, the reflection coefficient (Salisbury et al., 2000) of each cell is calculated for a cell, using the acoustic impedance of that cell and the cell immediately below it.

To interpret the vertical reflection coefficient model, reflection coefficients greater than 0.06, in general, will result in a very strong positive reflection, and a reflection coefficient smaller than -0.06 will result in a very strong negative reflection (assuming vertical incidence, Salisbury et al., 2000). More complex methods to calculate the seismic response of an RT model are beyond the scope of this abstract. A possible scheme could be that of Hobbs (2003).

An example: the gravity response of an RT model

For this example, we used the listric fault model of Cleverley et al. (2006), created physical property distributions, and then calculated the density response for a gold deposit presently sitting at the base of 100 m of constant low-density (2000 kgm^{-3}) material, to simulate the regolith. The initial RT model was used to simulate an unaltered architecture, and the RT model after chemical alteration and fluid transport was used to simulate an architecture after alteration (Figure 1). This model also has been compared to the known gravity response over a mineralised region (Chopping et al., 2008).

The general pattern of the gravity response over this model is that alteration has increased the density laterally away from the site of gold deposition, and has reduced the gravity response directly above the zone of gold deposition. This decrease of gravity response above the site of gold deposition is approximately 8% of the unaltered response for the same region, which has the potential to be detected in a gravity survey, for station spacings approximately 1 km apart (Figure 2).

Conclusions

The prediction of geophysical responses for geochemical simulations provides a new tool for mineral exploration, especially in undercover regions. The calculations are likely to be fast enough to be implemented directly in the RT modelling code, although currently they are utilised by calculating on completed RT model time steps. By using these methods on a simple reactive transport model, there is the potential to identify targets using geophysical models. Such targets compare favourably with known mineralisation at the Victory-Defiance region of the St Ives Gold Mine (Chopping et al., 2008).

Acknowledgements

The work contained in this abstract reflects a distillation of ideas from Project A3 with some chemical modelling from Project M9. Project A3 would not have been possible without strong industry support from the *pmd*CRC* sponsors. Three sponsors in particular strongly supported the project, namely AngloGold Ashanti, Barrick Gold and Gold Fields International. N. Kositcin, R.J. Korsch, A.C. Barnicoat and T. Meixner provided constructive reviews.

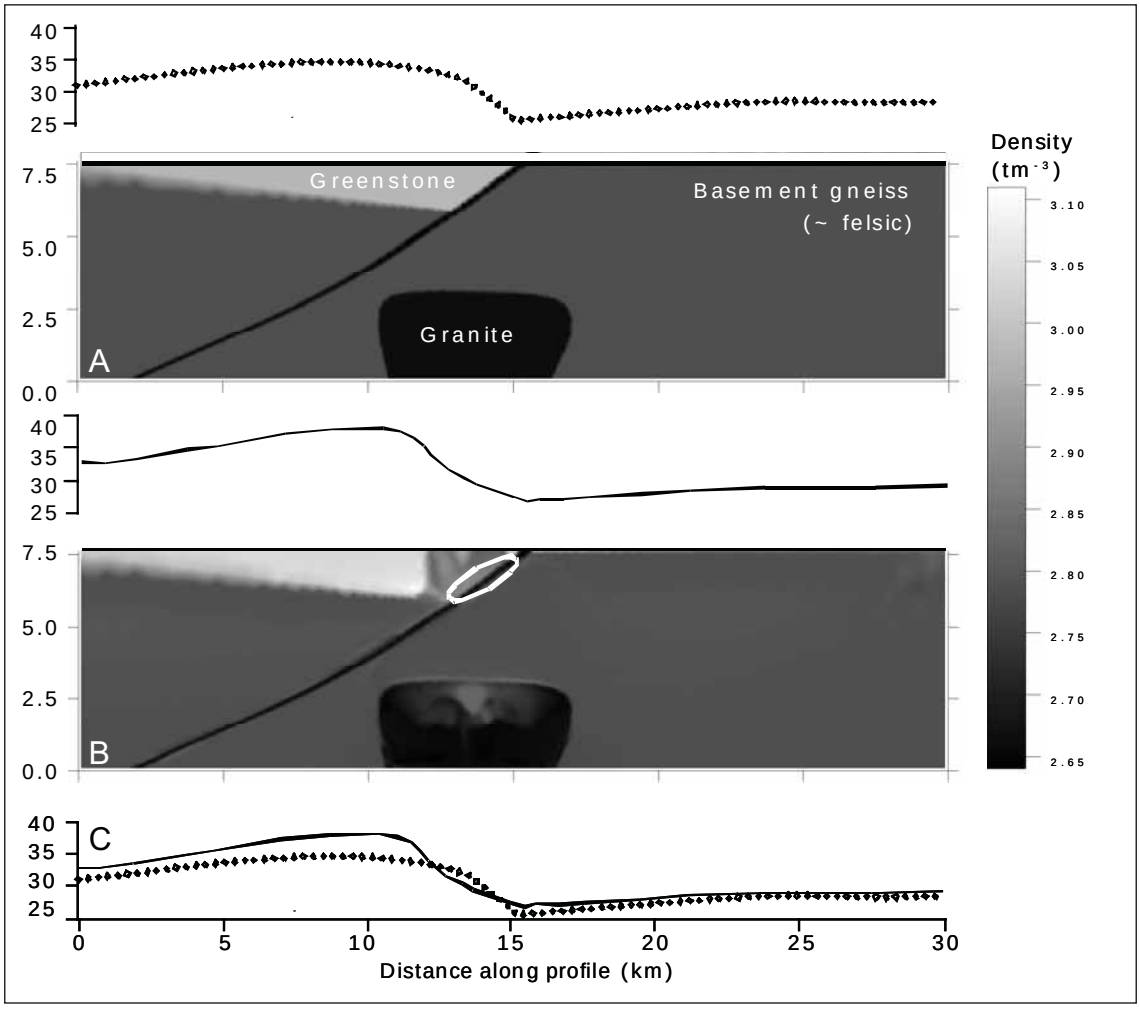

Figure 1. Physical property models, after simulation of erosion and regolith formation, of an unaltered (A) and altered (B) gold mineral system. The profile above each density model is the corresponding gravity response for that model. In general, alteration has increased the density of the greenstone package in the hangingwall of the fault. The density has also been increased, although by a smaller amount, in the footwall basement gneiss. The density has been decreased from the unaltered density in the vicinity of the gold deposit (oval); this includes alteration associated with the 'chimney' directly above the gold deposit. This decrease in density is caused by an increase in carbonate, quartz and some feldspar in this outflow zone. Correspondingly, there are increases in the gravity response, with respect to the unaltered gravity response, on either side of the deposit, and a decrease in gravity response directly above the position of the gold deposit. These differences are apparent when the two gravity profiles are plotted on the same graph (C).

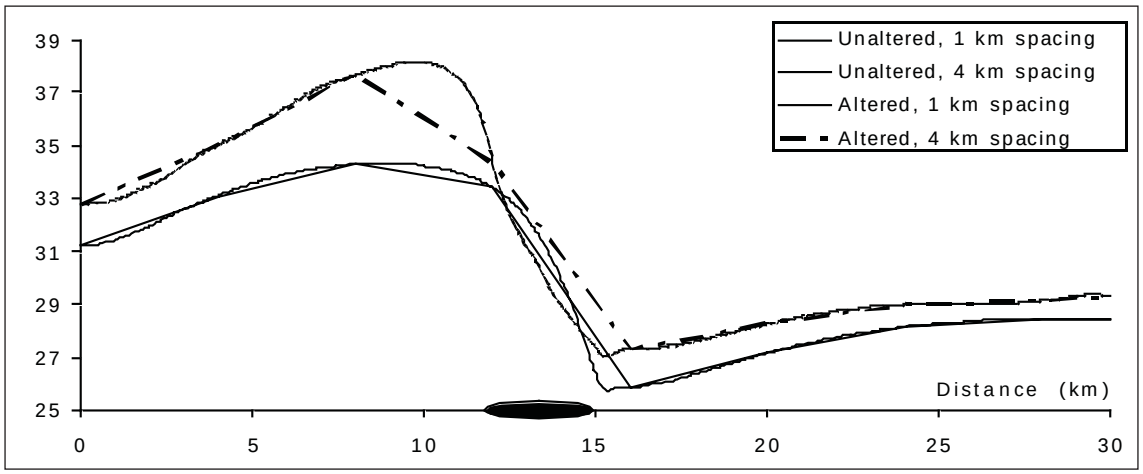

Figure 2. Gravity profiles over the Listric Fault Model (Cleverley et al., 2006), for both the altered and unaltered scenarios (Figure 1), at two different station spacings. The prediction of geophysical responses of reactive transport models allow the testing of different survey designs, verifying the minimum data spacing required to reliably interpret alteration features. Clearly this figure indicates that the subtle decrease in gravity response directly over the deposit location (filled oval) is only apparent using 1 km or better gravity station spacings. 4 km spaced gravity, it must be noted, is certainly sufficient for defining the gross architecture of this system.

References

Berryman, J.G., 1995. Mixture theories for rock properties. In: Ahrens, T.J., ed., Rock physics and phase relations: A handbook of physical constants. American Geophysical Union, 205-238.

Chopping, R., 2008. Geophysical signatures of alteration. ***pmd*****CRC* Project A3 Final Report. Predictive Mineral Discovery Cooperative Research Centre (pmd*CRC), Melbourne, 135pp.

Chopping, R., Cleverley, J.S., Henson, P.A. & Roy, I.G., 2008. Reactive transport models: from geochemistry to geophysics to targets. In: Blewett, R.S., ed., Concepts to targets: a scale-integrated mineral systems study of the Eastern Yilgarn Craton. ***pmd*****CRC* Project Y4 Final Report. Predictive Mineral Discovery Cooperative Research Centre (***pmd*****CRC*), Melbourne.

Cleverley, J.S., Hornby, P., & Poulet, T. 2006. Pmd*RT: Combined fluid, heat and chemical modelling and its application to Yilgarn geology. In: Barnicoat, A.C. & Korsch, R.J., eds., Predictive Mineral Discovery Cooperative Research Centre – Extended Abstracts from the April 2006 Conference. Geoscience Australia, Record. 2006/07, 23-29.

Emerson, D.W., 1990. Notes on mass properties of rocks – density, porosity, permeability. Exploration Geophysics, 21(3&4), 209-216.

Fannin, P.C., Scaife, B.K.P. & Charles, S.W., 1990. An experimental study of the magnetic susceptibility of colloidal suspensions of magnetite as a function of particle volume fraction. Journal of Physics, D: Applied Physics, 23(12), 1711-1714.

Grant, F.S. & West, G.F., 1965. Interpretation theory in applied geophysics. McGraw-Hill, New York, 583pp.

Guéguen, Y. & Palciauskas, V., 1994. Introduction to the physics of rocks. Princeton University Press, 294pp.

Hobbs, R.W., 2003. 3D modelling of seismic wave propagation using complex elastic screens with application to mineral exploration. In: Eaton, D.W., Milkereit, B. & Salisbury, M.H., eds, Hardrock Seismic Exploration. Society of Exploration Geophysicists, Tulsa, Oklahoma. 270pp.

Hornby, P. & Poulet, T., 2008. Reactive transport. In: ***pmd****CRC* Enabling Technologies Final Report. Predictive Mineral Discovery Cooperative Research Centre (pmd*CRC), Melbourne.

Li, Y. & Oldenburg, D.W., 1996. 3D inversion of magnetic data. Geophysics, 61(2), 394-408.

Li, Y & Oldenburg, D.W., 1998. 3D inversion of gravity data. Geophysics, 63(1), 109-119.

Mooney, H.M. & Bleifuss, R., 1953. Magnetic susceptibility measurements in Minnesota part II: Analysis of field results. Geophysics, 18(2), 383-393.

Owen, S.J., 1992. An implementation of natural neighbour Interpolation in three dimensions. MSc thesis, Brigham Young University, 118 pp. (unplublished) .

Parasnis, D.S., 1973. Mining geophysics, revised edition. Elsevier, Amsterdam, 395pp.

Salisbury, M.H., Milkereit, B., Ascough, G., Adair, R., Matthews, L., Schmitt, D.R., Mwenifumbo, J., Eaton, D.W. & Wu, J., 2000. Physical properties and seismic imaging of massive sulfides. Geophysics, 65(6), 1882-1889.

Shandley, P.D. & Bacon, L.O., 1966. Analysis for magnetite utilising magnetic susceptibility. Geophysics, 31(2), 398-409.

Telford, W.M., Geldart, L.P. & Sheriff, R.E., 1990. Applied geophysics (second edition). Cambridge University Press, Cambridge, 790pp.

Watt, J. P., 1988. Elastic properties of polycrystalline minerals: comparison of theory and experiment. Physics and Chemistry of Minerals, 15(6), 579-587.

Werner, S., 1945. Determinations of the magnetic susceptibilities of ores and rocks from Swedish iron ore deposits. Swedish Geological Survey, Series C472, #39, 79pp.

Wyllie, M.R.J, Gregory, A.R. & Gardner, L.W., 1956. Elastic wave velocities in heterogeneous and porous media. Geophysics 21(1), 41-70.

Deposition: Reactive transport modelling

JAMES S. CLEVERLEY

*pmd***CRC*, CSIRO Exploration & Mining, PO Box 1130, Bentley, WA 6102
James.Cleverley@csiro.au

Introduction

Reactive Transport (RT) Modelling is the technique of the coupled simulation of fluid-flow, heat and mass transport, and chemical reaction. This type of simulation can be used to understand the systems with coupling between many physical processes. In particular, the coupling and feedback between heat and mass advection, chemical reaction and porosity-permeability evolution is especially important at sites of active mineral deposition. While reactive transport modelling is commonly applied to environmental and contaminant/waste problems (i.e. nuclear repository, contaminant plume etc), it has received only limited, application in hydrothermal mineral system studies.

This work describes the reactive transport code being developed within CSIRO as part of the Predictive Mineral Discovery Cooperative Research Centre. Using a simple case, study this work demonstrates the potential application of this type of modelling and the implications for predictive exploration.

Software

The ***pmd*****CRC* RT modelling code is based around two Python modules, pmdPyRT and pmdPyGC, and a commercial chemical solver (WinGibbs) derived from the HCh modelling program (Shvarov & Bastrakov, 1999). Currently the RT code is run through a single graphical user interface for numerical modelling, the Desktop Modelling Toolkit (DMT). Technical descriptions of these codes, and the mathematics behind them are described in detail in the Enabling Technology Final Report (***pmd*****CRC* Projects M9 and F6, in press). The code and its application has been discussed previously (Cleverley and Bastrakov, 2005; Cleverley et al., 2006; Cleverley, 2007). The generalised workflow for reactive transport modelling includes:

a) Definition of a geometry and creation of a mesh.
b) Definition of a PDC (Problem Description, Conceptual) file based on the mesh and geometry, containing the inputs necessary to run the conceptual model.
c) Run fluid-flow, heat and transport models.
d) Run reactive transport models.
e) Analyse results using post-processing functions either in DMT or 3rd party software.

Concept Model

The concept model described in this work is based on a simplified granite-cover geometry that is an approximation of some Archaean lode gold systems. However this geometry could be used in a number of geological scenarios. The geometry is illustrated in Figure 1, along with the mesh used for the modelling. This scenario explores the interaction of magmatic-derived fluid from a cooling granite and its impact on a felsic volcanic-mafic rock stratigraphy. The whole model is 30 km wide and 15 km deep and contains ~15000 mesh elements.

In broad terms the concept model considers a reduced H_2S-bearing brine with gold released from the granite that interacts with the felsic volcanic and then mafic rock sequence.

General Physical Properties

The top of the model is fixed at 5 MPa and 40°C (corresponding to ~500 m depth) and the initial P-T conditions are based on hydrostatic pressures and 30°C_km geothermal gradient.The base of the model is constrained with a fixed heat flux (~85 mW_m2) (see Figure 1b).

The granite is initialised at 600°C (T_0) and is allowed to cool via heat advection and conduction. Heat flux at the base of the granite is elevated (100 mW_m2) beneath the granite for the first 0.15 m.y. model time, after which the value is the same as the rest of the base of the model.

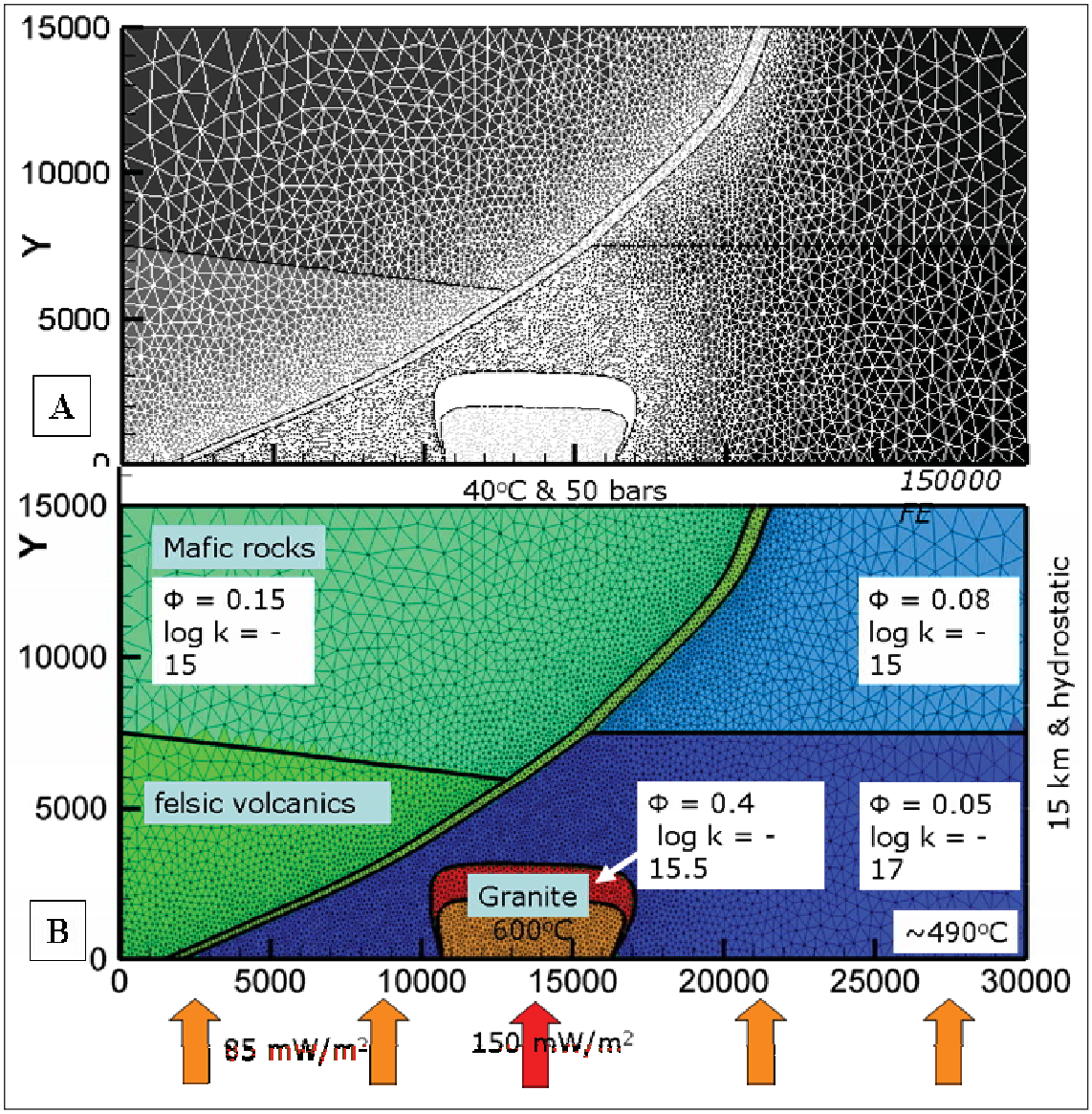

Figure 1. A. Geometry and mesh (v1) used in modelling of the listric fault – granite model described in this paper. Geological domains are coloured and the unstructured, triangular mesh is also illustrated. B. Physical properties of the rock units and boundary conditions for the initial modelling.

The initial porosity-permeability structure of the model is initialised at $0.15/10^{-15}$ m^{-2} in mafic units, $0.05/10^{-17}$ m^{-2} in the felsic basement, and $0.4/10^{-15.5}$ m^{-2} in the granite. The porosity is dynamic, calculated at each time step as a function of the liquid volume of the nodes and changes are a consequence of the precipitation or dissolution and transport of material. Permeability is calculated as a function of porosity using the Carman-Kozeny relationship, $\kappa = \kappa_0(\phi/\phi_0)^3$.

Chemistry

Initial solid and aqueous chemistries were defined for each of the model units, and the mineralogy broadly consists of:

- Mafic unit: albite-quartz-calcite-tremolite-chlorite-pyrrhotite-graphite;
- Felsic volcanics: quartz-albite-muscovite-k-feldspar-pyrite; and
- Granite: quartz-albite/anorthite-k-feldspar-biotite-magnetite with H_2S in the fluid.

The fluid phase is populated initially with a mixed brine (Na, K, Ca, Fe) at ratios close to equilibrium for that rock, $H_2S \pm SO_4$, Au^+ ($1e^{-9}$ and $1e^{-5}$ molal for background & granite respectively), and CO_2. The $\Sigma C_{(aq)}$ is minor in the mafic rocks (CH_4), dominant in the felsic volcanics (CO_2) and absent in the granite. The initial chemical step (calculated with no transport) calculates the fluid composition in full equilibrium with the rock at the fluid/rock defined by the specified porosity of that unit. As each bulk chemical composition is occurs across a range of temperatures and pressures, the equilibrium phase assemblage and fluid composition will also vary within the model units.

Evolution in Space

The model discussed in this section, with chemistry switched on, was run to 1.148 m.y., by which time the granite had cooled. Although the mesh was relatively coarse (although fine in areas of importance such as above the granite), with chemistry the model takes 5-6 days to complete. Currently there is no provision to parallelise or run the chemistry on supercomputing grids, due to limitations that include the use of a Windows-based, third party chemical solver. Future developments will seek to improvements to this situation.

Thermal-Flow Evolution

Figure 2 illustrates a composite of the thermal and flow fields after 0.15 m.y. (active gold deposition) showing the a) magmatic tracer and flow vectors and, b) the temperature field. The most striking feature of this model is the large-scale thermal and mass plume above the granite, even when the granite has cooled significantly (+100°C background at 0.15 m.y.). This upwelling causes the localisation of convection in the overlying basin, although convection is likely a consequence of the overall thermal gradient in the model and not just the interaction with the cooling granite. Localisation is also a function of the chemical-reaction influenced porosity/permeability changes discussed below.

Thermal modelling without the chemistry is relatively quick, models taking a few hours to completion, and as such tests can made using a range of parameters in the initial model setup. The DMT (Desktop Modelling Toolkit) can be used to submit multiple models to supercomputing facilities (such as iVEC, Perth) in order to quickly model large range of parameters. An extension of this work, with a finer mesh resolution, has been used to explore the influence of thermal gradient (10-40°C_km) with the presence of granite at different temperatures (650-800°C, and no granite) on the mass transport and flow evolution of this simple geometrical configuration.

Gold

Figure 3 shows the final distribution of gold in the model after ~1.2 m.y. There are two distinct places

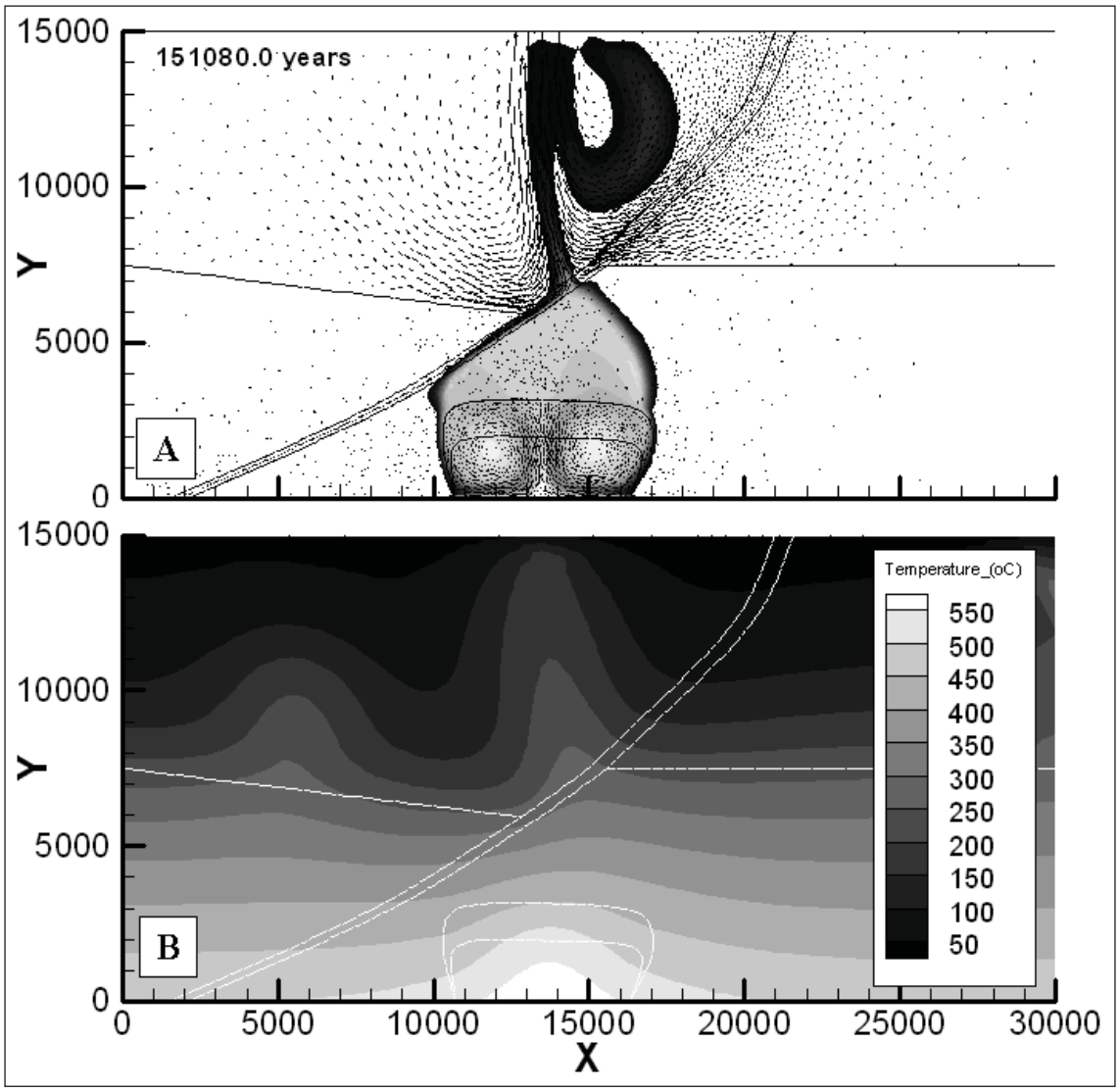

Figure 2. Thermal and flow results illustrated for 0.15 m.y. showing (A) the tracer from granite and flow vectors, and (B) the temperature field (°C).

that gold occurs (>0.01 g/t) in the model: 1) in the granite carapace and, 2) in the mafic rocks in a plume above the granite.

Gold occurring within the granite carapace in this model is a function of two effects. The permeability in the overlying rocks is low (10^{-16} m^{-2}), and this prohibits much total flux of gold-bearing fluid. There is also a large temperature gradient away from the granite (temperatures decrease from 600°C to 450°C), which will impact on the solubility of the gold-bearing fluid. The permeability of the host rocks is set at a uniform, mid-low value in this model, although it is likely that around granite carapaces the permeability of the host rocks will be enhanced by fracturing and granite emplacement deformation. A larger permeability would allow for a greater flux of total Au away from the granite, as well as permitting the temperature gradient to become more uniform (something noticed in granite-related fluid flow modelling of Dreisner & Geiger, 2007).

Gold occurring within the mafic rocks is a consequence of the interaction of reduced, $Au(HS)_2^-$ bearing, granite-derived fluid with the Fe-bearing mafic rocks. The shape of the gold distribution is complicated

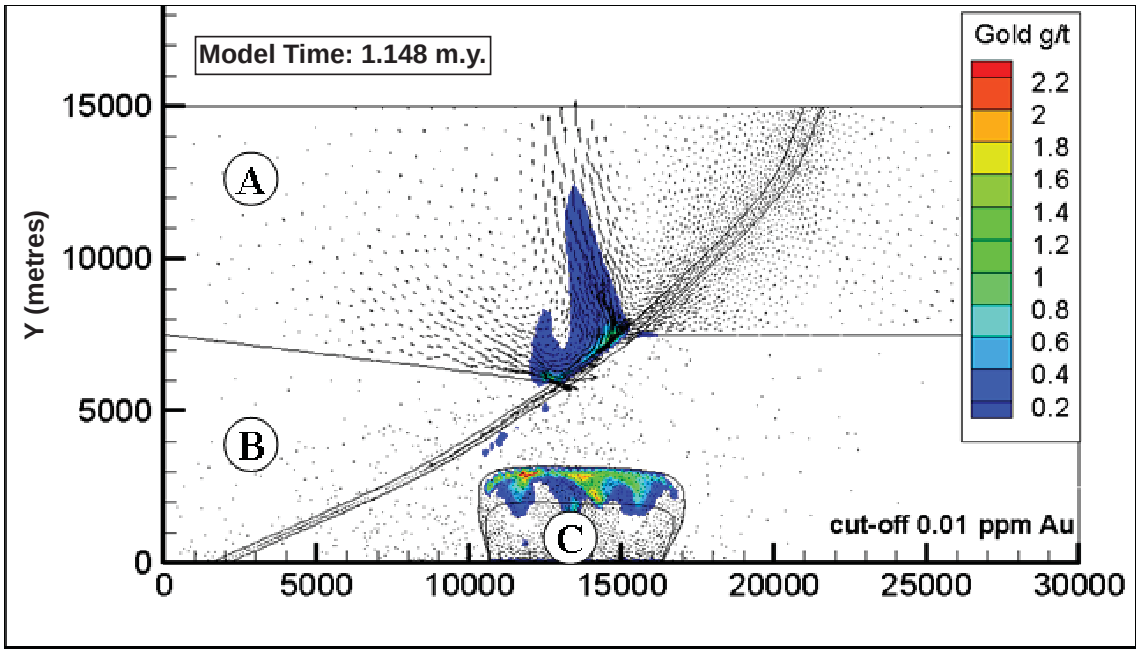

Figure 3. Distribution of gold (g/t, colours) after 1.14 m.y. overlain with fluid-flow vectors (black arrows).

and shows two prongs, not a single pathway as might be expected. There is also a large, low grade halo of gold above the zone. The highest Au grades occur at the interface between the felsic volcanics, fault and mafic rocks where grades reach 1.2 g/t. While this may not seem like very high, it must be remembered that this is a 2D model, and reality the focusing of fluids from the 3D into a single uplflow domain (i.e. there would be a greater total Au flux) in 3D. In addition, this result may indicate that the process of fluid-rock interaction is not sufficient on its own to create high-grade gold deposits.

Large-scale Alteration Patterns

Figure 4 shows the distribution of a) calcite and b) the approximate X_{Mg} of chlorite after 0.189 m.y. (in other words at the peak gold deposition time). These spatial plots of mineral assemblages show the extent to which the magmatic-derived fluid has impacted on the mineralogy throughout the 10 km section. The carbonate "chimney" is a function of CO_2 derived from the underlying felsic unit reacting with the mafic sequence. The gold is precipitated at the interface of this reaction zone. A zone of Mg-chlorite is formed above the granite, while the chlorite chemistry changes from Mg- to Fe-rich upwards away from the felsic-mafic interface. The structure of the "alteration chimney" above the gold zone is mirrored by the route of upward migration of tracer (as a proxy for magmatic fluid, see Figure 5).

Evolution in Time

Magmatic Upwelling

The position of the tracer away from the granite is not a single, static upwelling, but evolves in space through time. Figure 5 shows two time snapshots of the magmatic tracer at the interface between the felsic and mafic rock units (along with the fault). In this example, the locus of magmatic upwelling has migrated laterally ~3 km between 0.189 m.y. and 0.784 m.y. This is a function of the coupling between convective flow in the upper geological units effectively "pushing" the plume around and changes in the permeability of the host rock due to feedback from the chemical reactions (i.e. addition of carbonate). Figure 6 shows the permeability distribution in this area at 0.784 m.y. showing the change of an order of magnitude ($10^{-15.5}$ to $10^{-14.5}$ m^{-2}) caused by precipitation and dissolution reactions.

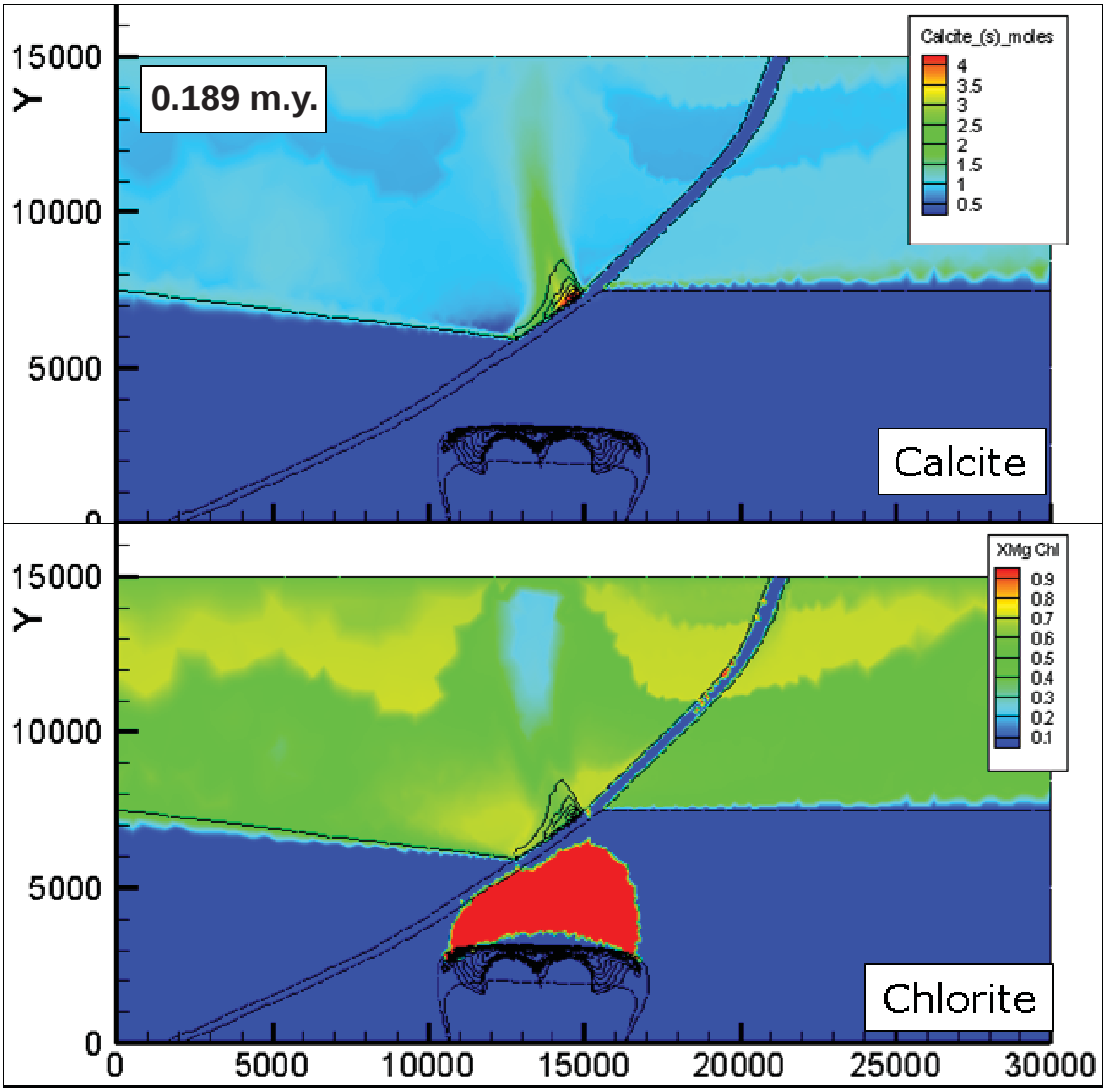

Figure 4. A. Distribution of calcite after 0.189 m.y., notice the steep carbonate plume in the mafic rocks above the granite. B. The calculated chlorite chemistry (X_{Mg}) in the model.

Simulated Paragenesis

Figure 6a shows a white dot where the magmatic fluid intersects the mafic rock units. This point has been used to generate a history of minerals through time and this is presented as a stacked plot (showing mineral volumes) in Figure 7. The initial assemblage consisting of quartz-epidote-chlorite-albite with minor carbonate-tremolite evolves with tremolite disappearing, quartz, chlorite and carbonate increasing and, muscovite replacing epidote during the phase of active gold deposition (see black line on Figure 7). This paragenesis is testable against real examples. In later stages of the calculated paragenetic history, the quartz and carbonate continue to increase, albite disappears and muscovite is reconverted to epidote.

Figure 5. (following page) Evolution of the tracer (proxy for magmatic fluid) at the interface between mafic-felsic units and the fault at (A) 0.189 m.y, and (B) 0.784 m.y. The precipitated gold at the time is illustrated as the black contours and shows that the final gold distribution is a function of the integrated passage of tracer through time.

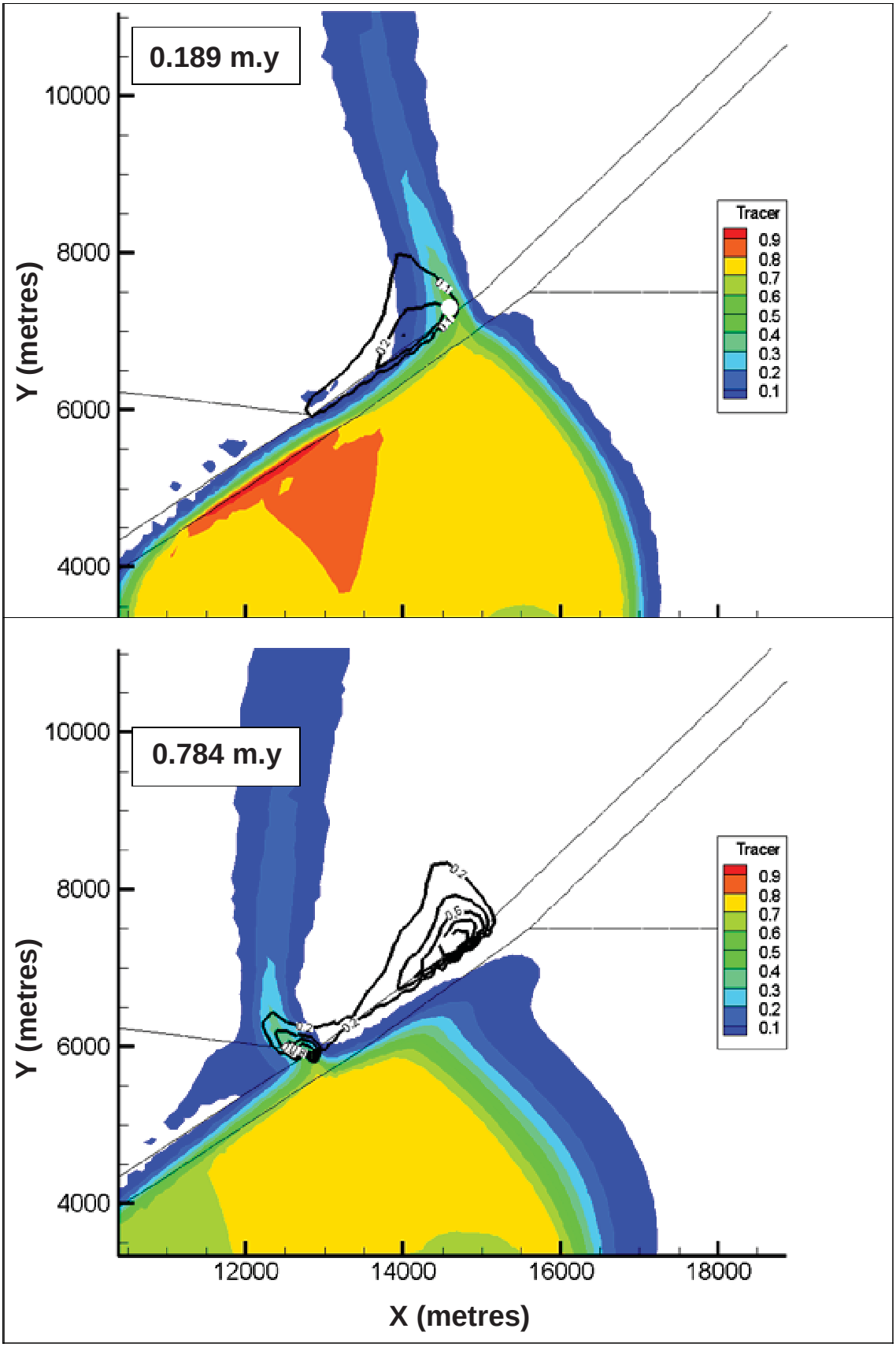

Figure 5 (caption on previous page

Graphite also starts to dominate in the later stages as the reduced mafic-derived fluids interact with the oxidised CO_2-bearing deeper fluids. This has implications for the modelling or consideration of isotopic signals of these processes (i.e. mixed carbon sources at different redox states).

The gold is actively precipitated over the period 0.71–0.51 m.y. in this location. The precipitation of gold at other locations would have occurred at different times but all within 1 m.y. While these time differences would be difficult to resolve within Archaean gold deposits, this may impact on our understanding of recent systems (younger than 50 Ma), where geochronology has a better resolution.

Conclusions

The pmdPyRT code can be used to develop and run combinations of thermal-flow-transport and chemical reaction models (reactive transport couples all of these processes). The code is run using the DMT interface and by the end of the ***pmd***CRC* at least the thermal-transport models can be run using the supercomputing facilities available on the grid.

The model discussed here explores the simple relationship between granite derived, Au-H_2S-bearing

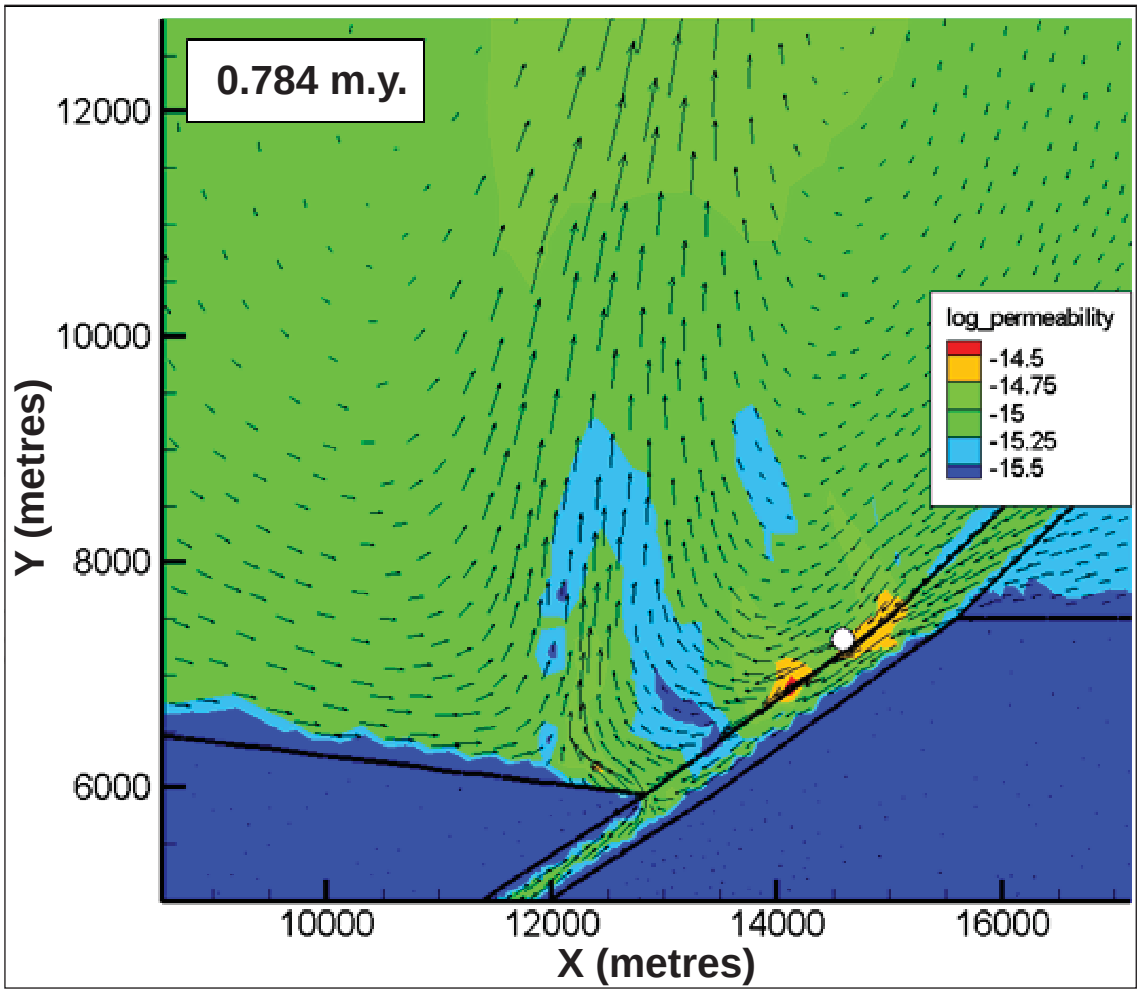

Figure 6. Permeability values and flow arrows for the critical interface region at 0.784 m.y., showing that the mafic units with initial permeability of 10^{-15} m^2 has evolved through chemical reaction to a range between 10^{-14} and 10^{-15} m^2. The influence of upwelling zones on the permeability can be seen with comparison to Figure 2. The white dot is the history point (Figure 7).

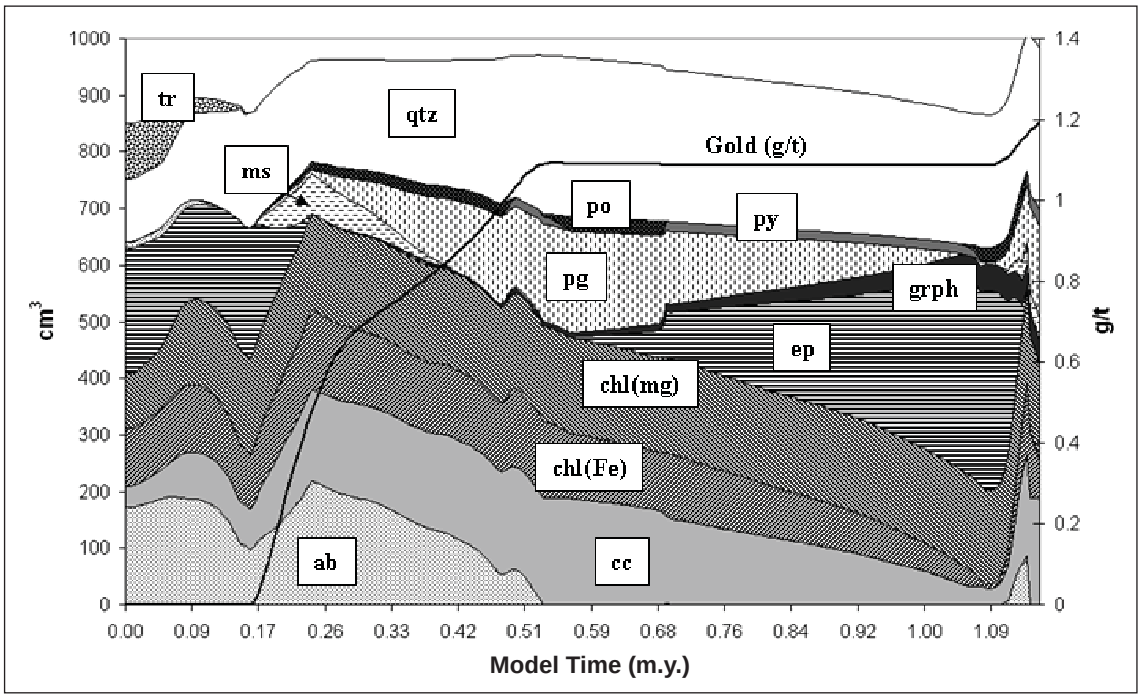

Figure 7. Evolution of mineral abundance (volume) over time for the history point illustrated in Figure 6. The gold concentration is given as a black line. This is a stacked plot so that variation in totals equates to variation in the bulk solid volume (1/porosity) value.

fluid as it interacts with a felsic basement and mafic composition upper sequence. The geometry and chemistry of the units is loosely applicable to many Yilgarn-type scenarios. In this model the granite causes focused upflow of mass and heat, but there is little influence on this upwelling plume by the fault. During the passage of the fluid through the felsic basement the fluid maintains the reduced, Au-bearing capacity, while interaction with the mafic sequence causes processes of reduction-oxidation (by fluid-rock and fluid-fluid interaction) to precipitate gold and associated assemblages including muscovite-carbonate. Carbonate maps out the upwelling plume and has been used in other work to model the gravity lows around some Yilgarn gold systems (see Chopping, this volume).

References

Cleverley, J.S., 2007. Large scale finite element reactive transport modelling as a tool to aid understanding and prediction in mineral systems. In: In: Andrew, C.J. et al., eds, Digging Deeper. Proceedings of the Ninth Biennial Meeting of the Society for Geology Applied to Mineral Deposits, Irish Association for Economic Geology, vol. 2, 1439-1442.

Cleverley, J.S. & Bastrakov, E.N., 2005. K2GWB: Utility for generating thermodynamic data files for The Geochemist's Workbench (R) at 0-1000 degrees C and 1-5000 bar from UT2K and the UNITHERM database. Computers and Geosciences, 31,756-767.

Cleverley, J.S., Hornby, P. & Poulet, T., 2006. Reactive transport modelling in hydrothermal systems using the Gibbs minimisation approach. Geochimica et Cosmochimica Acta, 70(18), Supplement 1, p.A106.

Driesner, T. & Geiger, S., 2007. Numerical simulation of multiphase fluid flow in hydrothermal systems. Reviews in Mineralogy and Geochemistry, 65, 187-212.

Shvarov, Y.V. & Bastrakov, E.N., 1999. HCh: a software package for geochemical equilibrium modelling. User's Guide. Australian Geological Survey Organisation, Record, 1999/25, 60pp.

Deposition: Modelling uranium deposition

L. FISHER[1], F. ELMER[1,2], J. CLEVERLEY[1], P. SCHAUBS[1] AND W. POTMA[1]

[1]*pmd**CRC*, CSIRO Exploration and Mining, PO BOX 1130, Bentley, WA 6102
[2]current address: Woodside Petroleum
Louise.Fisher@csiro.au

Introduction

Geochemical and reactive transport modelling of metal transport and deposition within uranium systems allows reverse engineering of ore formation and provides insights into the conditions required to form the observed deposits. Subsequent forward modelling can be used to predict the spatial distribution of associated alteration assemblages from which vectors for exploration can be developed. Two case studies are presented demonstrating this capability: the unconformity-related systems of the Alligator Rivers Uranium Field in the Northern Territory and the palaeochannel-hosted deposits of the Frome Embayment in South Australia.

Geochemical Modelling

HCh

Geochemical modelling of the formation of hydrothermal ore deposits and associated alteration can be used to enhance prediction of new ore deposits and develop vectors for exploration. The HCh software (Shvarov & Bastrakov, 1999; Shvarov, 1999) is a geochemical modelling code capable of describing local equilibrium dynamic models (Shvarov, 1999). Models can be run over a wide range of PT conditions; from 0 to 1000°C and 1 to 5000 bars making the software useful for simulating fluid–rock reaction processes at both surficial conditions and elevated pressures and temperatures (Cleverley & Oliver, 2005).

Reactive transport modelling

Reactive transport (RT) modelling represents the coupling between fluid flow, heat transport, solute transport and chemical reactions. This study uses pmdPyRT, the RT code developed by the ***pmd***CRC* (P. Hornby, pers. comm.; Cleverley et al., 2006; Cleverley, this volume), which consists of a Gibbs minimisation solver for calculating equilibrium chemistry (WinGibbs; Y. Shvarov, pers. comm.) coupled with a partial differential equation solver (Fastflo4; Gross, 2002). The RT code solves the equations of fluid flow, heat and mass transport, and equilibrium chemistry in a fluid-saturated porous medium, on a 2D or 3D finite element mesh. The fluid is a single phase and is assumed to be incompressible. Unstructured triangular and tetrahedral meshes enable realistic representation of geological features with arbitrary shapes, such as intrusions or wedges of sedimentary rocks. This is an advantage over other RT codes, such as Shemat (Clauser, 2003), for which the mesh must be structured and orthogonal. Each element or cell within the mesh holds information about the temperature, fluid pressure, composition and properties of the rock and fluid at that point. The initial chemistry is defined in terms of the volume fraction of minerals and moles or molality of chemical species in the fluid phase (Hornby & Poulet, 2008).

RT modelling allows predictions to be made on the distribution patterns of alteration and mineralisation.

Computation times are much faster than laboratory experiments and nature; hence it is possible to test multiple hypotheses for the formation of ore deposits, such as different sources of metals, the importance of faults in these systems, the fluid flow paths, etc. (for further discussion see Cleverley, this volume).

Modelling uranium deposition

Australia is the second largest producer of uranium in the world, with 19% of its resources coming from unconformity-related deposits and 4.4% from roll front/palaeochannel type deposits (Lambert et al., 2005). The Alligator Rivers Uranium Field in the Northern Territory hosts the majority of Australia's unconformity-related uranium deposits, including the Ranger, Nabarlek, Jabiluka and Koongarra deposits. Well known Australian examples of roll front-palaeochannel deposits include Beverley and Honeymoon in the Frome Embayment field, South Australia.

Unconformity-related uranium in the Alligator Rivers Uranium Field

The Alligator Rivers Uranium Field (ARUF) is part of the Proterozoic Pine Creek Orogen. All known uranium deposits are located in the basement, hosted by the Cahill Formation schists and Myra Fall Metamorphics (Lally & Bajwah, 2006). The metamorphosed basement consists of carbonate, calc-silicate, greywacke, carbonaceous schist, quartz ± feldspar ± mica schist, quartzite and amphibolite, with depositional ages of ≥1860 Ma, and is unconformably overlain by the Katherine River Group, a succession of sandstone, conglomerates and mafic volcanics. Unlike the Athabasca region of Canada, to which the ARUF is often compared, no economic mineralisation has been found above the unconformity.

Geochemical modelling of unconformity-related uranium deposits in the ARUF provides insight into ore genesis and places constraints on the conditions required to form these basement-hosted deposits. HCh and RT simulations were used to test a genetic model in which saline, oxidised, U-bearing basinal fluids sourced from the overlying sandstone sequence penetrate the basement through faults or zones of brecciation, where they are reduced by reaction with basement rocks (chlorite-graphite) resulting in deposition of uraninite.

Fluid infiltration models using HCh (Shvarov & Bastrakov, 1999) predict that as the oxidising ore fluid infiltrates the basement lithologies, uraninite will be deposited at the redox front within the basement. As infiltration continues the buffering capacity of the host rock is consumed and the redox front migrates downwards. With increasing oxidation of the basement units, uraninite is progressively stripped from the rocks and redeposited at the new redox front. The HCh models also predict the formation of chlorite alteration zones adjacent to mineralisation, which correlates with observed alteration at the deposits (Wilde & Wall, 1987; Polito et al., 2004).

The RT model represents a vertical section, 2 km by 2 km. A faulted basement is unconformably overlain by two sandstone units, which are given different chemical compositions. The fluid pressure and temperature conditions were defined to represent the unconformity at 5 km depth. Porosity and permeability were defined so that sandstone ≥ fault > basement. The chemical compositions of the host rocks and fluids were based on those used for HCh modelling.

Initial RT modelling tested a two stage scenario with 50,000 years of pre-ore fluid flow followed by 150,000 years of syn-ore fluid flow. The modelled fluid flow path passed from an evaporitic environment, through uraninite bearing sandstone and into a quartz mica schist basement. The results predict alteration of the basement with destruction of K-feldspar and formation of amphibole and chlorite alteration zones. As the model progresses deposition of uraninite along the unconformity is observed (Figure 1A). However, in this model, transport of uranium into the basement is limited even though a tracer shows that fluid is transported into the fault. Modelling the basement with a hematite bearing palaeo-regolith zone immediately below the unconformity did produce a small increase in the volume of uraninite deposited within the basement fault zones (Figure 1B). Increasing the permeability of the fault zone so

that it is equal to that of the overlying sandstone greatly increased predicted deposition of uranium within the basement (Figure 1C).

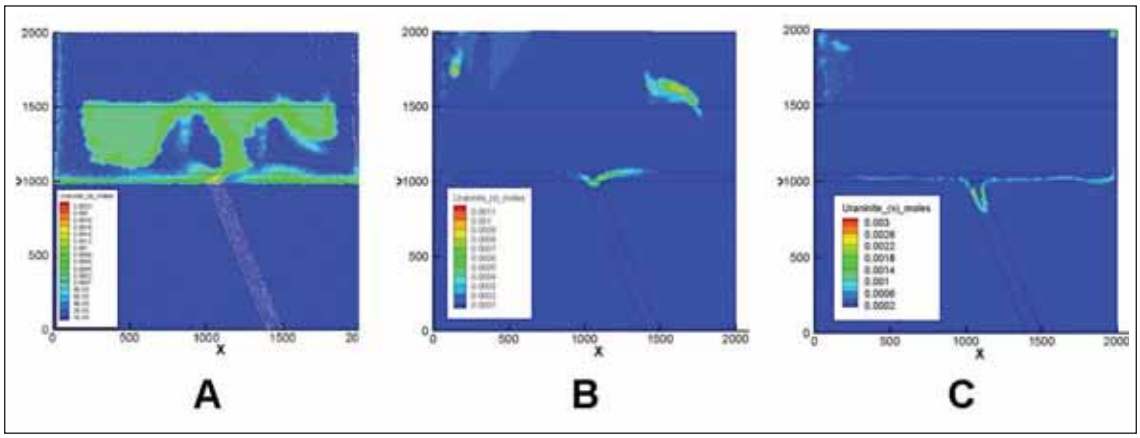

Figure 1: RT model outputs: A. after 150,000 years all mineralisation is localised along and above the unconformity; B. with basement modelled as 'pre-oxidised' and uranium in ore fluid, mineralisation is focused around the fault zone but no significant basement mineralisation is predicted; C. when the modelled permeability of the fault zone is increased to equal that of the sandstone units mineralisation of the basement is predicted.

Palaeochannel-hosted Uranium in South Australia

Geochemical and RT numerical modelling of palaeochannel-hosted uranium mineralisation was undertaken using HCh and PmdPyRT. The aim of the study was to produce numerical models to aid in the understanding of how palaeochannel-hosted 'roll-front' uranium deposits form.

A generic palaeochannel model was run simulating fluid flow from a topographic high, consisting of a uranium-rich granite, to a topographic low, within a palaeochannel which comprised reduced clays, oxidised sand and gravel layers. Modelling showed that oxidised fluid strips uranium from the granite and transports it along the palaeochannel. At reduced environments within the palaeochannel uranium is deposited as uraninite. The resulting deposition and associated alteration assemblages within the model reproduce what is observed within roll front deposits, showing how RT modelling can result in improved genetic concepts and lead to more predictive mineral exploration.

To refine this model and test various hypotheses on the formation of sandstone/palaeochannel-hosted uranium deposits, a mesh based on a schematic long-section representation of the Beverley deposit, within the Frome Embayment, was created to test different genetic hypotheses. It has been proposed that the source of uranium for sandstone/palaeochannel hosted deposits is granitic and/or felsic volcanic rocks with elevated uranium concentrations, and it has been observed that all known uranium deposits in Australia exhibit spatial relationships with uranium-enriched bedrocks (Lambert et al., 2005). In this model a tracer was placed in the granite region as a proxy for uranium, and the movement of the tracer over time shows the pathway of a fluid across the mesh. Figure 2 shows the tracer concentrations at 0 and 68,000 years.

After 68,000 years the tracer is spread out across the basement, and is mostly concentrated within the Eyre Formation. Although there are high fluid flow rates across the Namba Formation, fluid that passes through the granite region does not pass through the Namba Formation, which is host to the Beverley deposit. Assuming that the model geometry and permeability distribution is correct, this suggests that the in situ granite is unlikely to be the primary source of any uranium deposit within the Namba Formation.

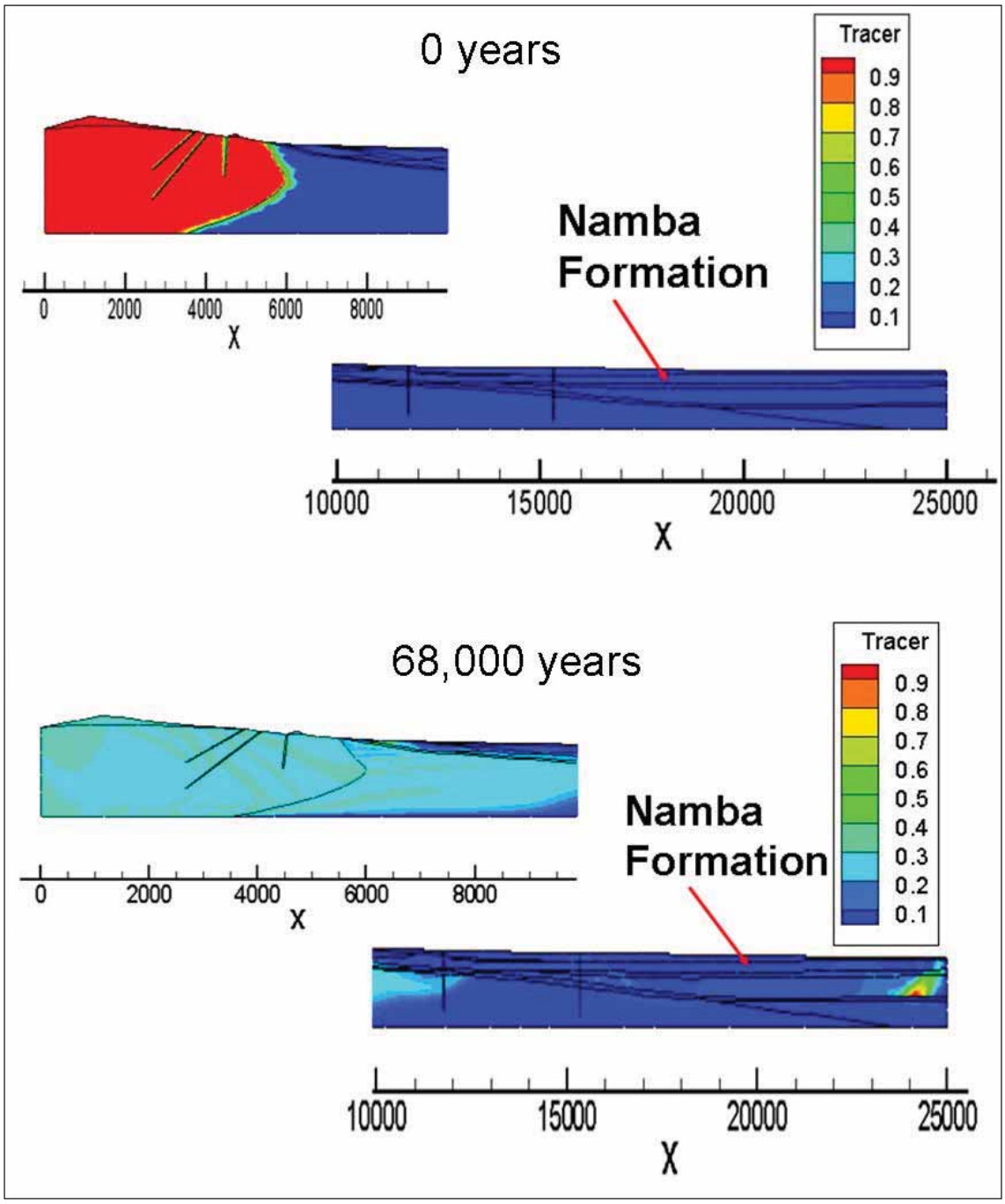

Figure 2: Tracer distribution in Beverley long-section model at 0 and 68,000 years.

Evaluating Genetic Models using Reactive Transport

The case studies described above illustrate how HCh and RT modelling of uranium systems provide an opportunity to compare and evaluate competing hypotheses for ore genesis. The recognition of the role of a pre-existing oxidised horizon/unit in the basement, and of high permeability fault zones in localising ore deposition in the basement of unconformity related uranium systems in the Alligator Rivers Uranium Field is one of the key results of this study.

Towards Prediction

Studies of the palaeochannel systems in South Australia highlight the role RT and geochemical modelling can play in developing predictive models for exploration. The results to date show how geochemical modelling methods can be used to provide a better understanding of the reactions and processes occurring within palaeochannel hosted uranium systems. Results presented here show, that when coupled with geological observations and data, numerical modelling can lead to a more quantitative understanding of the source of uranium, conduits for fluid flow, where fluid flow is focussed and the chemical traps which result in uranium deposition. Importantly, an improved understanding of fluid flow and the chemical processes involved in uranium transport and deposition will lead to a more predictive approach to exploration.

Acknowledgments

The predictive mineral discovery*Cooperative Research Centre, NTGS and PIRSA are thanked for their financial support.

References

Clauser, C., 2003. Numerical simulation of reactive flow in hot aquifers: SHEMAT and Processing SHEMAT. Springer, Berlin, 332pp.

Cleverley, J.S. & Oliver, N.H.S., 2005. Comparing closed system, flow-through and fluid infiltration geochemical modelling: examples from K-alteration in the Ernest Henry Fe-oxide-Cu-Au system. Geofluids, 5, 289-307.

Cleverley, J.S., Hornby, P. & Poulet, T., 2006. Pmd*RT: combined fluid, heat and chemical modelling and its application to Yilgarn geology. In: Barnicoat, A.C. & Korsch, R.J., eds, Predictive Mineral Discovery CRC - Extended Abstracts. Geoscience Australia, Record, 2006/7, 23-28.

Gross, L., 2002. Fastflo4. CSIRO Mathematical and Information Sciences Software.

Hornby, P. & Poulet, T., 2008. Reactive transport. In: pmd*CRC Enabling Technologies Final Report, in preparation.

Lally, J.H. & Bajwah, Z.U., 2006. Uranium Deposits of the Northern Territory. Northern Territory Department of Primary Industry, Fisheries and Mines, Report 20 (preliminary version).

Lambert, I., Jaireth, S., McKay, A. & Miezitis, Y., 2005. Why Australia has so much uranium. AusGeo News, Issue 80, 7-9.

Polito, P.A., Kyser, T.K., Marlatt, J., Bajwah, Z. & Drever, G., 2004. Significance of alteration assemblages for the origin and evolution of the Proterozoic Nabarlek unconformity-related uranium deposit, Northern Territory, Australia. Economic Geology, 99, 113-139.

Shvarov, Y.V. & Bastrakov E.N., 1999. HCh: a software package for geochemical equilibrium modelling. User's Guide. Australian Geological Survey Organisation, Record 1999/25, 60pp.

Shvarov, Y.V., 1999. Algorithmisation of the numerical equilibrium modelling of dynamic geochemical processes. Geochemistry International, 37, 571-576.1999)

Wilde, A.R. & Wall, V.J., 1987. Geology of the Nabarlek uranium deposit, Northern Territory, Australia. Economic Geology, 82, 1152-1168.

Architecture: Regional 3D maps and how to use them

P.A. HENSON[1], R.S. BLEWETT[1], J. McL. MILLER[2], I. G. ROY[1], Y. ZHANG[3] AND P.M. SCHAUBS[3]

[1]*pmd***CRC*, Geoscience Australia, GPO Box 378, Canberra, ACT 2601
[2]*pmd***CRC*, Centre for Exploration Targeting, School of Earth and Geographical Sciences, University of Western Australia, 35 Stirling Highway, Crawley, WA 6009
[3]*pmd***CRC*, CSIRO Exploration and Mining, Australian Resources Research Centre, 26 Dick Perry Avenue, Kensington WA 6151
Paul.Henson@ga.gov.au

The relatively new availability of widespread three dimensional software packages, designed for geological mapping, has changed the way we view and analyse geological data. Geological data collected at the surface of the can provide insights into the three dimensional extension of the surface outcrop and alteration associated with mineralising processes. Three dimensional maps (3D maps) have provided a medium where multidisciplinary data can be viewed and manipulated in georeferenced space. Relationships between these data can be compared and subsurface interpretations of stratigraphy, alteration and mineralisation can be constructed into physical objects and properties.

The uptake of 3D maps as a mainstream method to conduct geological research and exploration has encountered some scepticism. Most negative comments have been targeted at the inability of the user to ascertain the constraints, or the relative lack of constraints, used to construct 3D objects. To address this, it must be understood that the geometries within 3D maps are constrained using a variety of datasets. These data vary considerably and may involve several processing and interpretive phases before they are used in the interpretation of 3D objects. Data used to constrain 3D geometries can also vary considerably in their spatial distribution. An example of this is that magnetic and gravity data may provide a regional coverage, whereas a single seismic reflection line will only constrain subsurface interpretations locally. Construction of a 3D map is therefore a function of the integration of these variable constraints and hence will vary as a consequence of the available data types, their distribution and quality.

There are a variety of software packages currently available to construct 3D objects. These primarily consist of computer-aided design (CAD) based platforms, including gOcad™, which is currently widely used by Federal and State government organisations, universities and industry for a variety of applications (Figure 1). In addition, the semi-automated software program GeoModeller™ is gaining support due to its interactive potential field inversion and update capabilities.

Regional, camp and mine scale integration

Regional 3D maps are often constructed to provide an increased understanding of the 3D architecture and alteration associated with mineralisation. This is best done at a range of scales. Camp and mine scale data is significantly higher density and therefore can provide insights that can not be gained from regional data alone.

An example of 3D scale integration was conducted in the Laverton region located in the Eastern Goldfields Superterrane, Western Australia. Detailed structural analysis of both Wallaby and Sunrise

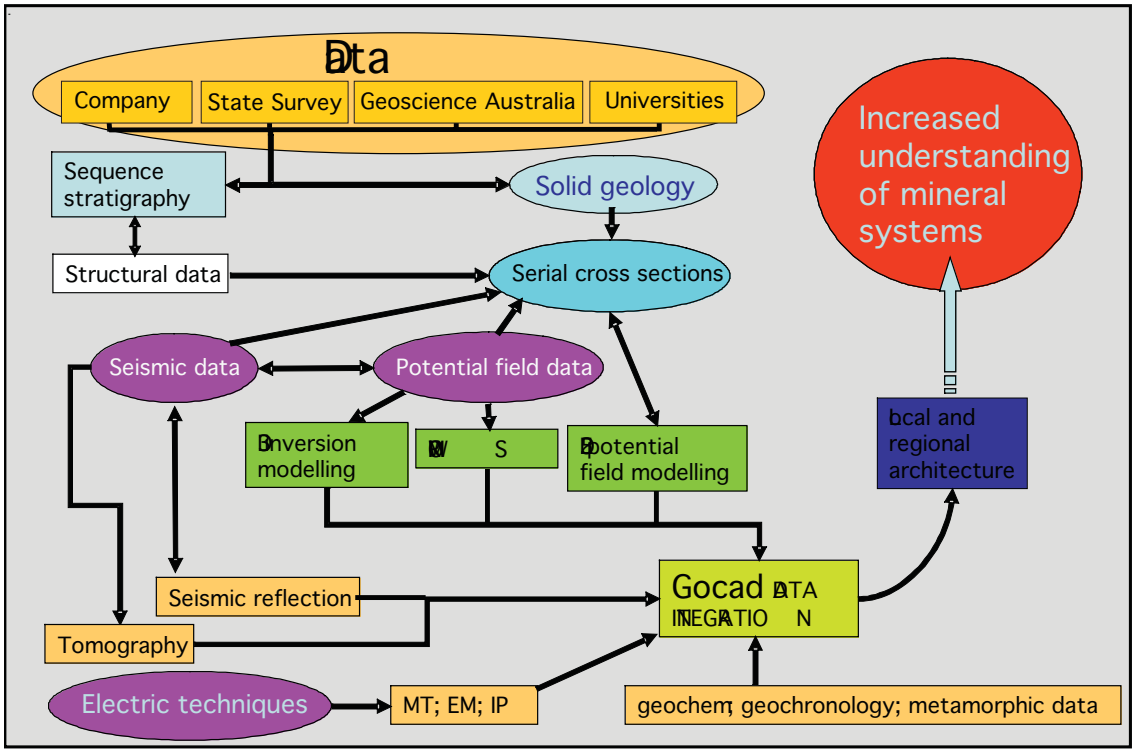

Figure 1. Workflow diagram for the construction of 3D maps using gOcad™.

Dam mines has provided new insights into gold formation. Mine scale structural analysis by Miller and Nugus (2006) at the Sunrise Dam mine and by Miller (2005) at the Wallaby mine, provided the basis for statistical analysis of 3D fault surfaces to ascertain preferential sites of fault reactivation and dilation during a northwest-southeast contractional gold event at both Wallaby and Sunrise Dam mines.

Using a 3D stress analysis approach, Miller and Nugus (2006) determined that the most favourable segment of faults to reactivate during the northwest-southeast contractional event were faults striking northeast-southwest and dipping at ~30° towards 310°. Mine scale 3D wireframes of the major shear zones in the Sunrise Dam deposit, combined with the actual occurrence of gold determined from drilling (Figure 2), provided a suitable test case to compare this stress vector against. Wireframes of the major faults and isosurfaces of the gold occurrences, generated using the software package Leapfrog™, were imported into the software package gOcad™ and assigned orientation parameters. This process highlighted areas along the faults that were within the ranges specified by Miller and Nugus (2006). Analysis of these data indicated that there is an almost one-to-one relationship between known gold occurrences and fault segments with these orientations at Sunrise Dam mine. It also highlighted down dip extensions distal to the known gold occurrences, which may provide additional targets during future near mine exploration.

In an attempt to test the importance of fault orientation regionally, the same principles were applied to the regional scale 3D faults in the Laverton region (Figure 3). Regional scale faults were constrained using both seismic reflection data and, to a lesser extent, potential field data. These data provided a suitable framework to apply the same fault parameters that were applied to the mine scale faults, to highlight suitably orientated segments on the regional scale. Application of this process highlights areas around Sunrise Dam, Wallaby and Lancefield mines as suitably oriented fault segments, but also highlighted other potential regions (Figure 3). These empirical relationships indicate that the orientation of faults is fundamental to the mineralisation process at least during northwest-southeast contraction event in the Laverton region. This work demonstrated that the dip of a fault is as important to the reactivation

process as the dip direction; hence it would not be possible to apply this type of analysis to 2D faults. In contrast, a well constrained 3D map is the only potential way of analysing these orientation parameters.

The integration of mine and camp scale studies highlights the power of scale integration when applied to a well constrained 3D map.

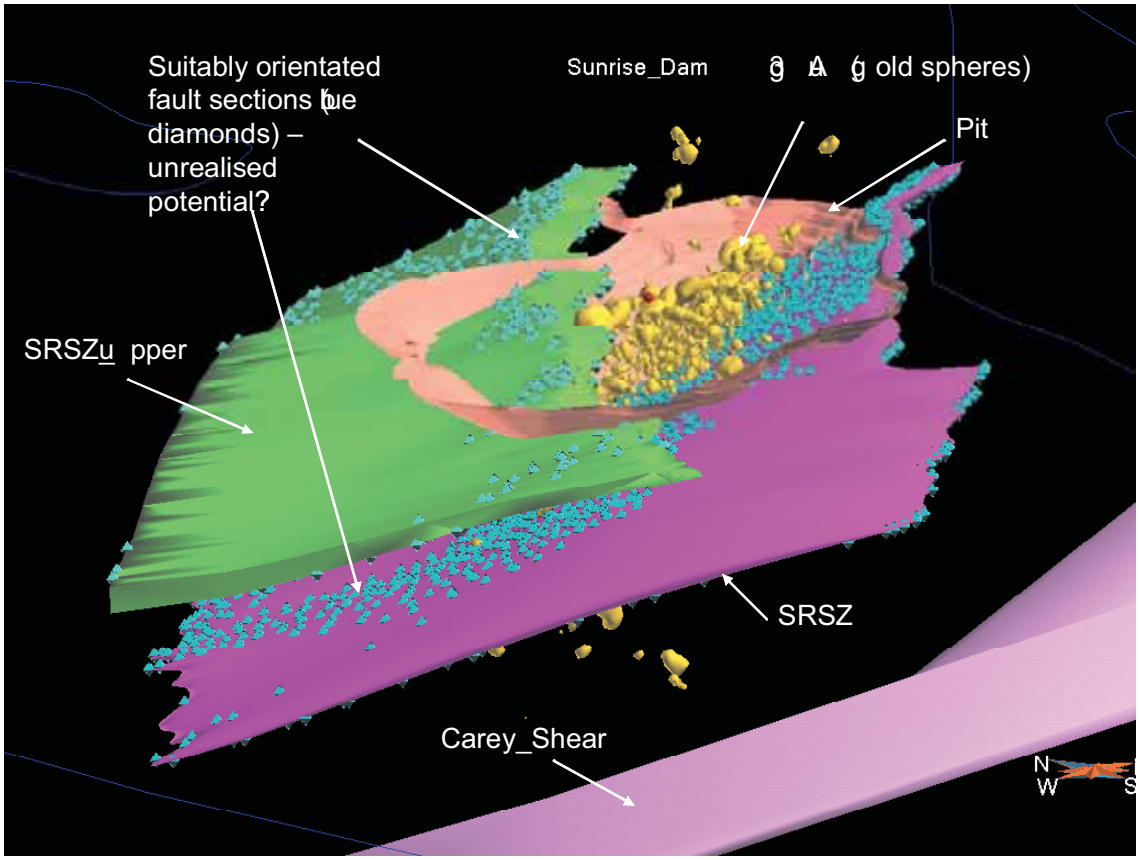

Figure 2. 3D image from gOcad™, looking to the northeast, of wireframes from Sunrise Dam mine. Blue diamonds show regions of suitably oriented fault segments to reactivate/dilate during a Northwest-Southeast contractional event.

3D maps and numerical modelling

The integration of 3D maps with numerical modelling has provided techniques for testing geological processes derived from a constructed 3D architecture. The process allows 3D conceptual geometries or 3D objects (constructed in gOcad™ or Geomodeller™, etc.), to be exported into 3D meshing packages (e.g., PATRAN) used for numerical modelling, where a variety of different parameters can be applied to simulate real geological processes. Numerical modelling applies mathematical code to 3D objects using different parameters in order to simulate a variety of geological processes. It also enables the researcher to test a range of different hypotheses using a variety of techniques including:

- Reactive transport
- Stress, strain and volumetric changes
- Heat flow - convection and conduction

These techniques have been applied to both conceptual and actual 3D surfaces and volumes (generated in gOcad™) (Figures 4 and 5). The process has determined location of shear and volumetric strain during

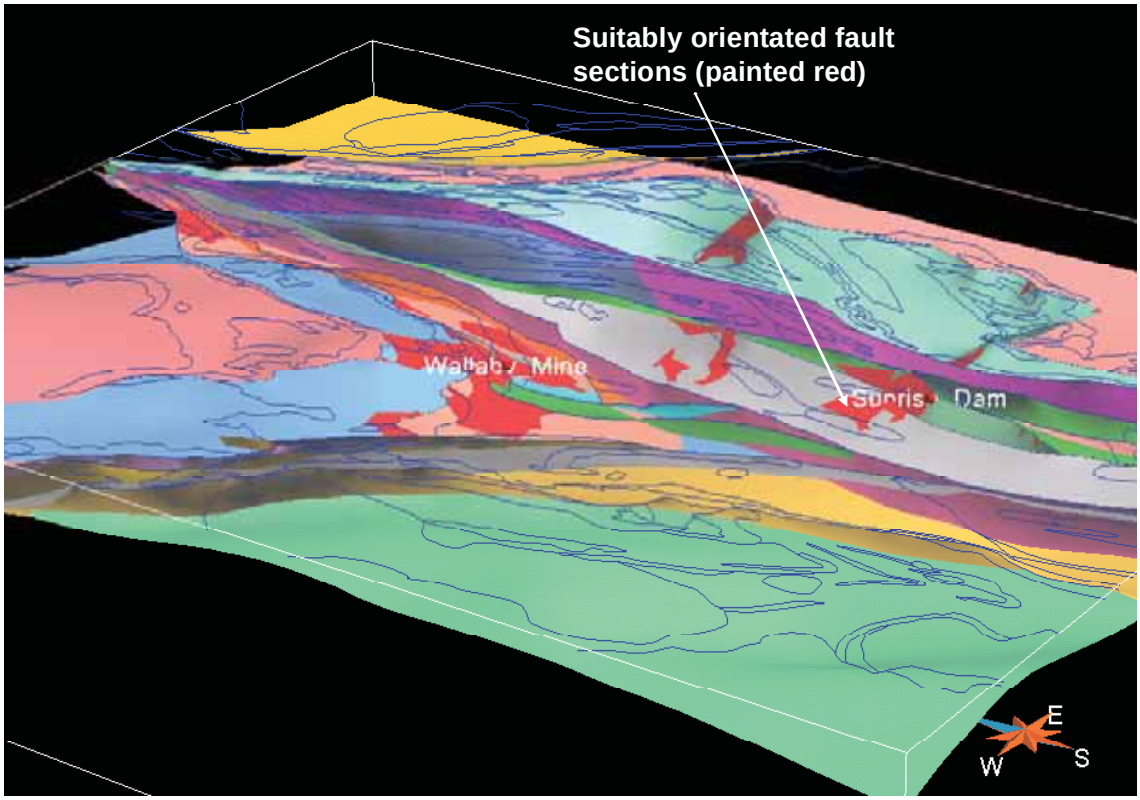

Figure 3. 3D image from gOcad™, looking to the northeast, of the regional faults in the Laverton region. Red surfaces show regions of suitably oriented fault segments to reactivate or dilate during a northwest-southeast contractional event.

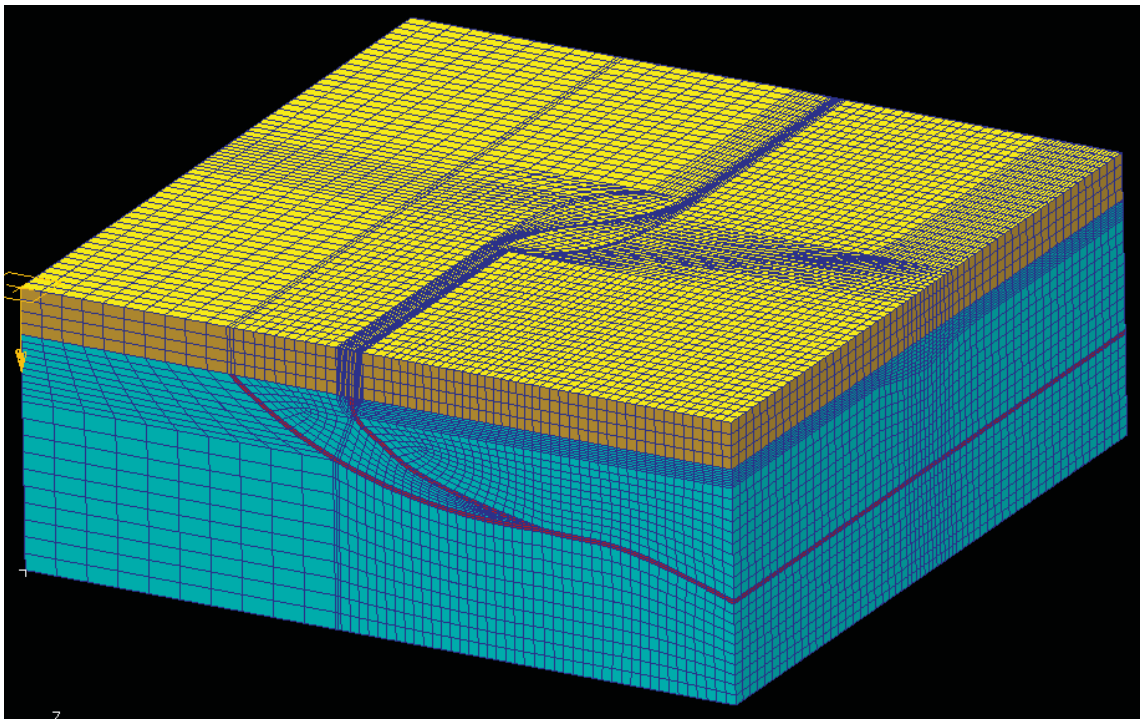

Figure 4. Image of the model of the 3D mesh displaying the fault geometries and lithological distributions and the mesh used.

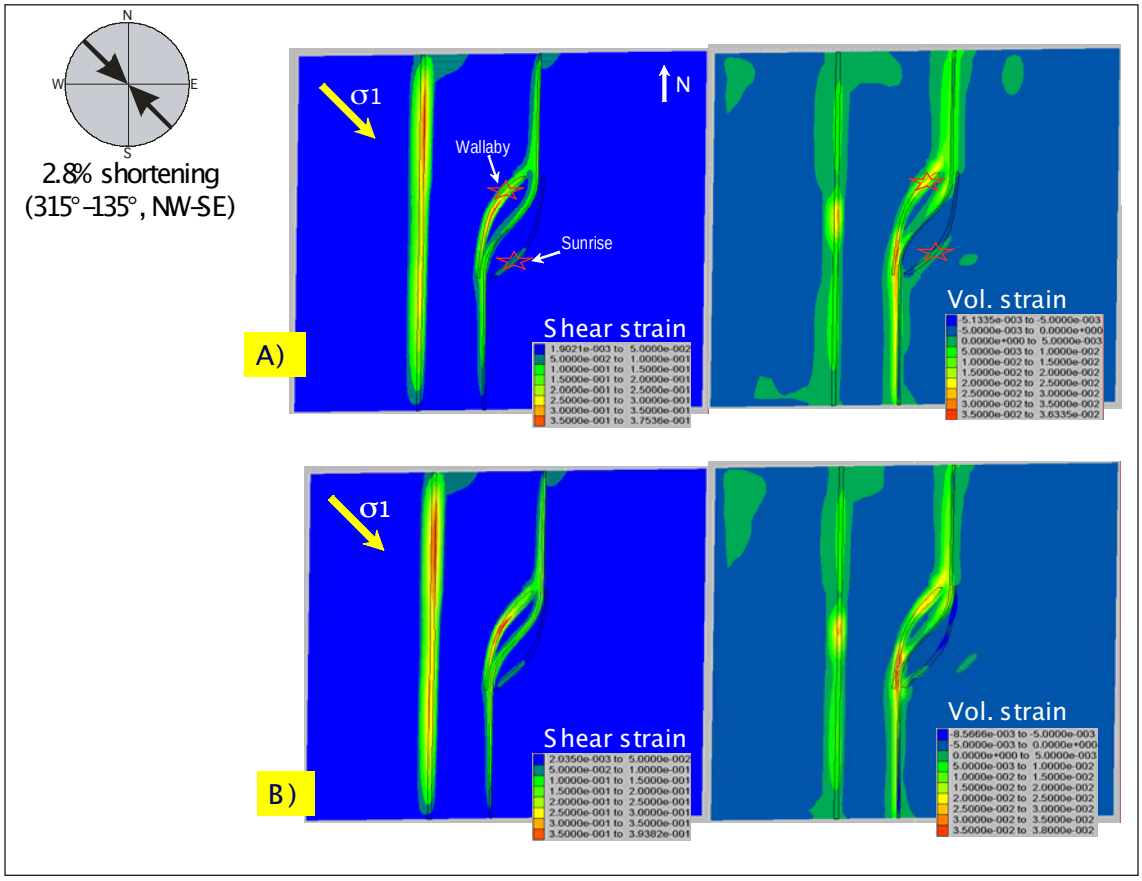

Figure 5. Image showing the Shear and Volumetric strain occurring during a northwest-southeast contractional event. A and B are plan views at 0.5 and 1.0 km below the top surface of the greenstone, which is the upper surface of the model in Figure 4. Clearly, greater shear and dilation localisation occurs at Wallaby compared to Sunrise Dam.

a variety of different stress directions. These data indicate the spatial distribution of regions displaying preferential dilation and, hence, regions of higher potential fluid flow and mineralisation.

Summary

The power of using 3D software packages to interpret geology is derived from data integration and display. Using this medium, we can no longer make interpretations in isolation or in a simple 2D sense. It is a powerful way of validating our hypotheses and cross checking geological relationships derived from multidisciplinary data sources and techniques.

References

Miller, J. M. & Nugus, M., 2006. The structural evolution of the Sunrise Shear Zone and the overlying Watu and Western Shear Zones, Sunrise Dam gold deposit, Laverton, W.A. Predictive Mineral Discovery CRC Project Y4 Report, November 2006.

Miller, J. M., 2005. The structural evolution of the Wallaby gold deposit, Laverton, W.A. Predictive Mineral Discovery CRC Project Y4 Report, July 2005.

Sources and Reservoirs: Noble gases as tools for constraining a mantle connection during orogenic-gold and IOCG mineralisation

M.A. KENDRICK[1], J.L. WALSHE[2], G. MARK[3], K. PETERSEN[4], T. BAKER[5], D. PHILLIPS[1], M. HONDA[6], N.H.S OLIVER[5], L. FISHER[5], D. GILLEN[5], P.J. WILLIAMS[5] AND B. FU[5,1]

[1]*pmd***CRC*, School of Earth Sciences, The University of Melbourne, VIC 3010
[2]*pmd***CRC*, CSIRO Mining and Exploration, Bentley, PO Box 1130, Bentley, WA 6102
[3]*pmd***CRC*, School of Geoscience, Monash University, VIC 3800
[4]*pmd***CRC*, School of Earth and Geographical Sciences, University of Western Australia, WA 6009
[5]*pmd***CRC*, School of Earth and Environmental Science, James Cook University, QLD 4811
[6]Research School of Earth Sciences, Australian National University, ACT 0200
Mark.Kendrick@unimelb.edu.au

Introduction

Mineralising fluids have diverse compositions and can have complex origins with multiple components acquired from different reservoirs. Chlorine is an essential ligand for complexing metals in aqueous solution and facilitates metal transport through the Earth's crust. Giant hydrothermal ore deposits result when a change in fluid physicochemistry leads to highly efficient metal precipitation. This can be triggered by a range of processes including fluid-rock interaction, fluid mixing, or the loss of volatiles. An improved understanding of these processes could improve our ability to predict giant hydrothermal ore deposits.

The noble gases (He, Ne, Ar, Kr and Xe) are powerful tracers for investigating fluids in the Earth's crust. They have well constrained isotopic compositions that vary by orders of magnitude between the Earth's mantle, crust and hydrosphere (Table 1); they have a low abundance, and they are famously unreactive; also being known as the rare or inert gases (Ozima & Podosek, 2002). The rarity of noble gases means their transport is coupled to that of the major volatile phases important for metal transport (e.g., H_2O, CO_2 and CH_4) and they never form a pure phase. Their inert behaviour means they are less easily reset during fluid-rock interactions than stable isotopes, and their huge variation in isotope composition enables mixing between very minor fluid components to be recognised. These characteristics mean the noble gases can help constrain, and in some cases provide definitive evidence for, mantle involvement in ore mineralisation (Simmons et al., 1987).

Simultaneous measurement of the noble gas and halogen (Cl, Br and I) composition of fluid inclusions enables the concentration of noble gases to be determined from fluid salinity (Kendrick et al., 2006b). The noble gas concentration in the fluid is more easily modified during fluid-rock interaction than its isotopic composition and noble gases can be 'lost' from the fluid during phase separation. As a result, the concentration of noble gases can provide information on the temperature of the fluids wall-rock

Table 1. Noble gas parameters for key reservoirs in the Earth.				
	Mantle	Lower Crust	Upper Crust	Hydrosphere
$^{40}Ar/^{36}Ar$	40,000	~1000? to >40,000	296-2,000*	296
$^{20}Ne/^{22}Ne$	12.5	9.8 to 5?	<9.8 to ~8	9.8
$^{21}Ne/^{22}Ne$	~0.03	0.029 to 0.8?	>0.029 to ~0.3	0.029
$^{3}He/^{4}He$ (Ra)	>6	0.02	<0.1	1

*Ra = the atmospheric $^{3}He/^{4}He$ value of 1.39×10^{-6}. References in Ozima and Podosek (2002) and Ballentine et al. (2002). *Based on typical sedimentary formation waters.*

interaction history and processes such as fluid boiling (Kendrick et al., 2001; Kendrick et al., 2006a). The halogens provide complementary information on the acquisition of salinity by a fluid (Hanor, 1994).

Application to IOCG mineral districts

The Cloncurry district of the Mt Isa Inlier (Figure 1), northeastern Australia, and the Wernecke Mountains, Canada, were chosen as two contrasting 1.6-1.5 Ga iron oxide copper-gold (IOCG) terranes. Most of the IOCG deposits in the Cloncurry district, including Ernest Henry which is the regions largest (167 Mt @1.1% Cu and 0.5 ppm Au), are temporally associated with intrusion of the regionally-extensive, post-1550 Ma, Williams-Naraku Batholith (Mark et al., 2006). The Osborne deposit is the second largest deposit in the region (15.2 Mt @ 3% Cu and 1ppm Au) and is unusual because its peak metamorphic age of 1595 Ma precedes regional magmatism by ~50 m.y. (Gauthier et al., 2001). In contrast to the Mt Isa Inlier, syn-mineralisation granites are unknown in the Wernecke Mountains, where large deposits are still to be found (Hunt et al., 2005). Quartz samples associated with mineralisation and barren Na-Ca alteration were collected from both districts and studied by microthermometry. Typical fluid inclusion assemblages include variably saline aqueous and carbonic varieties. However, fluids in the Mt Isa Inlier with higher salinity (up to 65 wt % salts) and CO_2 fluid inclusions are more common than in the Wernecke Mountains.

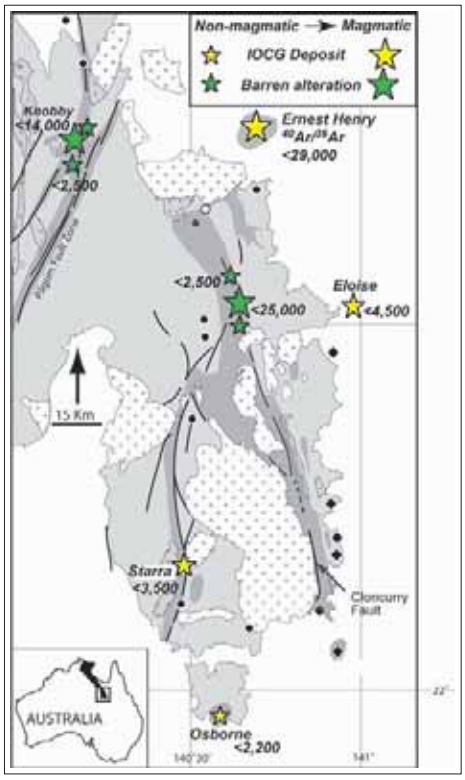

Figure 1. Summary map showing areas of intense Na-Ca alteration (dark grey shading) and summarising the maximum $^{40}Ar/^{36}Ar$ values determined for key study areas. Star size indicates interpreted involvement of magmatic fluids.

Mt Isa Inlier

High salinity fluid inclusions in samples from Ernest Henry are characterised by variable $^{40}Ar/^{36}Ar$ values of between <2500 and ~30,000 (Kendrick et al., 2007). The highest $^{40}Ar/^{36}Ar$ values are correlated with halogen signatures similar to magmatic fluids involved in porphyry copper mineralisation and are interpreted to represent a deeply-derived basement fluid of magmatic origin (Kendrick et al., 2007). Further work is required to determine if a mantle component is present. However, the Corella Formation is

interpreted as an important source of CO_2 in this deposit (Kendrick et al., 2007). The lowest $^{40}Ar/^{36}Ar$ values are correlated with low Br/Cl and I/Cl values (similar to the composition of halite) and are interpreted to represent sedimentary formation waters that have interacted with scapolite.

In contrast to Ernest Henry, fluid inclusions from the Osborne deposit have maximum $^{40}Ar/^{36}Ar$ values of <2200 (Fisher & Kendrick, 2008). These data do not favour the involvement of magmatic fluids and the abundant CO_2 fluid inclusions present at Osborne are inferred to have had a solely metamorphic origin (Fisher & Kendrick, 2008), compatible with the syn-metamorphic timing of mineralisation at Osborne (Gauthier et al., 2001). Available data for the Starra and Eloise deposits are intermediate between Osborne and Ernest Henry indicate maximum $^{40}Ar/^{36}Ar$ values of 3500 and 4500, respectively, which are intermediate between those of Ernest Henry and Osborne. These values could indicate minor involvement of magmatic fluids but suggest sedimentary formation waters dominated.

Noble gas and halogen data for regional (~1530 Ma) Na-Ca alteration in the Cloncurry district and Mary Kathleen Fold Belt indicate a similar range of fluid origins for barren alteration and economic IOCG mineralisation. Moderately saline fluid inclusions in samples from the Snake Creek Anticline have maximum $^{40}Ar/^{36}Ar$ values of ~25,000, that are interpreted to indicate a magmatic origin and correlated with the Saxby granite (Kendrick et al., 2008). Elsewhere aqueous fluids with $^{40}Ar/^{36}Ar$ values of <2700 dominate and are interpreted to indicate a dominantly non-magmatic fluid origin.

Samples from the Knobby Quarry are of special interest because they are dominated by CO_2 fluid inclusions: initial noble gas analysis indicated a maximum $^{40}Ar/^{36}Ar$ value of ~7,000 (Kendrick et al., 2008). This value is significantly lower than the magmatic value of ~30,000 determined in the Cloncurry district and the MORB mantle value of 40,000, suggesting significant portions of CO_2 had a local source from the Corrella Formation (Kendrick et al., 2008). Further work was undertaken to constrain a possible mantle CO_2 component and resulted in the maximum measured $^{40}Ar/^{36}Ar$ value increasing to ~14,000. This value is higher than could easily be generated by metamorphism of sedimentary rocks and it is positively correlated with $^{20}Ne/^{22}Ne$. The positive correlation between $^{20}Ne/^{22}Ne$ and $^{40}Ar/^{36}Ar$ is most easily explained as a mixing line. The end-members are modelled as ^{36}Ar-rich CO_2 obtained by devolatilisation of the Corella Formation and ^{36}Ar-poor CO_2 with a mantle origin. Depending on the input parameters, the maximum measured $^{40}Ar/^{36}Ar$ value corresponds with a maximum mantle CO_2 component of ~85% at the Knobby locality. This result is in good agreement with the proportions estimated independently from C and O isotope studies (Oliver et al., 1993; Oliver, 1995).

The Wernecke Mountains

Fluid inclusion bearing quartz and sulphide samples were collected from the Slats, Slab, Hoover, Olympic and Igor prospects described by Hunt et al. (2005). Despite the lack of contemporaneous granites outcropping in the Wernecke Mountains the Ar and halogen results are very similar to those obtained for Ernest Henry. The fluid inclusion $^{40}Ar/^{36}Ar$ values vary between 1000 and 40,000 and give a similar range of values in quartz and sulphide samples. The halogens are highly fractionated and include minimum Br/Cl and I/Cl values that are similar to halite. Fluid inclusions with high $^{40}Ar/^{36}Ar$ values can be attributed to either metamorphic or magmatic sources in the deep crust (Table 1). The highest $^{40}Ar/^{36}Ar$ value of 40,000 is within error of both the deep crust and the modern day MORB mantle (Table 1) and He and Ne isotope data preclude a mantle volatile component in these deposits (Figure 2).

Application to orogenic gold deposits

In the 2.65 Ga St Ives Gold Camp, gold is preferentially localised at the interface between different km-scale alteration zones with contrasting redox state. This observation has been critical in development of an unexpected new model for gold mineralisation that envisages hydrogen-rich deep-Earth fluids as a critical ingredient (Walshe et al., 2006; Neumayr et al., 2008). This model suggests hydric fluids could be important for either: reducing relatively oxidised Au-bearing metamorphic fluids and causing Au

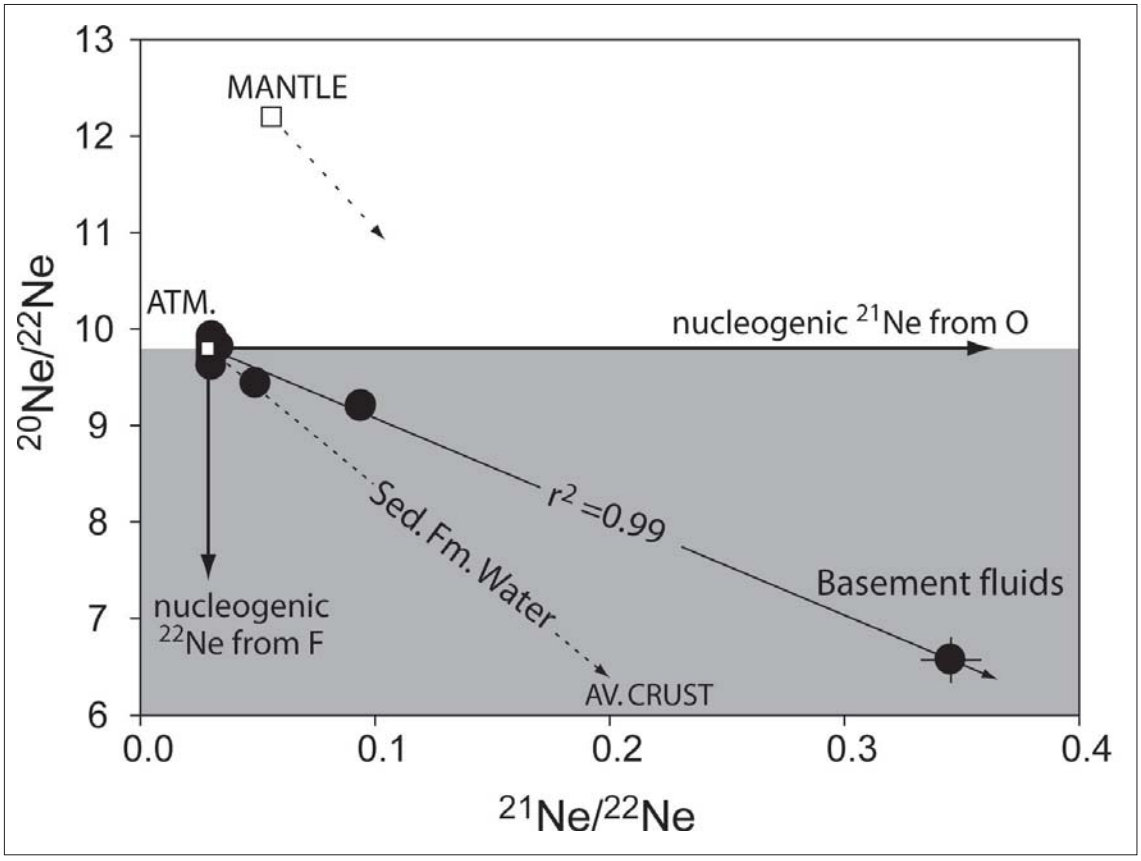

Figure 2. Ne isotope plot for fluid inclusions in Wernecke sulphide. Together with maximum ^{3}He/^{4}He value of 0.2 these data preclude a mantle component (Kendrick et al., 2008).

precipitation, or as a previously overlooked transporting medium that fluxes Au directly from the Earth's mantle to the crust during special mineralising epochs (Walshe et al., 2006).

The hydric fluids emphasised by this model do not appear to be present in very many gold deposits. Minor CH_4 fluid inclusions or CH_4 bearing mixed CO_2-H_2O fluid inclusions are commonly present but are generally explained by localised reduction of CO_2, or a minor source from hydrocarbons. A major difficulty in testing the deep Earth model is that the hydric fluids critical for mineralisation are destroyed by oxidation reactions during the mineralisation process, e.g.:

$$[CH_4 + AuHS + HCl(g)]_{mantle\text{-}fluid} + [H_2O + CO_2 + SO_2]_{magmatic\text{-}fluid}$$

$$= [CO_2 + H_2O + HCl(aq)]_{fluids} + H_2S + Au \pm C$$

If this model is correct then CH_4 (where present) should carry mantle-derived noble gases.

Fluid inclusion microthermometry has demonstrated that samples from oxidised pyrite-bearing quartz veins are dominated by CO_2-H_2O fluid inclusions that are similar to those reported for most other gold deposits (Petersen et al., 2007). These fluid inclusions have ^{40}Ar/^{36}Ar values of up to 17,000 and contain ppb levels of ^{36}Ar, observations consistent with the involvement of magmatic fluids. Samples from reduced pyrrhotite-bearing quartz veins are unusual in that they are dominated by high-purity CH_4 fluid inclusions (Petersen et al., 2007).

The CH_4 fluid inclusions have mantle-like ^{40}Ar/^{36}Ar values of up to 48,000 and contain parts per trillion

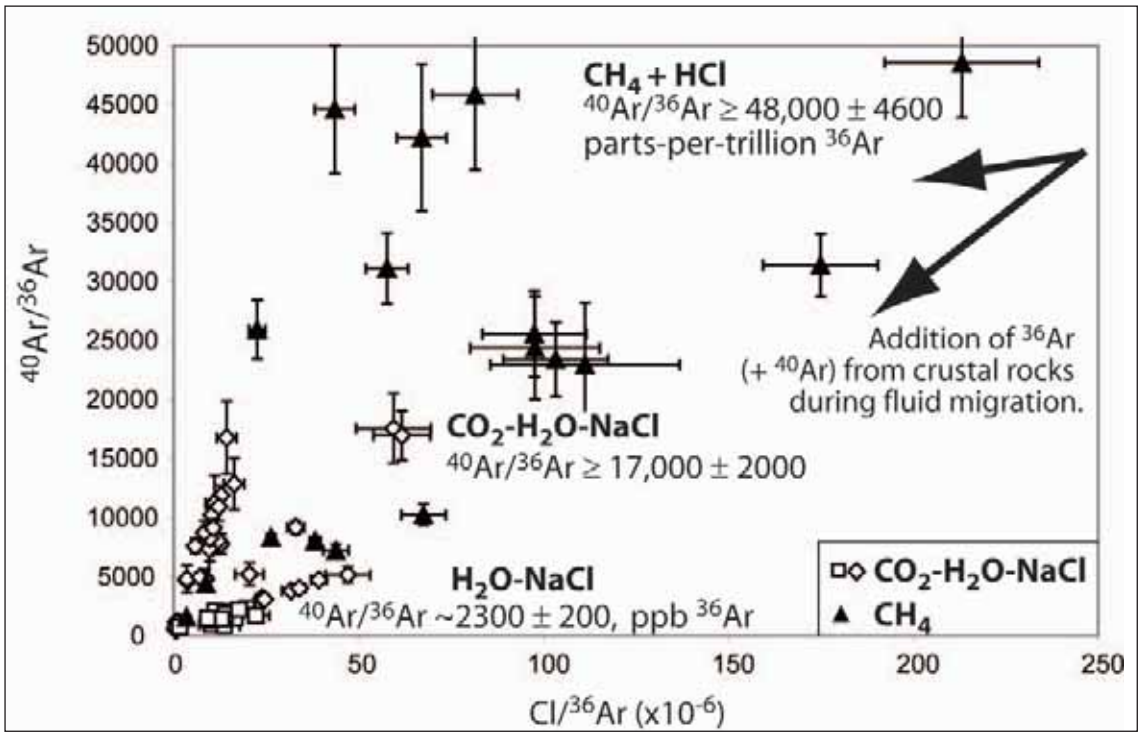

Figure 3. Ar data for six samples with different fluid inclusion types.

^{36}Ar concentrations (Figure 3). These data are compatible with a mantle origin for CH_4 at St Ives if noble gases have been recycled into the mantle since the Archaean (Holland & Ballentine, 2006).

An important feature of these data is that CH_4 fluid inclusions have lower ^{36}Ar concentration than CO_2 fluid inclusions. This implies CH_4 could not have formed by reduction of CO_2 due to wall-rock interaction: wall-rock interaction typically increases the ^{36}Ar concentration of the fluid (Kendrick et al., 2006a). In addition, the $^{40}Ar/^{36}Ar$ values are orders of magnitude higher than is typical of hydrocarbons in sedimentary basins (Table 1). The only viable alternative to a mantle origin for CH_4 is that CH_4 was sourced independently of CO_2 from the deep crust. Helium and Ne isotope analyses are underway to test these alternative origins.

Summary and conclusions

Combined noble gas and halogen analysis has proven a powerful tool for constraining fluid origins in both IOCG deposits and orogenic gold deposits. Compared to stable isotopes which vary by parts per thousand and can be reset during wall-rock interaction, the order of magnitude variation in noble gas and halogen signatures reveals new complexities and the possibility of definitive constraints.

Fluid sources are indicated to have been heterogeneous in IOCG deposits and the fractionated halogen signatures provide strong evidence that the dissolution of halite, or breakdown of scapolite, has been an important process for enhancing fluid salinity. Involvement of mantle CO_2 has been demonstrated in the Mary Kathleen Fold Belt, supporting independent conclusions based on C and O isotope studies. However, mantle volatiles are not a ubiquitous component of IOCG ore fluids, or the only source of CO_2 in the IOCG systems of the Mt Isa Inlier. Magmatic fluids are inferred to have had a purely crustal origin in the Wernecke Mountains; no magmatic source rocks are exposed. Deeply-derived magmatic fluids are interpreted to have been completely absent during mineralisation at the syn-metamorphic Osborne IOCG deposit. The similarity of fluid origins indicated for barren alteration and IOCG mineralisation in

the Mt Isa Inlier suggests that wall-rock interactions are a far more important control on the mineralising potential of IOCG ore fluids than their source.

Argon data demonstrate independent origins for CO_2 and CH_4 in the St Ives gold camp. These data are compatible with fluid mixing models for mineralisation and confirm that the existing model of metamorphic gold mineralisation needs to be re-evaluated. The mantle is a favoured source of CH_4 with exceptionally high $^{40}Ar/^{36}Ar$ values at St Ives. However, further work including He and Ne isotope analyses are required to constrain this definitively. In addition, other gold deposits must be examined to test the applicability of the hydric fluid model to other mineralised regions.

References

Ballentine, C.J., Burgess, R. & Marty, B., 2002. Tracing fluid origin, transport and interaction in the crust. In: Porcelli, D., Ballentine, C.J. & Wieler, R., eds, Noble gases in geochemistry and cosmochemistry. Reviews in Mineralogy and Geochemistry, 47, 539-614.

Fisher, L. & Kendrick, M., 2008. Metamorphic fluid origins in the Osborne Fe oxide–Cu–Au deposit, Australia: evidence from noble gases and halogens. Mineralium Deposita, in press (available online at journal website).

Gauthier, L., Hall, G., Stein, H. & Schaltegger, U., 2001. The Osborne Deposit, Cloncurry District: A 1595 Ma Cu-Au Skarn Deposit. In: Williams, P.J., ed., A Hydrothermal Odyssey. Economic Geology Research Unit, James Cook University, Contribution, 59, 58-59.

Hanor, J.S., 1994. Origin of saline fluids in sedimentary basins. In: Parnell, J., ed., Geofluids: Origin, Migration and Evolution of fluids in Sedimentary Basins. Geological Society of London, Special Publication, 78, 151-174.

Holland, G. & Ballentine, C.J., 2006. Seawater subduction controls the heavy noble gas composition of the mantle. Nature, 441, 186-191.

Hunt, J., Baker, T. & Thorkelson, D., 2005. Regional-scale Proterozoic IOCG-mineralized breccia systems: examples from the Wernecke Mountains, Yukon, Canada. Mineralium Deposita, 40, 492-514.

Kendrick, M.A., Baker, T., Fu, B., Phillips, D. & Williams, P.J., 2008. Noble gas and halogen constraints on regionally extensive mid-crustal Na-Ca metasomatism, the Proterozoic Eastern Mount Isa Block, Australia. Precambrian Research, 163, 131-150.

Kendrick, M.A., Burgess, R., Pattrick, R.A.D. & Turner, G., 2001. Fluid inclusion noble gas and halogen evidence on the origin of Cu-Porphyry mineralising fluids. Geochimica Cosmochimica Acta, 65, 2651-2668.

Kendrick, M.A., Duncan, R. and Phillips, D., 2006a. Noble gas and halogen constraints on mineralizing fluids of metamorphic versus surficial origin: Mt Isa, Australia. Chemical Geology, 235, 325-351.

Kendrick, M.A., Mark, G. & Phillips, D., 2007. Mid-crustal fluid mixing in a Proterozoic Fe oxide-Cu-Au deposit, Ernest Henry, Australia: Evidence from Ar, Kr, Xe, Cl, Br, and I. Earth and Planetary Science Letters, 256, 328-343.

Kendrick, M.A., Miller, J.M. & Phillips, D., 2006b. Part I. Decrepitation and degassing behaviour of quartz up to 1560 C: Analysis of noble gases and halogens in complex fluid inclusions assemblages. Geochimica Cosmochimica Acta, 70, 2540-2561.

Mark, G., Oliver, N.H.S. & Carew, M.J., 2006. Insights into the genesis and diversity of epigenetic Cu-Au mineralisation in the Cloncurry district, Mt Isa Inlier, northwest Queensland. Australian Journal of Earth Science, 53, 109-124.

Neumayr, P., Walshe, J., Hagemann, S., Petersen, K., Roache, A., Frikken, P., Horn, L. & Halley, S., 2008. Oxidized and reduced mineral assemblages in greenstone belt rocks of the St. Ives gold camp, Western Australia: vectors to high-grade ore bodies in Archaean gold deposits? Mineralium Deposita, 43, 363-371.

Oliver, N.H.S., 1995. Hydrothermal History of the Mary Kathleen Fold Belt, Mt Isa Block, Queensland. Australian Journal of Earth Science, 42, 267-279.

Oliver, N.H.S., Cartwright, I., Wall, V.J. & Golding, S.D., 1993. The stable isotope signature of kilometre-scale fracture-dominated metamorphic fluid pathways, Mary Kathleen, Australia. Journal of Metamorphic Geology, 11, 705-720.

Ozima, M. & Podosek, F.A., 2002. Noble Gas Geochemistry. Cambridge University Press.

Petersen, K., Hagemann, S.G., Neumayr, P. & Walshe, J.L., 2007. Multiple hydrothermal fluid pulses through time at the Kambalda gold deposits, Yilgarn Craton, Western Australia. In: Andrew, C.J. et al., eds, Digging Deeper. Proceedings of the Ninth Biennial Meeting of the Society for Geology Applied to Mineral Deposits, Irish Association for Economic Geology, vol. 1, 675-678.

Simmons, S.F., Sawkins, F.J. & Schlutter, D.J., 1987. Mantle derived helium in two Peruvian hydrothermal ore deposits. Nature, 329, 429-432.

Walshe, J.L., Neumayr, P., Petersen, K., Halley, S., Roache, A. & Young, C., 2006. Scale-integrated, architectural and geodynamic controls on alteration and geochemistry of gold systems in the Eastern Goldfields Province, Yilgarn Craton. Minerals and Energy Research Institute of Western Australia, Perth, Project M358, 200pp.

Architecture: New knowledge from seismic surveys

R.J. KORSCH

*pmd***CRC*, Geoscience Australia, GPO Box 378, Canberra ACT 2601
Russell.Korsch@ga.gov.au

Introduction

In undertaking a 'whole of system' approach to mineralisation, the Predictive Mineral Discovery Cooperative Research Centre (***pmd***CRC*) has adopted an integrated methodology across all scales using the Five Questions, as outlined by Price and Stoker (2002) and Barnicoat (2007). In understanding the architecture of a mineral system, the ***pmd***CRC* routinely constructs 3D geological maps in selected mineral provinces in Australia, to determine the geodynamic evolution and to examine regional scale controls on mineralisation and possible fluid pathways. To help constrain the architecture in the third dimension, the ***pmd***CRC* has been involved, with Geoscience Australia (GA), state government agencies and industry sponsors, in the acquisition (through the National Research Facility for Earth Sounding - ANSIR) and interpretation of a series of deep seismic reflection profiles (Figure 1) to provide information on mineral systems at scales ranging from the province to the deposit. Here we examine some of these seismic profiles in terms of their contribution to the understanding of mineral systems in the province.

In terms of the Five Questions, the deep seismic data can contribute to the understanding of several aspects, as underlined below:

1. What is the geodynamic setting and PT history of the system?
2. What is the architecture of the system?
3. What are the fluids, their sources and/or reservoirs?
4. What are the fluid flow drivers and pathways?
5. What are the metal and sulfur transport and deposition processes?

Northeast Yilgarn Craton (Orogenic Au, Ni)

The granite-greenstone terranes of the eastern Yilgarn Craton, in particular the Kalgoorlie and Kurnalpi Terranes, contain numerous world-class gold deposits that are spatially associated with major structures. The three-dimensional character of these major structures reveals information on the size and architecture of the gold mineral systems and the geodynamic processes responsible for their generation (Archibald, 1998; Goleby et al., 2002a).

In the northeastern Yilgarn region, the three-dimensional structure was poorly constrained. Geoscience Australia and the Geological Survey of Western Australia (GSWA), in conjunction with the ***pmd***CRC* and ANSIR, acquired over 430 km of deep seismic reflection data in the northeastern part of the Yilgarn Craton in Western Australia in 2001. The deep seismic reflection data were collected along two traverses, starting in the west within the Sons of Gwalia gold mine lease near Leonora and extended eastwards past Laverton and Yamarna before passing over the mineral exploration drill hole NJD1 and finishing in the Officer Basin. Shorter seismic lines were also acquired in the vicinity of Wallaby and

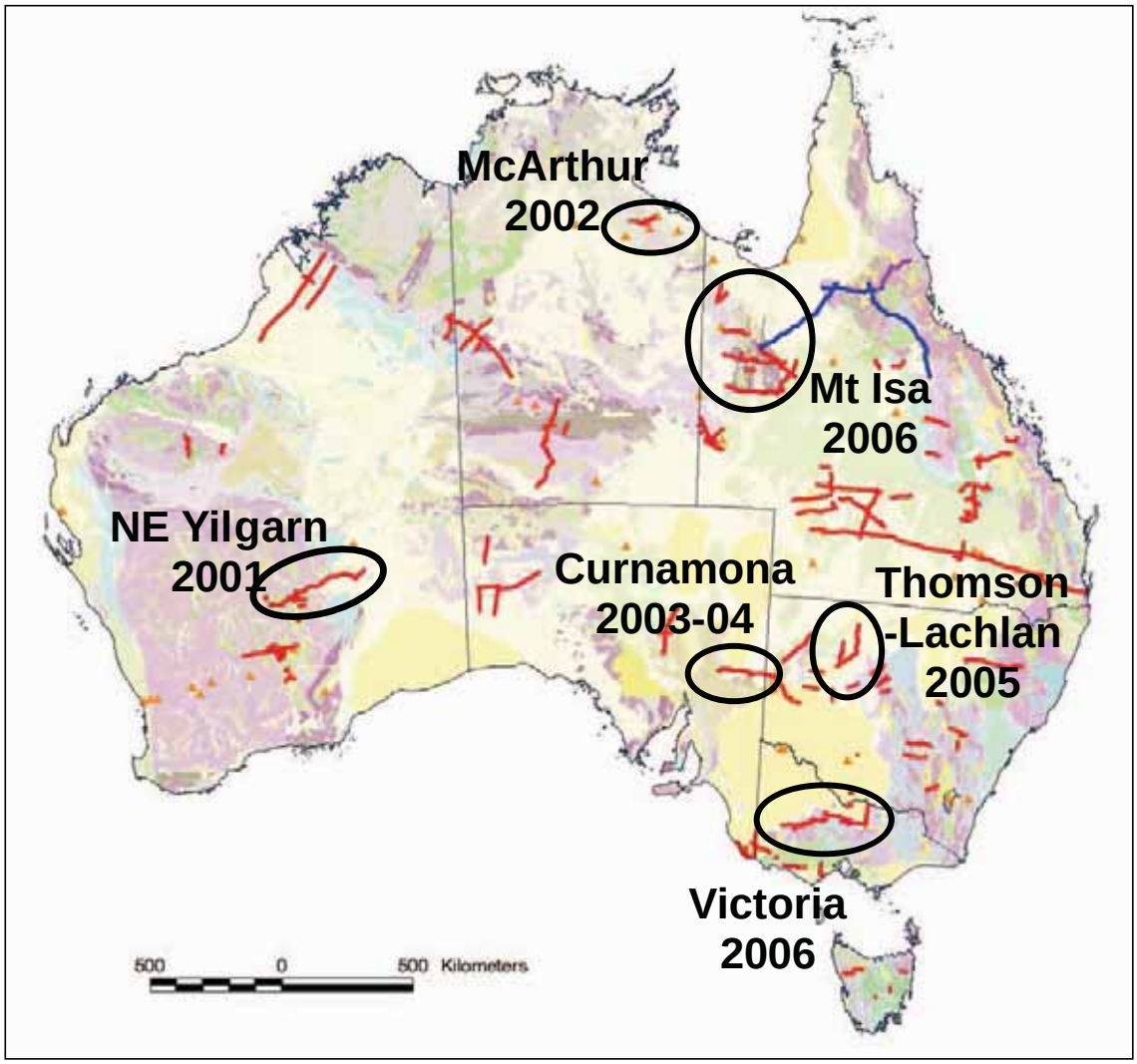

*Figure 1. Deep seismic reflection lines in Australia, showing the locations of the surveys that the pmd*CRC has been associated with.*

Sunrise Dam mines.

A summary of the main features of the deep seismic interpretation is presented in Goleby et al. (2002b, 2003, 2004). Blewett et al. (2002) discusses several of these observations within the western part of the survey, between Leonora and Laverton, in detail. A number of significant geological features of the northern Yilgarn deep seismic reflection traverse stand out. These are:

- The crust thickens eastwards as it approaches the Albany-Fraser Province. It deepens from about 13.5 s (40 km) beneath Leonora to 15.5 s (46 km) at the eastern end the traverse.
- The crust can be subdivided into three subhorizontal bands, a lower non-reflective ductile level, a middle level with numerous prominent east-dipping reflections and an upper level that can be grouped into packets of distinct reflectivity.
- There is a very pronounced east-dipping reflectivity along the entire seismic traverse, both in the middle and upper levels of the crust and have a shallow dip that is typically around 30°.

- There are three major, east-dipping, crustal-penetrating shear zones. Major orogenic gold systems are associated with the western (Leonora region) and central (Laverton region) shear zones. The third shear, recognised in the eastern part of the seismic line, in the Yamarna area, raises the potential for significant gold mineralisation in this area.
- In places, low angle shear zones have an extensional geometry, and late basins with synformal geometries sit in the hanging wall of the shear zones (Czarnota et al., 2007).
- The Neoproterozoic succession at the eastern end of the seismic traverse has been cut by several faults, indicating that there was some post-Proterozoic deformation. It is uncertain as to how far this deformational event extends westwards into the Yilgarn Craton.

McArthur Basin (Pb-Zn System)

The Palaeoproterozoic to Mesoproterozoic (<1850-<1490 Ma) southern McArthur Basin, Northern Territory, contains an unmetamorphosed, relatively undeformed succession of carbonate, siliciclastic and volcanic rocks that host the McArthur River (HYC) Zn-Pb-Ag deposit. Geoscience Australia, Northern Territory Geological Survey (NTGS), ***pmd****CRC* and AngloAmerican combined to fund a deep seismic reflection survey along a 110 km long east-west profile across this basin, which was acquired by ANSIR in late 2002. The main aim was to examine the fundamental basin architecture of the southern McArthur Basin, particularly the Batten Fault Zone (Rawlings et al., 2004).

The seismic data provide little evidence for pronounced stratigraphic thickening in the seismic section, with no evidence for the Batten 'Trough' being a separate depocentre, or for the presence of large asymmetric half graben, because the thick sedimentary succession extends both to the east and west, beyond the inferred boundaries of the 'trough'.

The western two-thirds of the seismic profile is dominated by a series of west-dipping low-angle faults that form part of a previously unrecognised major thrust belt that has propagated eastward, forming a forward-breaking sequence of thrusts. Displacement on the thrusts tends to be greatest in the west and diminishes to the east, with the frontal thrust of the system having only minor displacement and occurring ~6 km west of the Emu Fault Zone. In the west, the youngest strata of the McArthur Basin, the Roper Group, form the western limb of the Bauhinia monocline, which developed above the most western thrust ramp in the seismic data, and indicate a post-Roper timing for the thrust system. The thrusts continue at depth beyond the western limit of the seismic section, and this part of the thrust belt is now hidden beneath younger sedimentary cover.

In the eastern part of the basin, the Emu Fault Zone is interpreted as a near-vertical, braided strike-slip fault system. The seismic data suggest the likelihood of minor stratigraphic thickening adjacent to the Emu Fault during deposition of the McArthur Group, probably in a small pull-apart basin forming a negative flower structure. This interpretation is supported by the rectilinear nature of the fault system in map view. There have been at least two episodes of fault activity. The first involved sinistral movement in middle McArthur Group times, leading to possible thickened strata at transtensional fault bends. The second involved dextral transpression, which inverted earlier transtensional zones to form positive flower structures in post-Roper time.

For the giant McArthur River Zn-Pb-Ag deposit, it has been argued that the Emu Fault provides a conduit for ore forming fluids to move from source to depositional site (Williams, 1978). The depositional environment for the base metals is the thick accumulation of carbonaceous deep-water shales and siltstones of the Barney Creek Formation (middle McArthur Group), deposited in a sub-basin adjacent to the Emu Fault.

Numerical fluid flow models for base metal mineralisation at McArthur River (e.g. Garven et al., 2001) rely largely on the circulation of metalliferous brines in free convective cells of 20-50 km diameter,

which develop within the proposed lateral aquifer system. First order control on ore fluid focussing was discharge to the surface along the active Emu Fault, and recharge along the Tawallah Fault to the west. The subvertical orientation and deep-rooted nature of both the Emu and Tawallah faults and a subhorizontal aquifer is implicit to the initiation and maintenance of west-to-east brine transport and the proposed discharge and recharge points. Although the seismic data suggest that the Emu Fault is subvertical, this is not the case for the Tawallah Fault which is a thrust dipping shallowly to the west. Hence the architecture of the fluid flow model by Garven et al., (2001) for the formation of the McArthur River deposit is invalid and needs to be reconsidered.

The new seismic data suggest that the potential for McArthur style base metal deposits is increased within and to the east of the Batten Fault Zone. Given the strike-slip nature of the Emu Fault, segments of it now under cover to the north and south of the McArthur River deposit may also have formed sub-basins (negative flower structures) that would also be prospective for base metals.

The recognition of a previously unknown major thrust belt enhances the prospectivity of large areas of the McArthur Basin for exploration for younger (post-Roper Group) foreland basin type deposits such as Mississippi Valley types (MVT) as well as equivalent styles to the Century deposit, which possibly formed by topographically-driven fluid flow. Also, under cover well to the west of the seismic profile, in the core of the thrust belt (orogen), there may be potential for orogenic gold deposits under younger cover.

Curnamona Province (Ag-Pb-Zn, Cu-Au and U Systems)

The Curnamona Province contains the world class Broken Hill Ag-Pb-Zn deposit and consists of the Palaeoproterozoic (~1720-1640 Ma) Willyama Supergroup and coeval magmatic rocks that were deformed and metamorphosed during the ~1600 Ma Olarian Orogeny, which was followed by an early Mesoproterozoic magmatic event. In 2003-04, GA, PIRSA and the ***pmd****CRC* , in conjunction with ANSIR, collected ~200 km of deep seismic reflection data in the South Australian part of the Curnamona Province.

Data from a 1996-97 dynamite-sourced deep seismic reflection survey in New South Wales (Gibson et al., 1998) have been reprocessed using more recent seismic processing techniques and the results combined with the 2003-04 vibroseis-sourced deep seismic survey (Goleby et al., 2006) to produce a single 400 km long transect across the entire Curnamona Province from the Darling Basin in the east to the Flinders Ranges in the west. This transect across the Curnamona Province has provided the first seismic transect across an entire mineral province in Australia, and has provided insights into its crustal architecture and geological evolution (Korsch et al., 2006a).

The original interpretation of the seismic transect in New South Wales indicated that the dominant features seen in the seismic data were a series of reflections that had an apparent dip to the southeast (Gibson et al., 1998). These reflections were interpreted to represent shear zones, some of which were inferred to cut deep into the crust (e.g. Mundi Mundi Fault and King Gunnia Shear Zone). A short high resolution seismic line immediately to the east of Broken Hill acquired in 2005 has provided a much improved image of the upper ~3 km of the crust, including the region between the Stephens Creek and Globe-Vauxhall shear zones (Korsch et al., 2006b), which crosses the northeast extension of the Broken Hill line of lode. This confirmed the southeast dip and thrust geometry to the shear zones.

In South Australia, the seismic transect shows an upper crustal thrust belt, with east-dipping thrusts cutting the Willyama Supergroup, which has been folded to form hanging wall anticlines. This thrust belt sits on a "decollement" defined by strong reflectivity at ~6-9 km depth. The high level thrust belt propagated westwards, with the amount of displacement dying out to the west, and the shortening being accommodated into broad wavelength folds in the near surface.

The seismic transect shows the presence of a linked westward-propagating thrust belt. The thrusts are

thick skinned and cut deep into the crust in the core of the orogen in the vicinity of Broken Hill, whereas to the west, principally in South Australia, the thrust belt is thin skinned and consists of thrusts that link onto a shallow detachment at a depth of ~6-9 km.

Because the thrust belt includes individual folds and thrusts that are interpreted as D_3, it is inferred to have formed late during the ~1600 Ma Olarian Orogeny. Nevertheless, the structures may have been reactivated during later Neoproterozoic and/or Palaeozoic (Delamerian) deformational events. Shear zones exhibiting this timing are well documented at the surface in the southern Curnamona province, and Delamerian deformation is seen at the western end of the profile, where Neoproterozoic rocks are intensely deformed.

The Kalkaroo Cu-Au-Mo deposit, a large tonnage, relatively low grade polymetallic resource, located about 4 km to the north of the seismic line, appears to be associated with second order synthetic D_3 faults associated with hanging wall anticlines above a bounding east-dipping fault at depth. The fault beneath the anticline could have been the conduit for fluids moving from the deep crust to upper crustal levels where they could have migrated into favourable depositional sites associated with the second order structures.

The western limit of the Curnamona Province is defined by a possible suture zone between two different types of lower crust, with the crust in the west below the Flinders Ranges being overthrust by sub-Curnamona crust in the east. The eastern limit of the province is also defined by a crustal-scale, east-dipping structure that thrusts the Neoproterozoic-Phanerozoic Koonenberry Belt over rocks of the Curnamona Province.

The thin-skinned and thick-skinned deformation (D_3) forms a single, linked, westward-propagating thrust belt at c. 1600 Ma. Three geodynamic scenarios are feasible to explain the formation of the thrust belt:

1. The thrust belt is a retroforeland thrust belt formed due to backarc contraction, with a continental margin magmatic arc and subduction zone (with shallow west dip) located to the east,

2. The thrust belt could be part of a collision zone, with the other half of the collision zone (either continent-continent or arc-continent collision) located to the east, or

3. The thrust belt could result from continental intraplate deformation, implying more continental crust to the east.

In every scenario, the eastern part of the system is missing, presumably rifted off during the breakup of Rodinia, and replaced in the Neoproterozoic-Phanerozoic by the Koonenberry Belt during the assembly of Gondwana.

Thomson Orogen-Lachlan Orogen Boundary (Frontier Terrain)

The Neoproterozoic to middle Palaeozoic Thomson Orogen occupies a vast area of western and central Queensland and northwestern New South Wales, but very little is known about it because it is covered by Cainozoic sediments and the Mesozoic Eromanga Basin. A ~290 line km deep seismic reflection survey was conducted in 2005 in New South Wales by GA, Geological Survey of New South Wales (GSNSW) and ***pmd****CRC* , in conjunction with ANSIR, to examine the tectonic and metallogenic implications of a major east-west tectonic boundary with the Lachlan Orogen to the south flanked to the north by a major east-west gravity high, curvilinear aeromagnetic highs and mafic to intermediate igneous rocks reported from drill holes in the southern part of the Thomson Orogen (Glen et al., 2006, 2007).

In the seismic sections, the boundary between the Thomson and Lachlan orogens is imaged as a north-dipping fault zone that cuts through the entire crust and offsets the Moho. Latest movement was in the Carboniferous, during the Kanimblan-Alice Springs Orogeny, because Late Devonian rocks of the

Nelyambo Trough of the Darling Basin are truncated and deformed at the suture, where older rocks of the Thomson Orogen are thrust over the Late Devonian sedimentary rocks. The crust under the Thomson Orogen is much thicker than that under the Lachlan Orogen.

North of this boundary, the similarity of the gravity responses with those of accreted gold- and copper-rich Ordovician Macquarie Arc sampled by seismic reflection profiling in 1997 and 1999 (Glen et al., 2002) suggests that the boundary may be a convergent margin, marked by the possible development of island arc and ocean crustal igneous rocks. This is supported by the recent reporting by Burton et al. (2008) of calc-alkaline volcanic rocks of possible island arc affinity 35 km to the northeast of Bourke in the southern Thomson Orogen.

South of the boundary, there is now increased potential for mineral systems in Early Devonian rift basins (possibly of the style of the nearby Cobar Basin generated by movement on the Thomson-Lachlan boundary imaged by the seismic beneath Late Devonian strata in the Nelyambo Trough of the Darling Basin. The seismic also indicates the possibility of Mississippi Valley mineral systems along the along the margins of the Mt Jack High, that marks the thrust-related southern edge of the Nelyambo Trough.

Central Victoria (Orogenic Au Systems)

The ~400 km long Central Victorian deep crustal reflection seismic survey was carried out in 2006 as a collaborative project between Geoscience Australia, the Victorian Government (Department of Primary Industries and Department of Innovation, Industry and Regional Development, through Geoscience Victoria - GSV), the ***pmd*CRC*** , Gold Fields Australasia Pty Ltd, Lihir Gold Ltd and Northgate Minerals Corporation, using the facilities of ANSIR. The aim was to cross several basement zones and provide information on the crustal architecture, particularly across the highly prospective Palaeozoic rocks occurring along strike to the north of the major Victorian goldfields.

The primary aims of the seismic survey were to investigate (a) the internal structure of the Stawell, Bendigo and Melbourne structural basement zones, (b) the major faults that form the boundaries of basement zones, (c) the distribution of rock units in the crust, and (d) the relationship of major gold deposits to major regional structures in central Victoria. The new seismic data significantly enhance the understanding of the geological evolution of Victoria and help validate regional cross-sections being constructed concurrently for 3D interpretation and the building of a meaningful 3D map of Central Victoria. The new data and their detailed geological interpretation also provide the framework for understanding the controls on gold mineralisation in the western Lachlan Orogen.

The Moyston Fault is a major east-dipping planar fault near the eastern edge of the Delamerian Orogen. It cuts through the entire crust to the Moho. The boundary between the Stawell Zone and the Bendigo Zone farther to the east is the Avoca Fault, which appears to be a west-dipping listric fault that links to the Moyston Fault at a depth of about 22 km, forming a Y-shaped geometry. Internal faults in the Stawell and Bendigo zones are almost entirely west-dipping listric faults, which cut the highly reflective lower crust of these zones. Major gold deposits occur in the hanging wall of the thrust sheet above west-dipping thrust faults, which cut deep into the crust. There is increased potential for gold associated with those faults previously considered to be shallow, but shown by the seismic data to be major structures that cut deep into the crust.

The boundary between the Bendigo and Melbourne zones, the Heathcote Fault Zone, forms a zone of strong west-dipping reflections about three kilometres wide to a depth of at least 20 km, and possibly to the Moho. The Governor Fault, separating the Melbourne Zone from the Tabberabbera Zone, dips to the north at about 10° where the survey crosses it. The seismic character of the lower crust below the Melbourne Zone (the "Selwyn Block") is significantly different to that observed below the Bendigo and Stawell zones, and consists of several very strong subhorizontal reflections about 5-6 km thick starting at about 18 km depth, with a less reflective zone below it.

Mt Isa Province (Pb-Zn, IOCG and U Systems)

In late 2006, GA, Geological Survey of Queensland, ***pmd*****CRC* and Zinifex Limited, in conjunction with ANSIR, undertook deep seismic reflection profiling along six traverses in the Mount Isa region to improve the understanding of the linkages between crustal architecture, fluid flow and regional scale mineral systems and to assist in the discovery of further mineral resources. These traverses complement the regional deep seismic survey conducted by the Australian Geodynamics CRC in 1994 (Drummond et al., 1998; MacCready et al., 1998; MacCready, 2006), and has been reprocessed as part of this project.

The scientific objectives included:

1. Determining the structural and crustal setting of known mineralisation as a guide to finding similar ore bodies and attempt to directly image known fluid conduits and/or alteration systems
2. Imaging the major basement-penetrating faults and shear zones that controlled basin formation plus any major basin-bounding structures that may have acted as fluid conduits for known mineralisation during or subsequent to basin formation
3. Determining the depth, geometry and distribution of pre-1800 Ma basement beneath the Leichhardt and Calvert Superbasins
4. Investigating the relative importance of north-south versus east-west trending structures in basin formation for the Leichhardt River Fault Trough, and northeast- versus northwest-trending structures on the Lawn Hill Platform and determine the extent to which the associated basin architecture is developed farther east in the Eastern Fold Belt
5. Determining the extent of basin inversion related to north-south and/or east-west crustal shortening.
6. Defining the extent, distribution and geometry of Proterozoic rocks below much younger Cambrian rocks and regolith cover to the west and south of Mt Isa, thereby providing an additional interpretative tool to better understand unexposed basement that can be targeted by complementary geophysical methods (e.g. aeromagnetics, gravity and multispectral analysis).

Processing and interpretation of the deep seismic reflection traverses is in progress and the results will be released at a public domain workshop in Mount Isa in late June 2008.

Conclusions

Deep seismic reflection profiles in mineral provinces in Australia are identifying the main crustal-scale architecture which is the key to determining regional scale controls on mineralisation and possible fluid pathways, thus contributing significantly towards the Five Answers to the Five Questions. The results have implications for regional geodynamics and constrain the crustal architectures during the building of 3D geological maps of the regions. The seismic results are challenging our current understanding of the geology, mineral system and ore deposit models, and contributing to the potential prospectivity of Australia.

Acknowledgements

I thank the many geoscientists who have been involved in various stages of the seismic acquisition, processing or interpretation phases for their input, and apologise to any whom I have omitted inadvertently from the list below:

- ***pmd*****CRC* @ **GA:** Bruce Goleby, Richard Blewett, George Gibson, Paul Henson, Karol Czarnota, David Huston, David Champion, Kevin Cassidy, Barry Drummond, David Maidment, Ben Bell, Alan Whitaker, Mike Barlow, Richard Lane, Helen Keogh

- ***pmd*CRC* and ANSIR @ GA:** Tim Barton, Leonie Jones, David Johnstone, Tanya Fomin, Ross Costelloe, Aki Nakamura, Jenny Maher, Hugh Tassell, Erdinc Saygin, Josef Holzschuh.
- **3D, Graphics and Visualisation @GA:** Malcolm Nicoll, Joe Mifsud, Silvio Mezzomo, Angie Jaentsch
- ***pmd*CRC* @ Melbourne University:** Barry Murphy, Ben Jupp, Tim Rawling, Chris Wilson, Lawrence Leader, Alison Dugdale,
- **GSWA:** Bruce Groenewald, Greg Carlsen
- **NTGS:** David Rawlings
- **GSNSW:** Dick Glen, Yvette Poudjom Djomani, Ricky Mantaring, Steve Dick, Barney Stevens
- **PIRSA:** Colin Conor, Wolfgang Preiss, Stuart Robertson, Andy Burtt
- **GSV:** Ross Cayley, David Moore, Vince Morand, Peter O'Shea, Clive Willman, Tim Rawling
- **GSQ:** Laurie Hutton, Ian Withnall
- **Industry:** Angela Lorrigan, Larry Stewart (Zinifex), Neil Norris, Andrea Reed (Northgate), Geoff Turner (Gold Fields)

References

Archibald, N. 1998. 3-D Geology and Tectonic Synthesis of the Kalgoorlie terrain. In: Geodynamics and gold exploration in the Yilgarn. Australian Geodynamics Cooperative Research Centre, Workshop Abstracts, 17-22.

Barnicoat, A.C., 2007. Mineral systems and exploration science: linking fundamental controls on ore deposition with the exploration process. In: Andrew, C.J. et al., eds, Digging Deeper. Proceedings of the Ninth Biennial Meeting of the Society for Geology Applied to Mineral Deposits, Irish Association for Economic Geology, vol. 2, 1407-1410.

Blewett, R., Champion, D., Whitaker, A., Bell, B., Nicoll, M., Goleby, B., Cassidy, K. & Groenewald, B., 2002. A new 3D model of the Leonora-Laverton Transect: implications for the tectonic evolution of the eastern Yilgarn Craton. In: Vearncombe, S. (ed. Applied Structural Geology of Mineral Exploration and Mining. Australian Institute of Geoscientists Bulletin, 36, 18-21.

Burton, G.R., Dadd, K.A. & Vickery, N.M., 2008. Volcanic arc-type rocks beneath cover 35 km to the northeast of Bourke. Quarterly Notes of the Geological Survey of New South Wales, 127, 1-23.

Czarnota, K., Blewett, R.S., Champion, D.C., Henson, P.A. & Cassidy, K.F., 2007. Significance of extensional tectonics in orogenic gold systems: an example from the Eastern Goldfields Superterrane, Yilgarn Craton, Australia. In: Andrew, C.J. et al., eds, Digging Deeper. Proceedings of the Ninth Biennial Meeting of the Society for Geology Applied to Mineral Deposits, Irish Association for Economic Geology, vol. 2, 1431-1434.

Drummond, B.J., Goleby, B.R., Goncharov, A., Wyborn, L.A.I., Collins, C.D.N. & MacCready, T., 1998. Crustal-scale structures in the Proterozoic Mount Isa Inliert of north Australia: their seismic response and influence on mineralisation. Tectonophysics, 288, 43-56.

Garven, G., Bull, S.W. & Large, R.R., 2001. Hydrothermal fluid flow models of stratiform ore genesis in the McArthur Basin, Northern Territory, Australia. Geofluids, 1, 289-311.

Gibson, G., Drummond, B., Fomin, T., Owen, A., Maidment, D., Gibson, D., Peljo, M. & Wake-Dyster, K., 1998. Re-evaluation of crustal structure of the Broken Hill Inlier through structural mapping and seismic profiling. Australian Geological Survey Organisation, Record, 1998/11, 55pp.

Glen, R.A., Korsch, R.J., Direen, N.G., Jones, L.E.A., Johnstone, D.W., Lawrie, K.C., Finlayson, D.M. & Shaw, R.D., 2002. Crustal structure of the Ordovician Macquarie Arc, eastern Lachlan Orogen, based on seismic reflection profiling. Australian Journal of Earth Sciences, 49, 323-348.

Glen, R.A., Korsch, R.J., Costelloe, R.D., Poudjom Djomani, Y. & Mantaring, R., 2006. Preliminary results from the Thomson-Lachlan Deep Seismic Survey, northwest New South Wales. In Lewis, P., ed., Mineral exploration geoscience in New South Wales. Extended Abstracts, Mines and Wines Conference, Cessnock, NSW. SMEDG, Sydney, 105-109.

Glen, R.A., Poudjom Djomani, Y., Korsch, R.J., Costelloe, R.D., & Dick, S., 2007. Thomson-Lachlan seismic project – results and implications. In: Lewis, P., ed., Mines & Wines 2007: Mineral Exploration in the Tasmanides. Australian Institute of Geoscientists Bulletin, 46, 73-78.

Goleby, B.R., Korsch, R.J., Fomin, T., Bell, B., Nicoll, M.G., Drummond, B.J. & Owen, A.J., 2002a. A 3D interpretation of the Kalgoorlie region, Eastern Goldfields, Western Australia from deep seismic reflection and potential field data. In: Korsch, R.J., ed., Geodynamics of Australia and its mineral systems: mineral provinces, Australian Journal of Earth Sciences, 49, 917-933.

Goleby, B.R., Blewett, R.S., Champion, D.C., Korsch, R.J., Bell, B., Groenewald, P.B., Jones, L.E.A., Whitaker, A.J., Cassidy, K.F. & Carlsen, G.M., 2002b. Deep seismic profiling in the NE Yilgarn: insights into its crustal architecture. In: Vearncombe, S., ed., Applied Structural Geology of Mineral Exploration and Mining. Australian Institute of Geoscientists Bulletin, 36, 63-66.

Goleby, B.R., Blewett, R.S., Groenewald, P.B., Cassidy, K.F., Champion, D.C., Jones, L.E.A., Korsch, R.J., Shevchenko, S. & Apak, S.N., 2003. The 2001 Northeastern Yilgarn deep seismic reflection survey. Geoscience Australia, Record, 2003/28, 143 pp.

Goleby, B.R., Blewett, R.S., Korsch, R.J., Champion, D.C., Cassidy, K.F., Jones, L.E.A., Groenewald, P.B. and Henson, P., 2004. Deep seismic reflection profiling in the Archaean northeastern Yilgarn Craton, Western Australia: implications for crustal architecture and mineral potential. Tectonophysics, 388, 119-133.

Goleby. B.R., Korsch, R.J., Fomin, T., Conor, C.H.H, Preiss, W.V., Robertson. R.S. & Burtt, A.C., 2006. The 2003-2004 Curnamona Province seismic survey. Geoscience Australia, Record, 2006/12, 96 pp. http://www.ga.gov.au/about/corporate/ga_authors/record2006_12.jsp

Korsch, R.J., Fomin, T., Conor, C.H.H., Stevens, B.P.J., Goleby, B.R., Robertson, R.S. & Preiss, W.V., 2006a. A deep seismic reflection transect across the Curnamona Province from the Darling Basin to the Flinders Ranges. Geoscience Australia, Record, 2006/21, 102-109. https://www.ga.gov.au/image_cache/GA8853.pdf

Korsch, R.J., Fomin, T. & Stevens, B.P.J., 2006b. Preliminary results of a high resolution seismic reflection survey at Broken Hill. Geoscience Australia, Record, 2006/21, 110-115. https://www.ga.gov.au/image_cache/GA8853.pdf

MacCready, T., Goleby, B.R., Goncharov, A., Drummond, B.J. & Lister, G.S., 1998. A framework of overprinting orogens based on interpretation of the Mount Isa deep seismic transect. Economic Geology, 93, 1422-1434.

MacCready, T., 2006. Structural cross-section based on the Mt Isa deep seismic transect. Australian Journal of Earth Sciences, 53, 5-26.

Price, G.P. & Stoker, P., 2002. Australian Geodynamics Cooperative Research Centre's integrated research program delivers a new minerals exploration strategy for industry. Australian Journal of Earth Sciences, 49, 595-600.

Rawlings, D.J., Korsch, R.J., Goleby, B.R., Gibson, G.M., Johnstone, D.W. & Barlow, M., 2004. The 2002 Southern McArthur Basin Seismic Reflection Survey. Geoscience Australia, Record, 2004/17, 78pp. https://www.ga.gov.au/image_cache/GA5568.pdf

Williams, N. 1978. Studies of the base metal sulfide deposits at McArthur River, Northern Territory, Australia; II, The sulfide-S and organic-C relationships of the concordant deposits and their significance. Economic Geology, 73, 1036-1056.

Geodynamics: Linking geochronology and structural evolution at Stawell

JOHN MILLER[1], CHRISTOPHER WILSON[2] AND DAVID PHILLIPS[2]

[1]*pmd***CRC*, Centre for Exploration Targeting, School of Earth and Geographical Sciences, University of Western Australia, 35 Stirling Highway, Crawley, WA 6009
[2]*pmd***CRC*, School of Earth Sciences, University of Melbourne, VIC 3010
jmmiller@cyllene.uwa.edu.au

Previous geochronology studies have identified multiple episodes of gold mineralisation between 455 Ma and 380 Ma in the Palaeozoic Victorian goldfields (Foster et al., 1998; Bierlein et al., 1999, 2001; Arne et al., 2001). This implies a long-lived geodynamic history. The structural complexity and gold-lode styles of the two largest primary gold deposits, at Stawell and Bendigo, however, are totally different (Miller & Wilson, 2002), despite similar ca. 440 Ma ages reported for ore-related minerals (Foster et al., 1998). The Stawell gold deposit has four major phases of deformation, with gold developing at a late stage in the fourth deformation event within poly-deformed and refolded rocks. In contrast, the Bendigo and Ballarat deposits occur in simple, upright folded successions. All of these deposits have previously been defined as occurring within the Lachlan Orogen, which lies to the East of the older Cambrian Delamerian Orogen.

$^{40}Ar/^{39}Ar$ age data from rocks that host the Stawell deposit indicate that the rocks are actually part of the older Cambrian Delamerian Orogen that was reworked during later orogenesis associated with the development of the Lachlan Orogen and the formation of ca. 440 Ma gold deposits (Miller et al., 2005). This has major implications for the tectonic evolution of the Tasmanides, and also raises the possibility of more ca. 440 Ma world class ore bodies lying within other reworked parts of the Cambrian Delamerian Orogen in Victoria and New South Wales.

The revised tectonic model places the Stawell gold deposit within a Cambrian metamorphic belt (=Delamerian age orogenesis) in the western Stawell Zone of the Palaeozoic Tasmanides System of southeastern Australia. The Ross and Delamerian systems of Antarctica and Australia reflect deformation processes associated with a Cambrian subduction zone that dipped towards the Gondwana supercontinent. $^{40}Ar/^{39}Ar$ age data indicate rapid cooling of the rocks in the Stawell region at about 500 Ma, temporally associated with calc-alkaline volcanism, followed by clastic sedimentation. Extension in the overriding plate of a subduction zone is interpreted to have exhumed the metamorphic rocks that host the Stawell gold deposit. Some of this geodynamic history has similarities to the evolution of the Western Tasmanian Cambrian Tyennan Orogen that hosts major copper, gold, and lead-zinc systems within the Cambrian Mount Read Volcanics.

The orogenesis that formed the Western Lachlan Orogen occurred about 40 million years after the Delamerian Orogeny. This closed a marginal ocean basin by west-directed underthrusting that produced a thrust belt with west-dipping faults. The major ca. 440 Ma orogenic gold deposits in the western Victorian goldfields have markedly different structural complexity, but all formed during east–west shortening. The structural complexity of the ca. 440 Ma Stawell gold deposit reflects its location in a reworked part of the Cambrian Delamerian Orogen, whereas the structurally simpler ca. 440 Ma Bendigo deposit is hosted by younger Ordovician turbidites that had not been deposited when the Cambrian deformation and metamorphism affected the rocks that host the Stawell deposit. At Stawell, a strike-change along a pre-existing Cambrian fault system above a major lithospheric boundary was reactivated during the ca. 440

Ma gold event. This boundary can be traced to a depth of 90 kilometres by P-wave velocity variations (Graeber et al., 2002). In the Bendigo Zone, 440 Ma orogenic-gold deposits have a trend oblique to the dominant structural grain and this is parallel to the western edge of an inferred underlying crystalline basement block that was defined as the Selwyn Block by Cayley et al. (2002).

During the evolution of the Lachlan Orogen, major variations in the regional stress fields occurred between 425 and 370 Ma. Some world class (> 4 million ounces) gold deposits formed between 380 Ma and 370 Ma. Field mapping at Stawell, integrated with existing geochronology, indicates that the 425–400 Ma period at Stawell records sinistral strike-slip faulting associated with gold mineralisation, southeast-directed faulting, intrusion-related gold mineralisation and extensive high-level Early Devonian plutonism. The gold deposits that formed in the 425–400 Ma period have relatively small endowments, but they introduce a marked amount of mineralogical and structural complexity to the gold province, and in places cause up-grading of deposits containing older stages of gold mineralisation.

Acknowledgements

This work evolved from ARC SPIRT Grant C39805027 (Completed January 2002), ARC LINKAGE Grant LP0211491 and work funded by the Predictive Mineral Discovery Cooperative Research Centre.

References

Arne, D.C., Bierlein, F.P., Morgan, J.W. & Stein, H.J., 2001. Re-Os dating of sulfides associated with gold mineralization in central Victoria. Economic Geology, 96, 1455-1459.

Bierlein, F.P., Foster, D.A., McKnight, S. & Arne, D.C., 1999. Timing of gold mineralization in the Ballarat goldfields, central Victoria: constraints from ^{40}Ar-^{39}Ar results: Australian Journal of Earth Sciences, 46, 301-309.

Bierlein, F.P., Arne, D.C., Foster, D.A. & Reynolds, P., 2001. A geochronological framework for orogenic gold in central Victoria, Australia. Mineralium Deposita, 36, 741-767.

Cayley, R.A., Taylor, D.H., VandenBerg, A.H.M. & Moore D.H. 2002. Proterozoic - Early Palaeozoic rocks and the Tyennan Orogeny in central Victoria: the Selwyn Block and its tectonic implications. Australian Journal of Earth Sciences, 49, 225-245.

Foster, D.A., Gray, D.R., Kwak, T.A.P. & Bucher, M., 1998. Chronology and tectonic framework of turbidite hosted gold deposits in the western Lachlan Fold Belt, Victoria: ^{40}Ar-^{39}Ar results. Ore Geology Reviews, 13, 229-250.

Graeber, F.M., Houseman, G.A. & Greenhalgh, S., 2002. Regional teleseismic tomography of the western Lachlan Orogen and the Newer Volcanic Province, southeast Australia. Geophysical Journal International, 149, 249–267.

Miller, J.McL. & Wilson, C.J.L., 2002. The Magdala Lode System, Stawell, southeastern Australia: structural style and relationship to gold mineralization across the western Lachlan Fold Belt. Economic Geology, 97, 325-349.

Miller, J.McL., Phillips, D., Wilson, C.J.L. & Dugdale, L.J., 2005. Evolution of a reworked orogenic zone: the boundary between the Delamerian and Lachlan Fold Belts, southeastern Australia. Australian Journal of Earth Sciences, 52, 921-940.

Architecture: using Leapfrog to link structure and spatial data

JOHN MCLEOD MILLER

*pmd**CRC, Centre for Exploration Targeting, School of Earth and Geographical Sciences, University of Western Australia, 35 Stirling Highway, Crawley, WA 6009
jmmiller@cyllene.uwa.edu.au

Traditional structural mapping approaches, using section and plan mapping and interpretation, can result in a large amount of mapping time that is not efficiently targeted, with non-critical areas being mapped as a result. This can delay the implementation of other research avenues that can have a major impact. Traditional sectional structural analysis approach is also commonly restricted by an inability to rapidly access 3D mine data, and can also be hampered by a lack of integration with geochemical data sets (e.g., arsenic, gold, etc.). This paper describes a laptop analysis approach integrated into structural mapping programs. Whilst there are multiple software packages available, this paper highlights the utilisation of FracSIS (Runge Ltd) to integrate and visualise data and also Leapfrog (Zaparo Ltd) to model drillhole databases and visualise existing wireframes with the newly generated isosurfaces. A description of the approach, and a short overview of a case study at the Wallaby gold deposit, Western Australia, is given below.

A revised structural mapping approach is as follows:

1. Utilise a program such as FracSIS (Runge Ltd) to compile mine data (development, grade shells etc.)
2. Utilise Leapfrog (Zaparo Ltd) to generate isosurfaces of grade, rock types, alteration and any other code recorded in the diamond drillhole database that could be relevant. These are then incorporated into the digital model with the mine data. Leapfrog isosurfaces are normally initially run as isotropic fits and also with anisotropy parallel to existing trends observed within the compiled mine wire frames.
3. Use the digital model to target surface or underground mapping areas (or drillholes).
4. Undertake standard systematic structural mapping in these target areas.
5. Run additional Leapfrog models using the knowledge gained from observations made during the mapping. Additional models commonly isosurface key alteration types linked to ore, or incorporate new mapping data (such as dyke, bedding or foliation trends) to run anisotropic models.

The Leapfrog isosurfaces of rock and alteration types are produced as follows:

- Drilling data composited to mid points (interval depends on scale)
- Code all units that are to be incorporated into the wire frame as 2
- Code all other units as 1
- Use Leapfrog to produce a isosurfaces between 1 and 2 (1.3 to 1.5 are common values used)
- Initially run isotropic models, but also anisotropic models are run.

Whilst the isosurfacing approach using Leapfrog is restricted by drilling density (and the consistency of drillhole logging), it has the advantage of being very quick; poor modeling outcomes do not adversely

affect the time frame of the study. The approach is not restricted totally by the current view of a given deposit (and the existing wire frames), with the ability to generate new isosurfaces that can be field tested immediately. This produces feedback loops where the 3D model can aid in identifying key field sites to map, which then leads to new isosurfaces being generated that further aid the understanding of a system. The result is a flexible 3D model with multiple generations of wireframes for different elements of a given system that is responsive to new data input. It also incorporates geology data logged from drill core that are not present in many existing 3D models.

Application to the Wallaby gold deposit, Laverton, Western Australia

The Wallaby gold deposit occurs within an Actinolite-Magnetite-Epidote-Calcite (AMEC) alteration pipe associated with a pipe-like syenite body that intruded a massive conglomerate unit (Salier et al., 2004). The low-angle gold lodes overprint the AMEC pipe with the assemblage dolomite-quartz-pyrite-calcite-sericite±hematite (Salier et al., 2004). As part of a structural mapping program done within the Predictive Mineral Discovery Cooperative Research Centre, Leapfrog models of the Wallaby Syenite were produced using isotropic and anisotropic fits (Figure 1). The anisotropic fits modeled the syenites

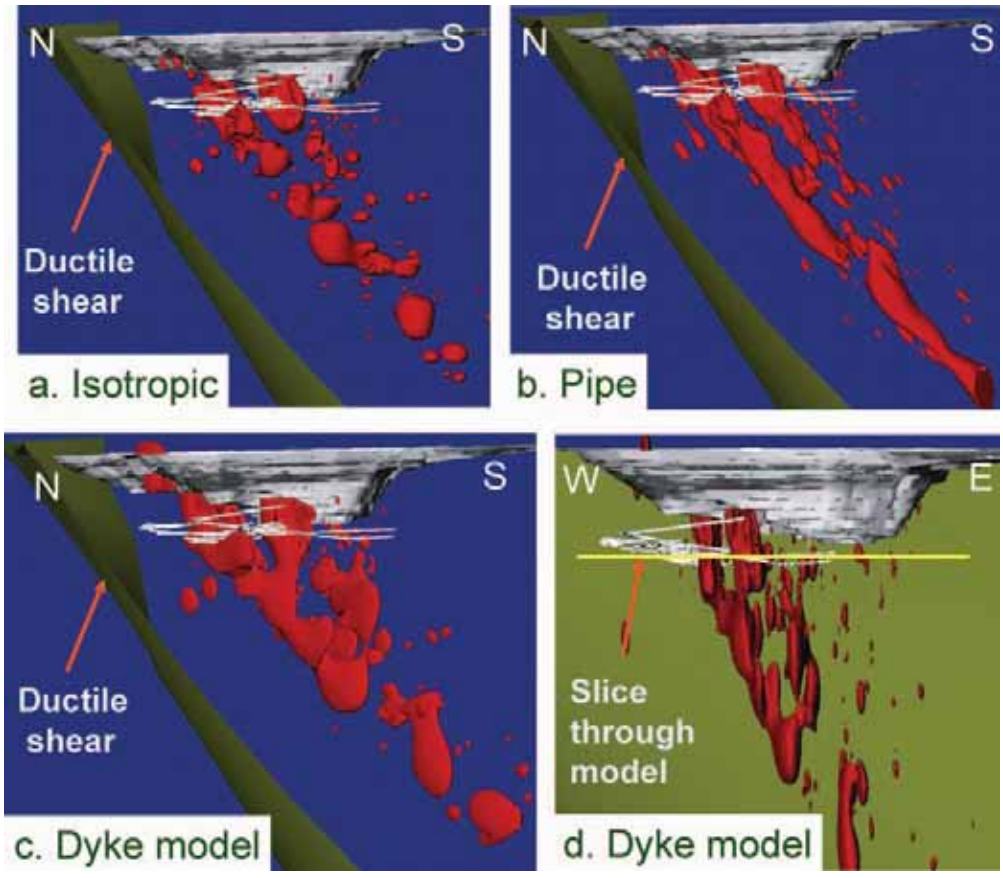

Figure 1. Leapfrog models of intrusive rocks viewed in FracSIS (combines all intrusive rocks except for lamprophyres), ductile footwall shear, pit shell and development also shown. Ductile shear wireframe produced by geology staff from Barrick Gold of Australia Limited. (a) Isotropic fit. (b) Pipe geometry (fitted for a plunge of 60° to the south with Leapfrog anisotropy of 2 1 1). (c and d) Two views of the dyke model. This used an anisotropic fit that followed the dominant syenite dyke trend in the open pit (north-northeast), Leapfrog anisotropy of 4 4 1. Line highlights position of section plan in Figure 3. In reality, the actual system is a combination of dyke and pipe geometries, with more than one dyke trend.

as a 'pipe' and with the dominant dyke trend present in the existing mine wire frames ('dyke fit'; Figure 1). Models of geology-logged, alteration types that had an association with gold were also generated.

A key feature observed within the 3D digital model prior to mapping, was that the syenite appeared to be offset in directions inconsistent with preexisting structural models. Also the complex 3D distribution of the syenites (e.g., pinch and swell geometries) appeared to have a control on the gold lode locations, with lodes located across thinner 'neck' regions of the intrusive bodies (Figure 2). The Leapfrog alteration models also showed complex distributions.

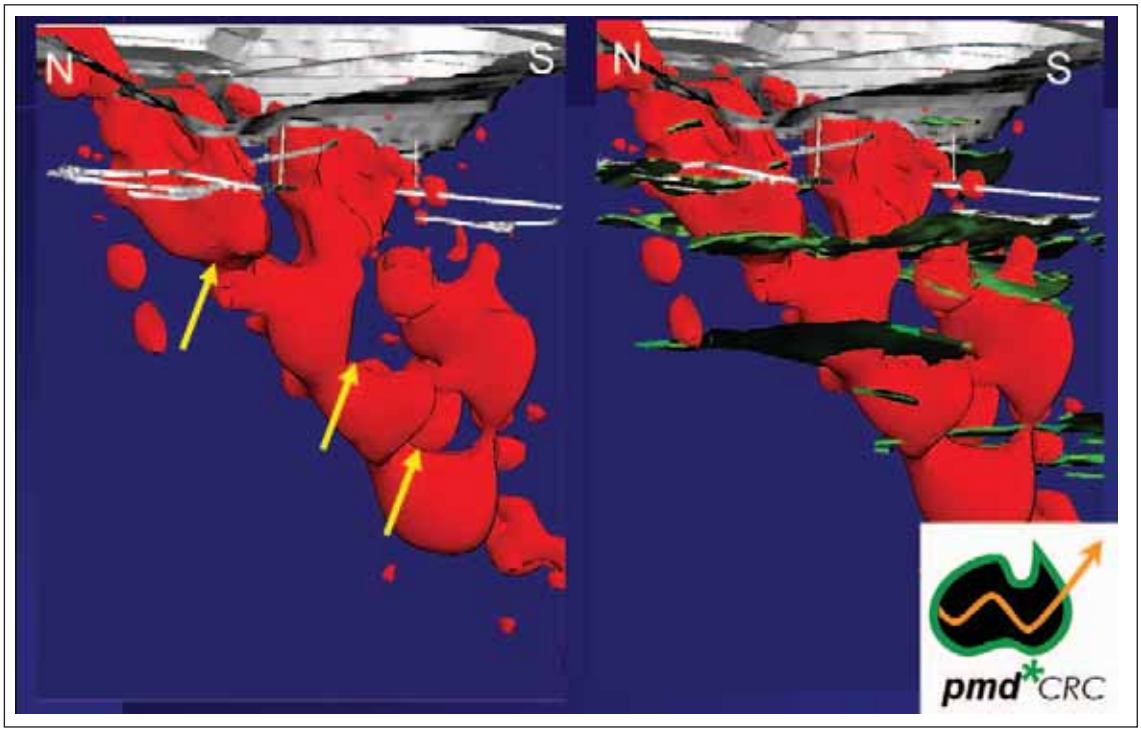

Figure 2. Leapfrog models of intrusive rocks viewed in FracSIS highlighting the lodes (green grade shells) being linked to breaks within the syenite intrusives. Grade shells produced by geology staff from Barrick Gold of Australia Limited.

Underground mapping (Figure 3) of the syenite contact with the conglomerates confirmed that the 'dyke' Leapfrog model was a close match to reality (the contact was normally within 5 metres, with exceptions being areas where the geology was defined by extensive syenite dykes). Furthermore, the observed offset direction of the syenites across the gold lodes in the Leapfrog model was also correct. Systematic structural mapping of fault-vein intersections (with niche sampling of grade) delineated the trends of fracture-mesh associated mineralisation within the deposit. The geometry of these fracture meshes was linked back to the existing grade shells, producing a good correlation between meso- and macro-scale features.

One key observation from the mapping was that there were actually two phases of fracture-mesh hosted gold lodes that could be linked back to the existing grade shells (this was interpreted to reflect a change in σ_2, and thus σ_2 permeability, with a resultant change in ore shoot orientation). The earliest set of lodes was associated with hematite alteration that had more gently dipping fault-vein intersections compared to later fracture-meshes. These early hematite-associated lodes were offset and deformed by the younger fracture-meshes. Apart from there being a difference in fracture-mesh geometry, the disseminated wall rock alteration linked to the hematite-associated lodes had different gold grades (compared to later fracture-meshes). These two observations meant that delineating the distribution

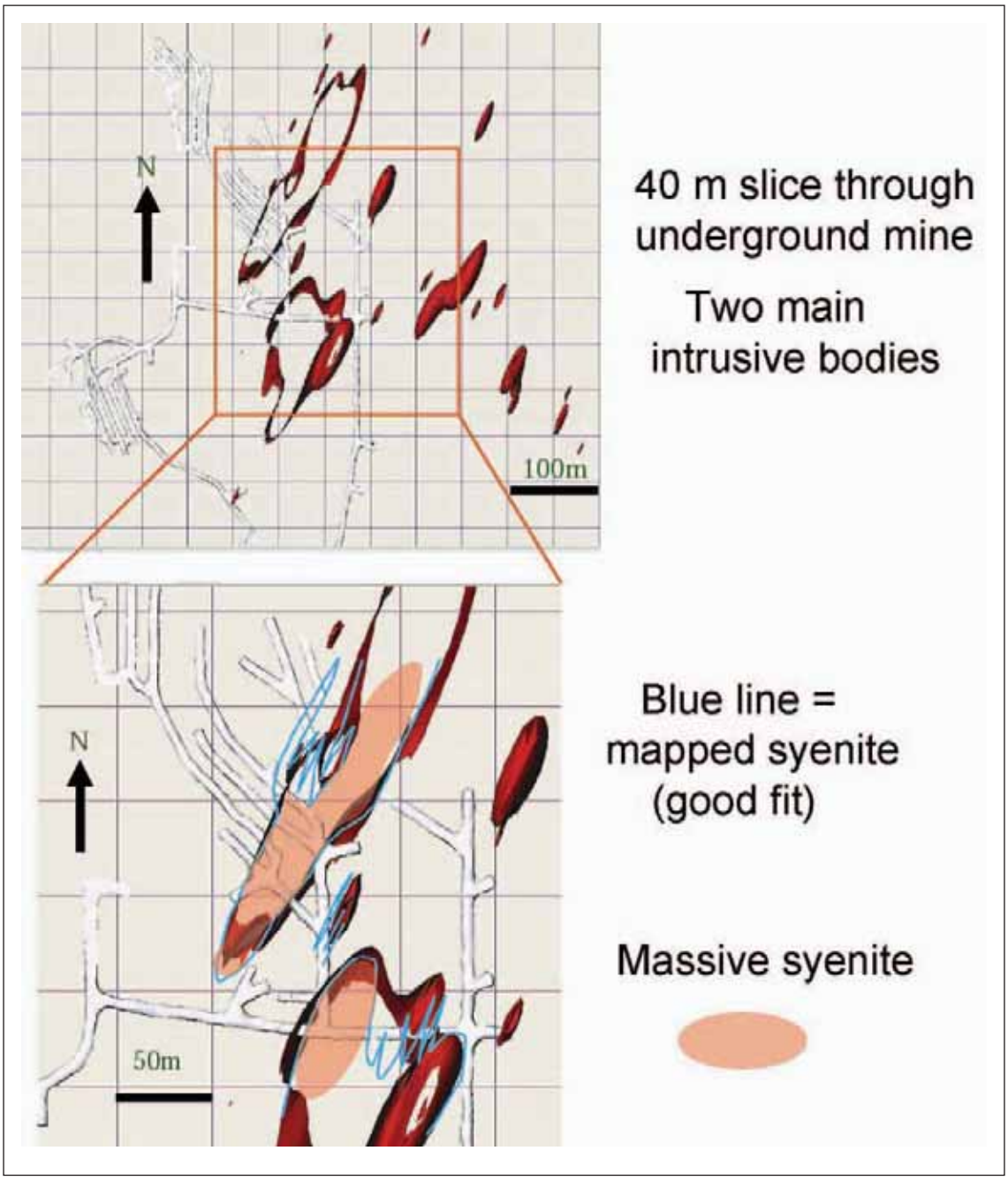

Figure 3. Horizontal slice through Leapfrog dyke fit to rocks viewed in FracSIS (line in Figure 1 highlights slice location). Note: two intrusive bodies were delineated in the model. This was confirmed by underground mapping (blue line). The major deviations from the model to actual distributions occurred where the intrusion split into multiple dykes. Note light red coloured areas are regions where massive syenite (instead of sheeted dykes) occurs.

of the hematite-lodes was one key aspect to understanding the grade distribution within the deposit. Additional Leapfrog models of the hematite alteration (rock code ASRH) were generated as a result of the field observations; these successfully identified the major structures linked to hematite-associated ore within the deposit.

The initial structural mapping underground was able to constrain the geometry of the fracture-mesh associated ore shoots. The Leapfrog alteration models for one area of the deposit, however, had a grade-related alteration trend that was substantially different to ore shoots linked to the intersection of the observed brittle deformation features. Based on its Leapfrog alteration pattern within the 3D digital model (Figure 4), this area of the mine became a key priority area to map, as it appeared to represent a well-defined, broad and continuous package of ore-related alteration, although it did not follow any trends apparent in the brittle features mapped in the mine. The mapping of this area found that localised zones of ductile shears and associated foliation had a major control on the formation of the gold lodes. The ore shoots in the Leapfrog alteration model actually reflected the intersection between these ductile shears and cross-cutting brittle faults, with a substantial amount of wall rock alteration following the pre-existing ductile shears (Figure 5a). The intersection of these two features (Figure 5b) matched the observed alteration shoot produced in the 3D Leapfrog model by modeling geology-logged alteration codes (Figure 4). Compared to areas with massive conglomerate, the presence of ductile shears was linked to the development of wider zones of alteration that are economic to mine. This highlighted the need for the Wallaby mine geologists to not just focus on the brittle features, but to understand the distribution of ductile zones of shearing within the deposit. The ductile shears are inferred to both chemically and mechanically prepare the rocks making them more susceptible to developing ore-related alteration around intersecting brittle faults. The mine geologists subsequently domained these ductile zones throughout the entire ore body.

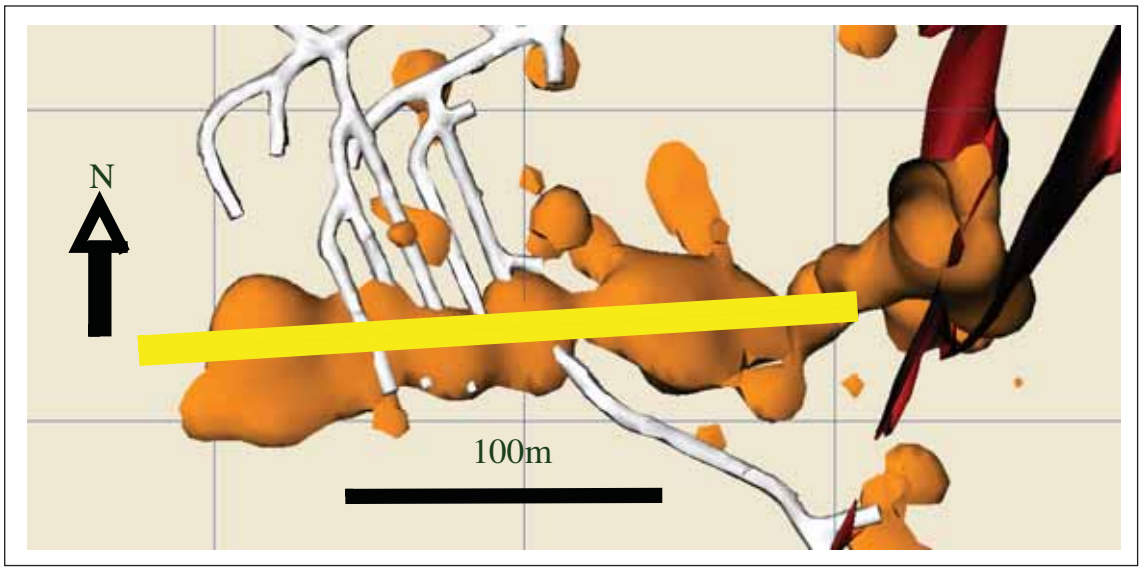

Figure 4. Snapshot of Leapfrog model (B21, B22 area, Wallaby Mine) of ore-related alteration (this combined all geology-logged rock codes linked to gold), viewed in FracSIS. This produced a strong east-trending alteration shoot which matches the mapped faults/foliation intersection (Figure 5).

Summary of mapping approach

The Wallaby project is an example of a structural mapping approach that integrated the existing mine data into a 3D model and also generated models of geology logged rock and alteration codes prior to and during the underground and pit mapping. This minimised the mapping of non-critical areas and extracted critical additional knowledge from the drillhole database.

Acknowledgements

This work has been done as part of the Y4 *pmd**CRC program. Susan Drieberg was critical in facilitating

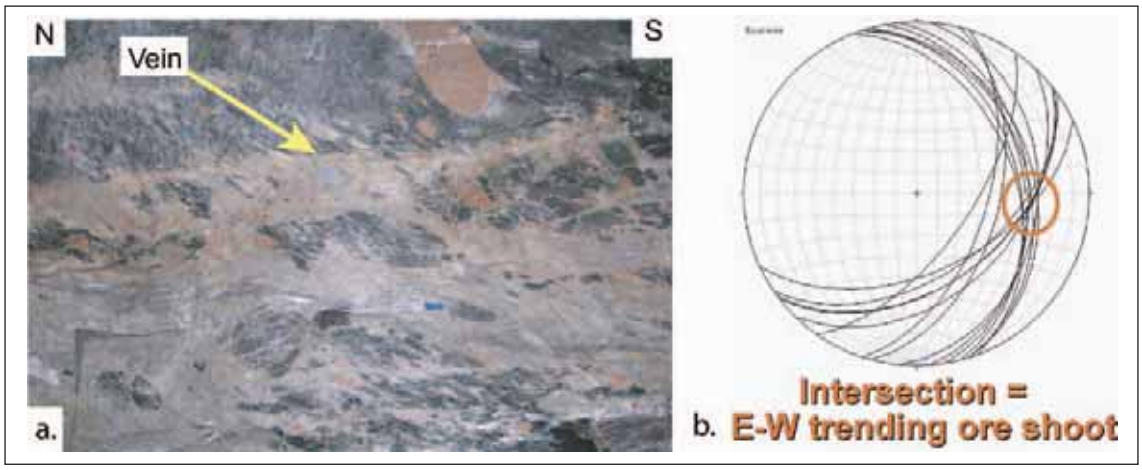

Figure 5. (a) Photo of hematite-associated alteration following earlier ductile shear/foliation. The intersection of these matches the ore shoot (see Figure 4). (b) Stereonet plot of faults (east-dipping) and foliation/ductile shears (southeast- to south-southeast dipping) in the B210-200 drive. The intersection is east-trending and matches the alteration trend in Figure 4.

the initial research and also demonstrated all of the key alteration types and intrusive rocks. Bruce Robertson is thanked for extensive aid in accessing drill data, wire frames and mapping, and making the project work.

Reference

Salier, B.P., Groves, D.I., McNaughton, N.J. & Fletcher, I.R., 2004. The world-class Wallaby gold deposit, Laverton, Western Australia: An orogenic-style overprint on a magmatic-hydrothermal magnetite-calcite alteration pipe? Mineralium Deposita, 39, 473–494.

Architecture: Worms and what they can show

F. C. (BARRY) MURPHY

*pmd*CRC*, School of Earth Sciences, University of Melbourne, VIC 3010
bmurphy@unimelb.edu.au and fcm@fractore.com

Introduction

Mineral explorers must make area reduction decisions based on some a priori knowledge and understanding of a range of data inputs with varying reliability. In particular, huge investments are made in the acquisition of gravity and aeromagnetic data, yet the interpretation of such data can fall short of the mark because there is a high degree of uncertainty or ambiguity involved with its interpretation. Ambiguity in potential field interpretation arises from the fact that an infinite number of 3D distributions of susceptibility or density can derive from the same measurements in the magnetic or gravity fields respectively. Gradients in the potential field are important, as they reflect density and/or magnetic susceptibility contrasts due to changes in rock composition. The positions and nature of such gradients are a key element in developing a geological interpretation of the architecture. A range of image processing and 2D edge enhancement techniques are commonly applied such data. Notwithstanding this, the ambiguity and range of possible interpretations remains large.

To reduce this ambiguity, CSIRO in collaboration with Fractal Graphics, through the Australian Geodynamics Cooperative Research Centre (AGCRC), developed an automated edge detection routine, using wavelet-based algorithms, to detect the positions of maximum gradients across multiple heights of upward continuation (loosely termed 'worms'; Hornby et al., 1999; Archibald et al., 1999; Holden et al., 2000). The advantage of this approach is that it provides a 3D floating point representation of the gradient fields that permits rapid, repeatable interpretations of the data. Although there is still ambiguity in how to interpret such data, in effect, the worms help to 'steady the hand' of the interpreter and give a 3D appreciation of the gradients that is superior to traditional 2D image enhancement methods.

Once generated, however, the interpreter is faced with a huge volume of data points (up to millions) which are cumbersome to manipulate and visualise in 3D and, especially, in 2D platforms. The 3D FracSIS software platform was developed in response to the need to visualise such information. On a 2D platform, an optimisation routine was developed through the ***pmd*CRC*** to convert the 3D data into 2D images and related vector outputs, using the ***pmd*CRC***'s Geoscope software. This makes the worm data more amenable to quantitative GIS treatments.

What are worms?

Worms are points of maximum gradient derived through a process of wavelet transformation and upward continuation of potential field grids. These points are 'floating' in 3D space and, when visualised across multiple levels of upward continuation, appear to coalesce as 3D worm 'sheets' (Hornby et al., 1999; Archibald et al., 1999). The points record the position (xyz) and amplitude (w) of gradients (Figure 1). Hornby et al. (1997) have shown that, with the use of an appropriate wavelet, derived from Green's function of gravitational acceleration, the measured potential field, or its spatial derivatives, can be treated as transforms of the source distribution. In other words, a complete or observed signal is broken down into a series of components or wavelets. Importantly, there is equivalence between the potential field

upward continuation and the change in scale in wavelet analysis. Through selection of appropriate scaling and gridding functions, this relationship is optimised for the production of worms. Worms at the lowest level of upward continuation are termed 'fine-scale' worms, and are short wavelength-high frequency edges in the near-surface environment. Worm sheets persist to varying heights of upward continuation, depending on the nature of the geological edge. Those that continue to high levels of upward continuation are termed 'coarse-scale', being long wavelength-low frequency edges. With some exceptions, coarse-scale worms generally relate to deeper levels and more persistent crustal sources.

A key assumption underlying the interpretation is that apparent edges in the potential field relate to a geological contact (Archibald et al., 1999). Synthetic models (e.g., Figure 1) indicate that, up to the w maxima (Holden et al., 2000), the dip direction of a worm sheet can be a mirror image of the related geological contact (e.g., folds, faults, intrusive bodies). Using the height (z) and length persistence of worms, inferences can be made about the depth of penetration of a geological edge (Murphy et al., 2004).

Naturally, contacts with no density contrast across them (e.g., some faults) are 'blind' to the edge picking algorithm. Such faults, however, can be inferred through linear breaks in, and offsets of, the worm sheets. As the worming process requires a regular grid of data, and regional surveys rarely conform to this, data may need to be introduced to 'pad out' the grid and, in some instances, the survey boundary may itself create an artificial worm.

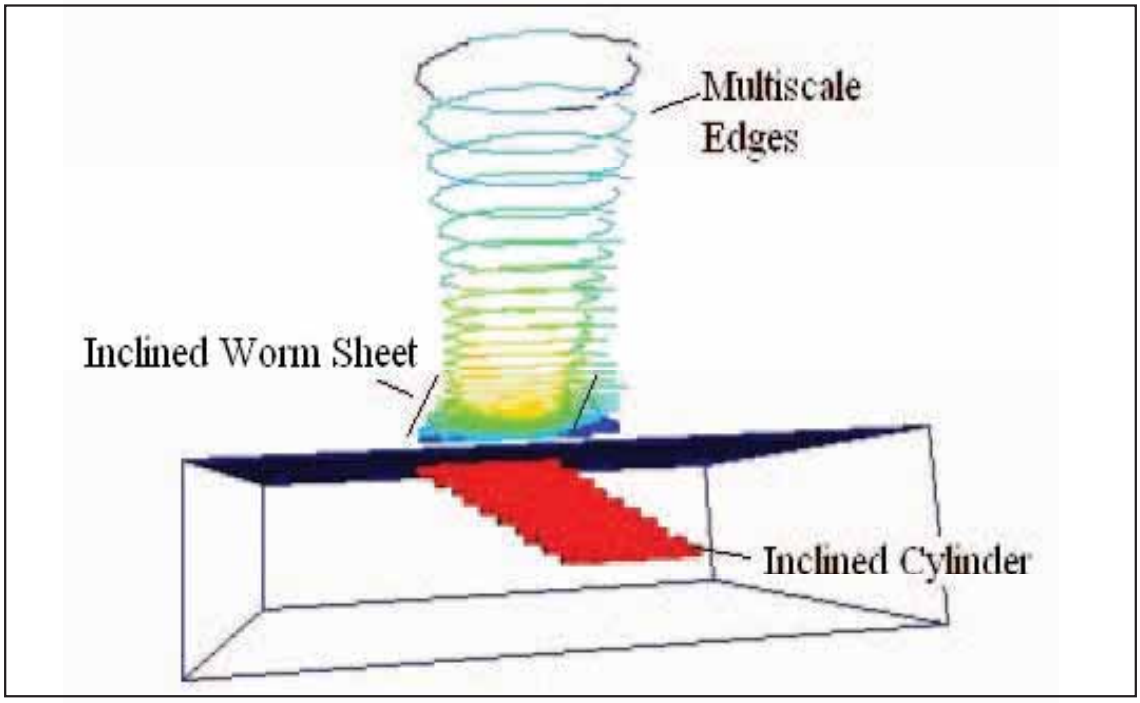

Figure inclined worm sheet mirrors the dip of the cylinder, and the amplitude (w) increases with height (z) towards a maximum (warmer colours); modified from Archibald et al. (1999).

What to do with worms?

The 3D nature of the worm data provides key information on the location, dip direction and depth extent of gradients. Such interpretations, however, need to be made in combination with other data sets, rather than used in isolation, as ambiguity remains an issue. In profile view, the upward continued

levels help to constrain the nature of geological contracts and, in combination with other geophysical and geological data, such outputs can be used in building 3D geological models derived from serial geological cross sections, such as in Western Victoria (Figure 2; Murphy et al., 2006) and in Tasmania (Murphy et al., 2004).

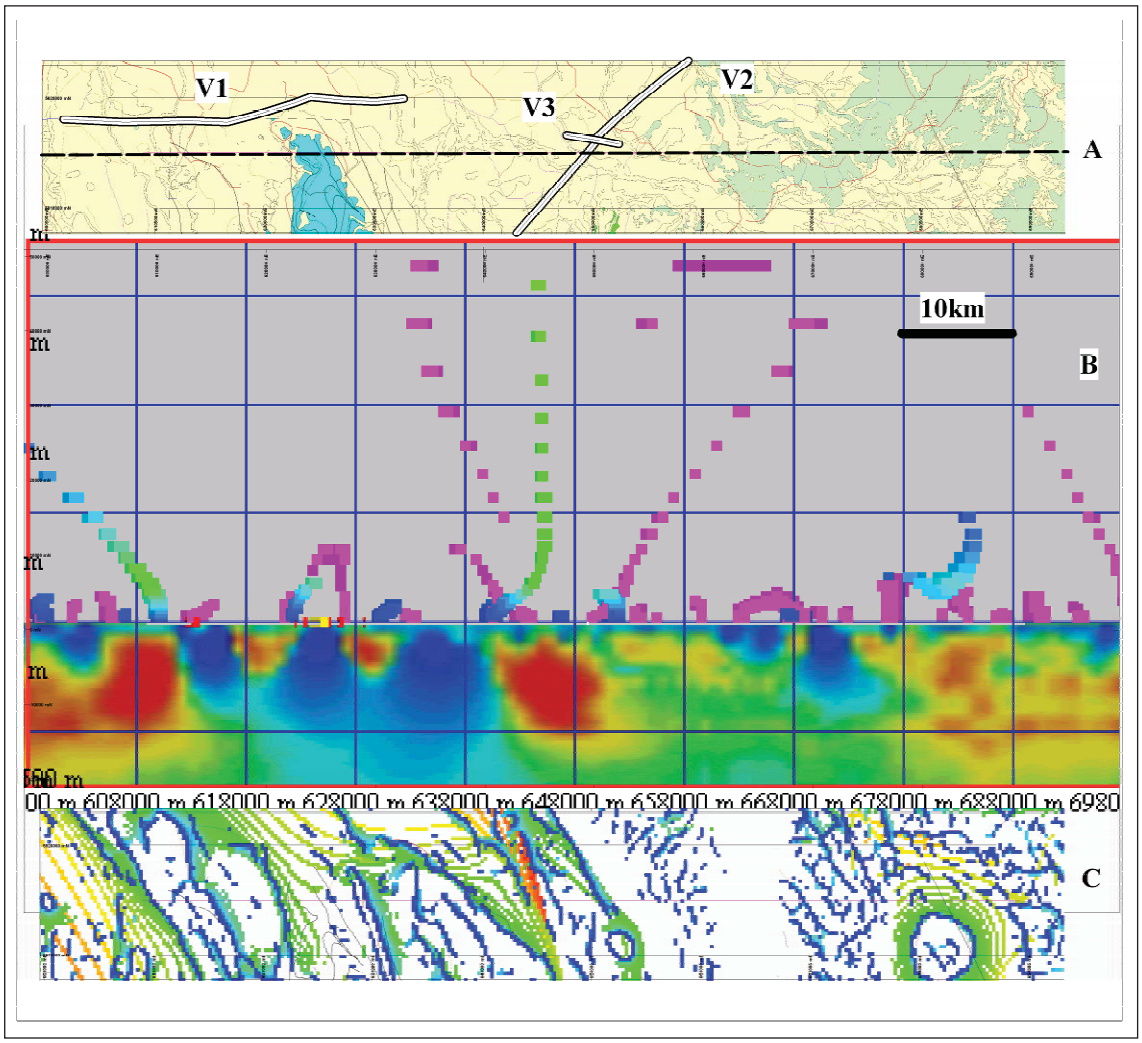

Figure 2. Template used for construction of geological cross sections in western Victoria. A. Geological map with superimposed positions of seismic traverses (V1, V2, V3) and line of section (dashed line labelled A); B. vertical profile of worm points at different heights of upward continuation above ground surface (magenta are gravity worms, blue-green are magnetic worms coloured by amplitude); C. below ground, vertical image of unconstrained gravity inversion to 20km depth (red are more dense bodies); D. map of aeromagnetic worms at same location as geology map. Scale bar is 10km, V=H (reproduced with permission from Murphy et al., 2006).

The *pmd***CRC*'s Geoscope software renders the 3D gradients (Figure 3a) as thematic maps of worm height (Figure 3b), worm amplitude and height migrated images. The post-processing routine uses nearest-neighbour analysis to generate vector lines from the worm points that are attributed with a range of parameters (trend, length, straightness, height). Figure 4 shows an example of gravity gradients at the 3 km upward continued level for the Mt Isa region. These worm lines have been filtered according to a minimum length criteria (>2 km long) and mapped according to three trend distributions. Such outputs help to constrain spatially distinct domains.

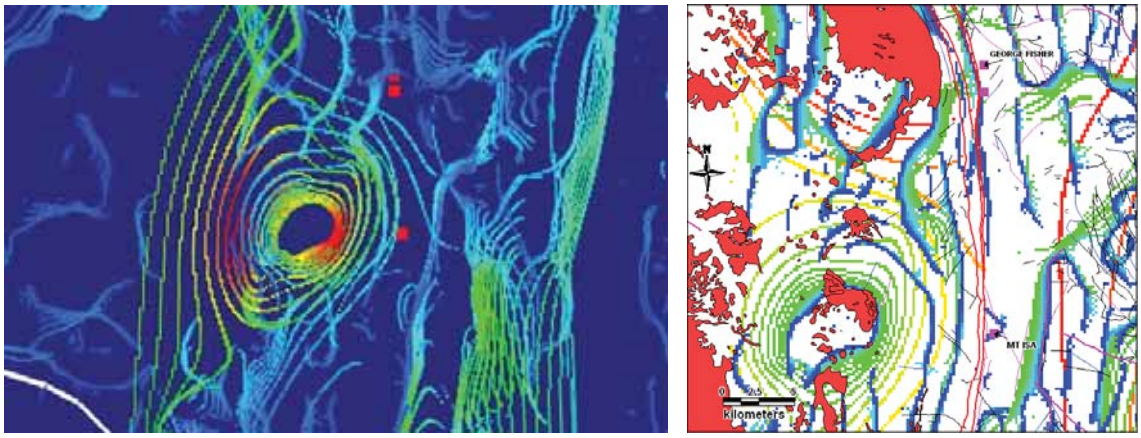

a) b)

Figure 3. Aeromagnetic worm image, Mt Isa region. A. 3D perspective (in FracSIS) of worm sheets from 5 to 30 km height, coloured by amplitude (w), with major deposits (red dots), and B. 2D map (from Geoscope) of slightly bigger area shaded at different levels of upward continued height (z), and showing position of major deposits (magenta), major faults (red) and Sybella Batholith (red).

Strike length is a unifying character of the gravity and aeromagnetic data sets. A key part of the interpretation routine involves a definition of the fault architecture from the worm data. This demands some subjectivity in determining where faults end, are offset or are terminated. Ockham's Razor ('entities should not be multiplied unnecessarily') is employed in the interpretation routine, seeking to emphasis continuity rather than segmentation (as per the original data). From this fault line interpretation, images of strike length can be readily derived. Examples of the ***pmd***CRC*'s application of worms to constraining regional architecture and their relationship to metal distribution include the Yilgarn Craton (Bierlein et al., 2006) and Tasmania (Murphy et al., 2004). Figure 5 shows aspects of the data used in the 3D model construction of Tasmania, and the relationship of worm length to the VHMS deposits in Western Tasmania. The magnetic worms for the whole of Tasmania (Figure 5a) have been interpreted in relation to strike length attributes (Figure 5b) to reveal the positions of the major fault elements. In this region, there is a well known association of massive sulphide deposits with regional scale faults, such as the Rosebery, Henty and Great Lyell Faults. Worming of gravity and aeromagnetic data in this region reveals a spatial association of major deposits with large dimension worm features. This is emphasised though imaging strike length parameters of the data (Figure 5b and 5c). In these figures, the warmer areas represent regions of longer structural elements and seem to have higher potential to host major deposits.

Conclusions

Worms are one facet of potential field gradients that significantly reduce ambiguity in interpretation. Being an automated edge detection technique, an advantage of using such data lies in the ability to visualise gradients across different levels of upward continuation at multiple scales. The worm sheets have an inherent geological appeal as, in many cases, they can mirror image geological contacts. In the development of 3D maps, worms should be used in conjunction with other data sets rather than in isolation. In under cover regions, there is a heavy reliance on gravity and aeromagnetics, the worm data provide a unique 3D representation of the richness of the gradient field that is superior to other traditional edge enhancement routines. Analysis of such data can be done in 3D platforms, such as FracSIS or, using ***pmd***CRC*'s Geoscope tool, in a 2D GIS environment.

For regional scale construction of 3D maps, the large dimension faults are modelled in the first instance and, in the absence of other supporting data, strike length can be a proxy for depth of penetration. An

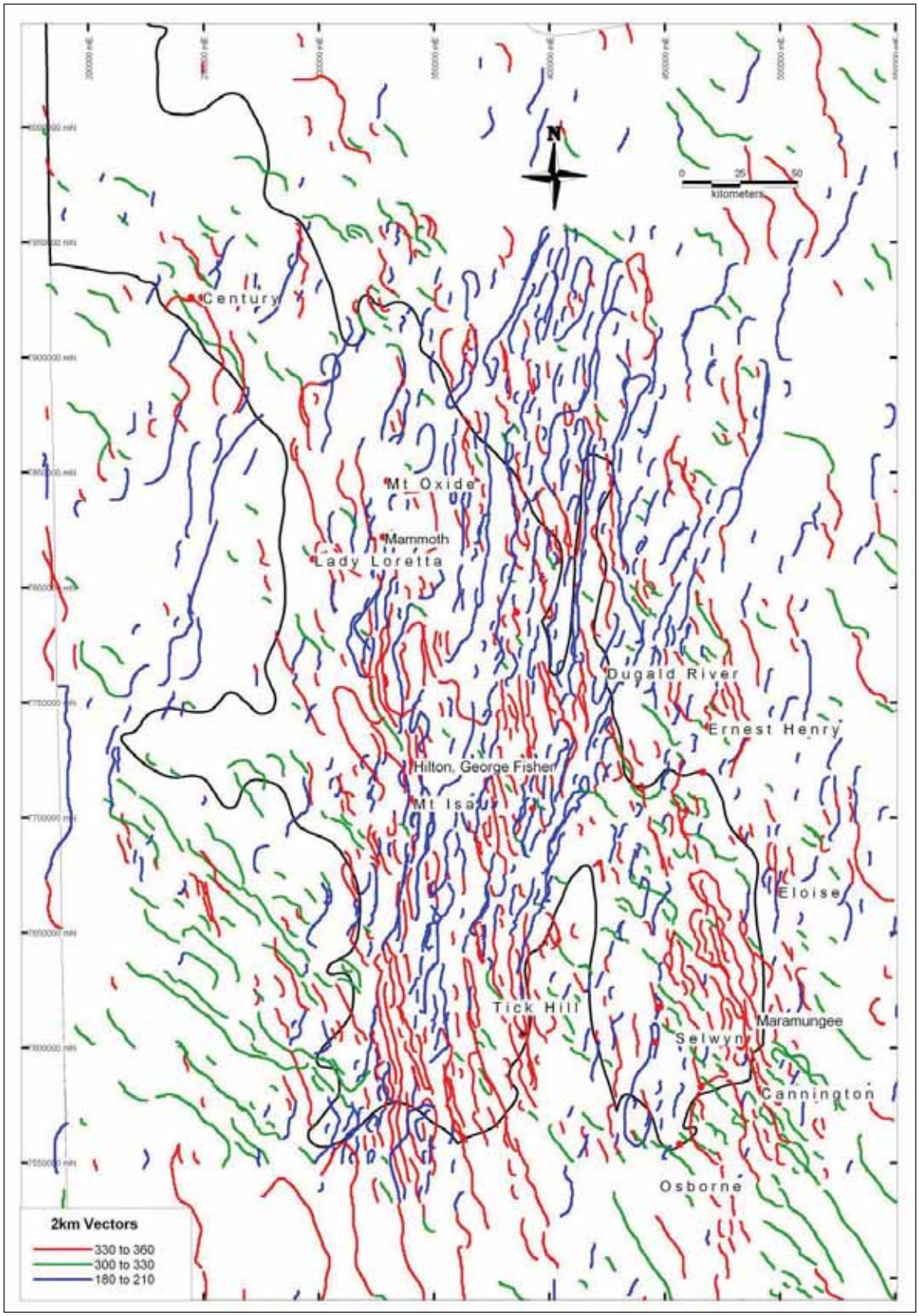

Figure 4. Thematic map of gravity worm lines that exceed 2 km length in the Mt Isa region. These are coloured by trend (as three subsets) at 3 km upward continuation height.

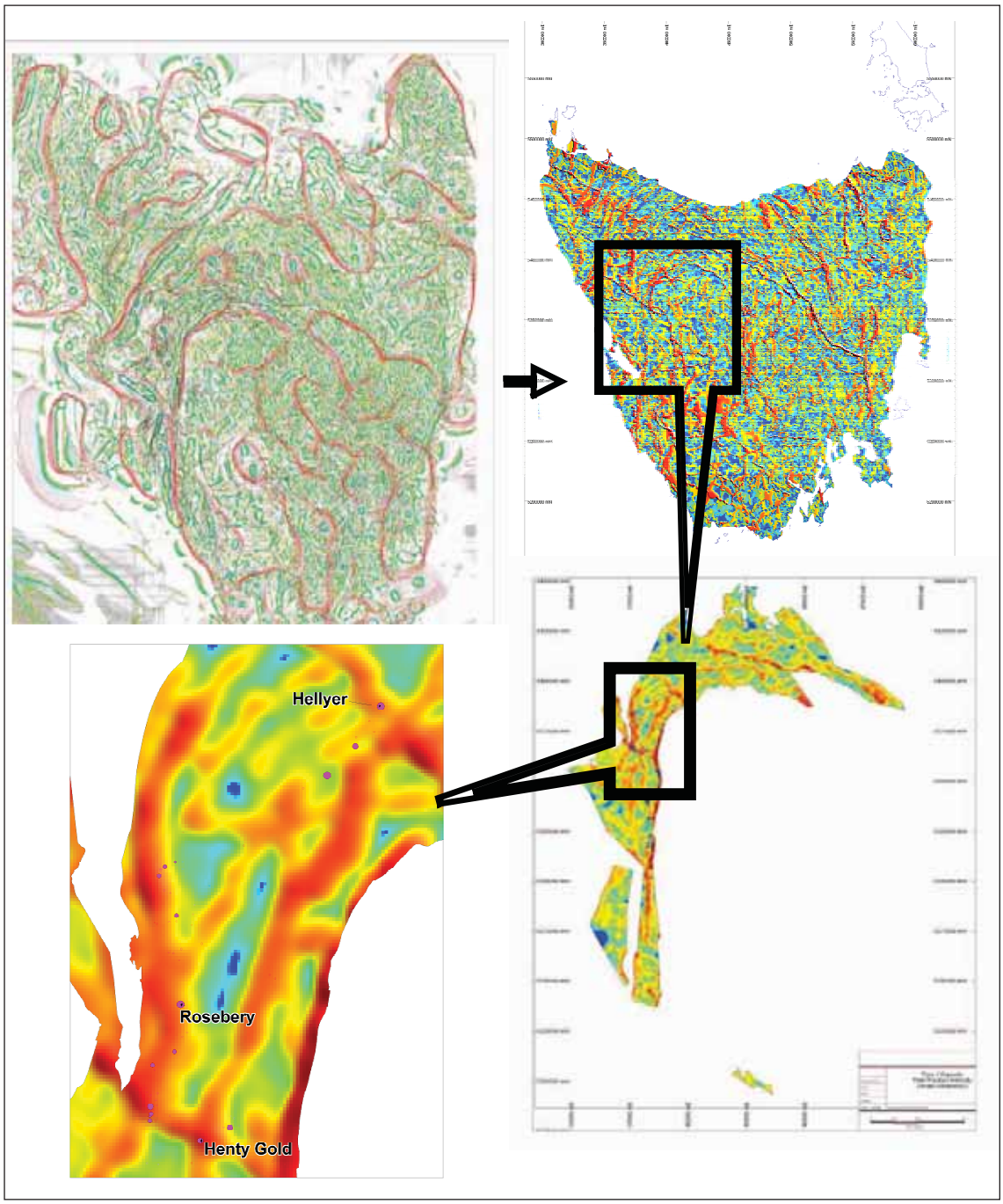

Figure 5. Tasmania: a. aeromagnetic worms colour coded by level of upward continuation (Z), green = fine scale, red = coarse scale; b. strike length image of combined aeromagnetic- and gravity-interpreted faults, warmer colours = longer length; c. Mt Read VHMS belt as fault strike length image; d. detail of strike length image and locations of major massive sulphide deposits (east-west field of view ~10km) (from Murphy et al., 2004).

analysis of gravity and aeromagnetic gradients provides a basis for generating interpreted fault length images of regions. This has relevance to fault-related hydrothermal deposits, particularly when exploring in under-cover regions where there is a heavy reliance on potential field data. It is commonly found that long wavelength, strike extensive gradients correlate with major fault discontinuities. Such large

dimension structures are intrinsically weaker, wider damage zones that can be conduits for hydrothermal fluids at different crustal levels.

References

Archibald, N., Gow, P. & Boschetti, F., 1999. Multi-scale edge analysis of potential field data. Exploration Geophysics, 30, 38-44.

Bierlein, F.P., Murphy, F.C., Weinberg, R.F. & Lees, T., 2006. Distribution of orogenic gold deposits in relation to fault zones and gravity gradients: targeting tools applied to the Eastern Goldfields, Yilgarn Craton, Western Australia. Mineralium Deposita, 41, 107-126.

Hornby, P., Horowitz, F., Boschetti, F. & Archibald, N., 1997. Inferring geology from geophysics. AGCRC Geodynamics and Ore deposits Conference, 120-122.

Hornby, P., Boschetti, F. & Horowitz, F.G., 1999. Analysis of potential field data in the wavelet domain. Geophysical Journal International, 137, 175-196.

Holden, D.J., Archibald, N.J., Boschetti, F. & Jessell, M.W., 2000. Inferring geological structures using multiscale edge analysis and forward models. Exploration Geophysics, 137, 617-612.

Murphy, F.C., Denwer, K., Keele, R., Green, G., Korsch, R.J. & Lees, T., 2004. Prospectivity analysis, Tasmania: where monsters lurk? In: McPhie, J. & McGoldrick, P., eds, Dynamic Earth: Past, Present and Future. Geological Society of Australia, Abstracts, 73, 102.

Murphy, F.C., Rawling, T.J., Wilson, C.J.L., Dugdale, L.J. & Miller, J.McL., 2006. 3D structural modelling and implications for targeting gold mineralisation in western Victoria: Australian Journal of Earth Sciences, 53, 875-889.

Deposition: Tarmoola Au numerical modelling - from reverse engineering of a deposit to multi-scale predictive targeting

WARREN POTMA

*pmd**CRC*, CSIRO Minerals Down Under Flagship, PO Box 1130, Bentley WA 6102
Warren.Potma@csiro.au

Introduction

The Tarmoola gold deposit is located on the eastern margins of the Tarmoola Granodiorite, north of Laverton in the Eastern Goldfields of the Yilgarn Craton, in what appears to be a largely structurally-controlled ore system hosting gold within both the granodiorite and carbonated komatiite sequences the granodiorite intrudes. Gold is closely associated with both tensile and shear veins. Tensile veins dominate within the granodiorite where the majority of mineralisation is located close to the margin of the intrusion, whereas large mineralised shear veins commonly mark the contact between the intrusion and the carbonated komatiite sequence. The carbonated komatiites host a combination of tensile and shear veins.

The highest grades and best ore tonnages commonly occur close to the contact, and there is a high-grade ore shoot plunging south-southeast, coincident with embayments in the granodiorite.

Reverse engineering of deposit

The first critical step towards numerically reverse engineering the system is to understand why the deposit is where it is in the local architecture. Why is one location on the margin of the granitoid mineralised in preference to others? The starting premise for the numerical modelling is that the Tarmoola deposit represents a classic competency contrast-driven, heterogeneous strain distribution problem, where deformation induced strain localisation proximal to the margins of a competent granitoid intrusion, which is hosted within a relatively weak altered ultramafic sequence, is providing the driving mechanism localising fluid flow.

To test this hypothesis, a 3D model of the granodiorite was created (Figure 1) from a combination of detailed drill hole data and mine mapping in and around the existing Tarmoola pit. Additionally, interpretations of geophysical datasets including gravity worms, and inversions of the gravity datasets were used as constraints on the geometry west of the pit. Using the resulting wireframe, a complex irregular 3D volumetric mesh was generated, and assigned physical and fluid-flow properties, which represented the geometry of the competent granodiorite hosted within a weaker komatiite matrix.

A large range of numerical models were then run to test the impact of varying the far-field stress direction and deformation regime (compression versus transpression versus strike slip). This resulted in a small group of models that developed strain and fluid flow anomalies in similar locations, and with similar morphologies to the Tarmoola mineralisation (Figure 2).

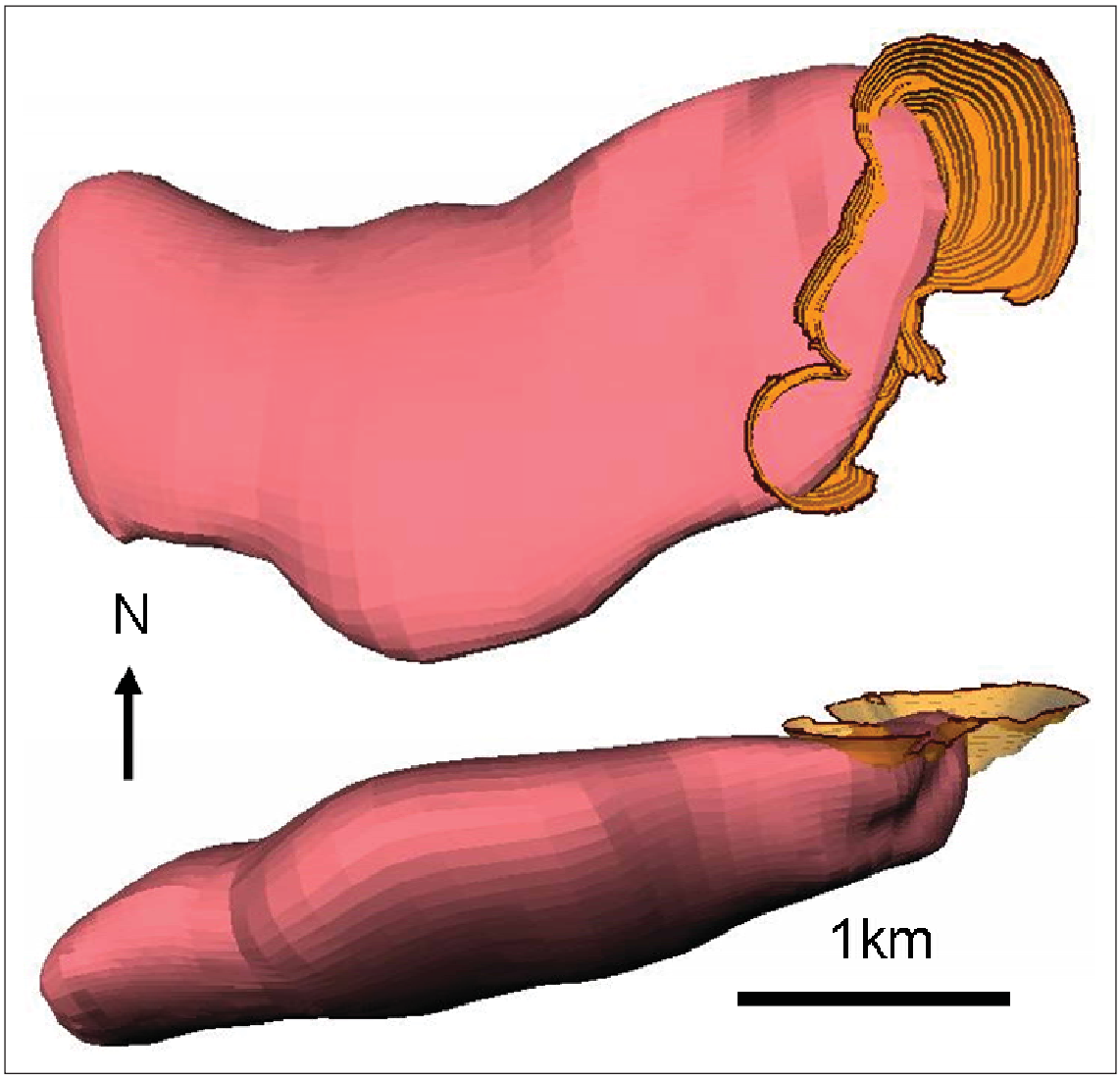

Figure 1. Tarmoola Granodiorite surface with the existing Tarmoola pit shell superimposed.

The best-fit reverse engineering model results reproduced:

- The observed distribution of dilation and tensile veining within the granodiorite proximal to the contact.
- The high shear strain and associated dilation on the flat upper eastern contact of the granodiorite proximal to the pit (where a contact parallel shear vein hosts mineralisation).
- The high shear strain within the host rocks to the east of the brittle mineralised domain proximal to the steep eastern granodiorite contact, including reproducing the greatest dilation anomaly coincident with the high-grade south-southeast plunging shoots of high-grade mineralisation.
- The greatest fluid flow at sites proximal to the margin of the granodiorite, coincident with the strain anomalies.

Multi-scale predictive targeting

The group of models that yielded a good fit with the observed distribution of mineralisation at Tarmoola also highlighted 3 other previously unidentified anomalies on the margins of the Tarmoola granodiorite

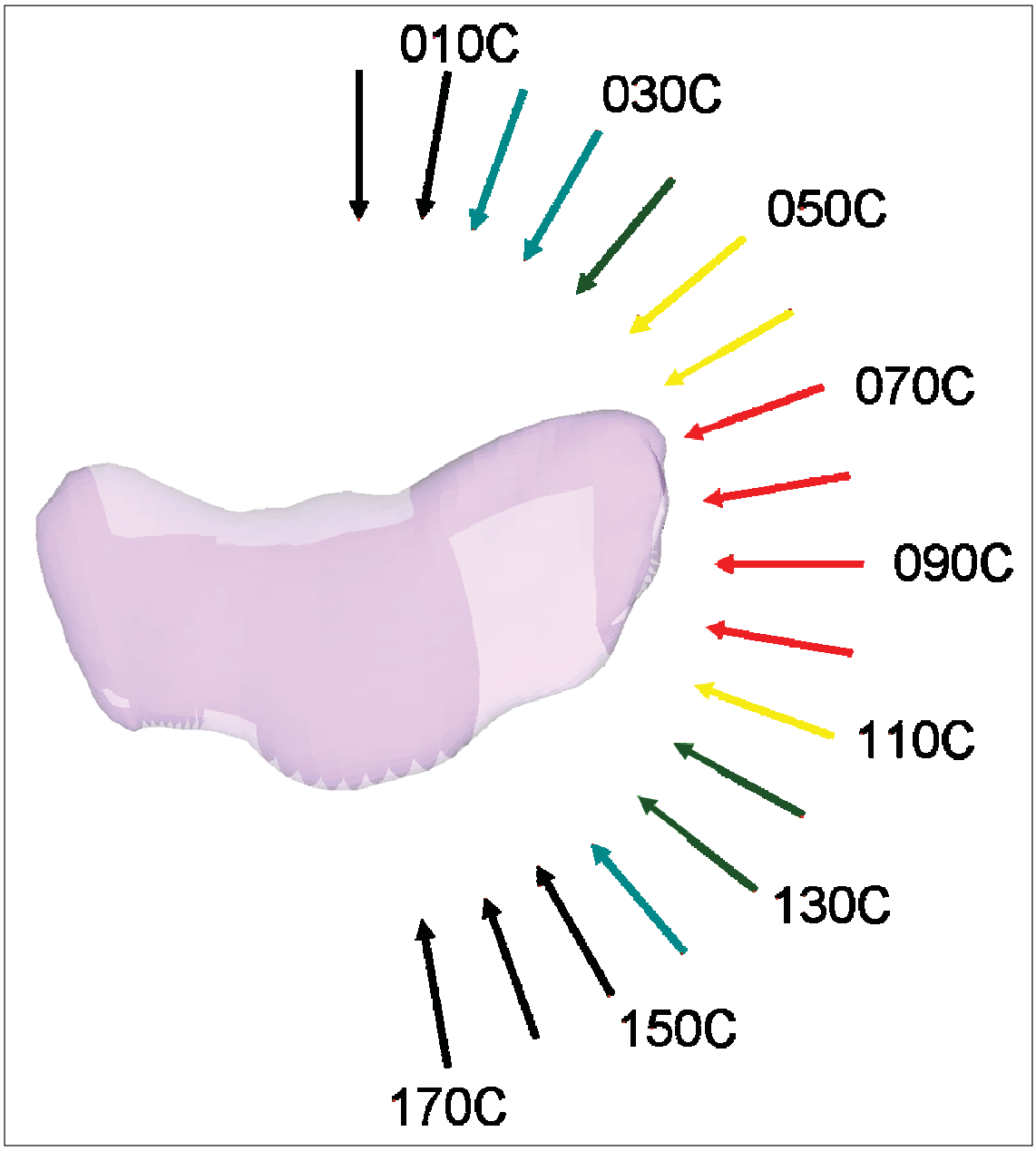

Figure 2. Models with east-west to east-northeast - west-southwest compression directions yielded anomalous strain and fluid flow distributions that best matched the known distribution of mineralisation and veining in the Tarmoola deposit. Sinistral transpression models with 050° compression components also yielded comparable results.

(Figure 4). The model results also produced an indication of the expected geometry of these targets as well as the style of mineralisation or host structure to be expected at each site.

The results of the Tarmoola modelling work can also be applied to regional predictive targeting of the most prospective portions of the margins of Tarmoola-like intrusive bodies throughout the region. The regional far-field stresses at the time of mineralisation are relatively well constrained, and the approximate shapes of other covered granitoids in the region can be derived from geophysical interpretations with sufficient accuracy to produce a generalised 3D shape to use as the basis for predicting the most prospective regions on the margins of the granitoids. Preliminary drilling can then be used to refine the

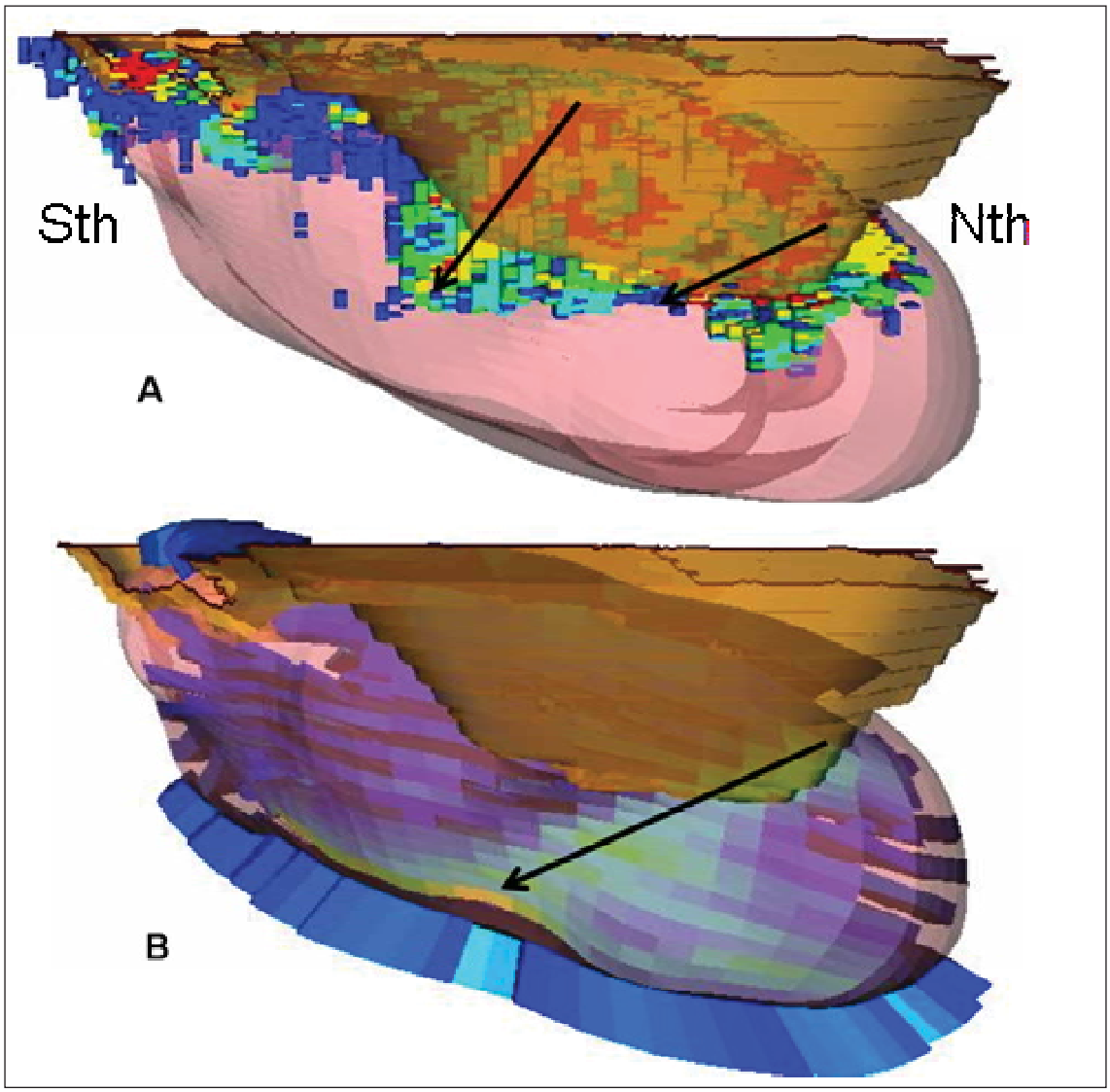

Figure 3. A. Tarmoola resource model; warm colours = higher grade. B. Cumulative dilation results from numerical reverse engineering model.

interpretation of the granitoid shape and subsequently refine the numerical model to improve the quality of predictive modelling outputs.

Acknowledgements

St Barbara Limited are acknowledged for allowing these results to be published and, in particular, Ian O'Grady and Bob Love for their contributions to this project. Digirock provided the first pass wireframe and interpretation of the Tarmoola Granodiorite, which was subsequently reinterpreted and refined by CSIRO. Guillaume Duclaux is also thanked for his assistance in preparing some of the results in this abstract.

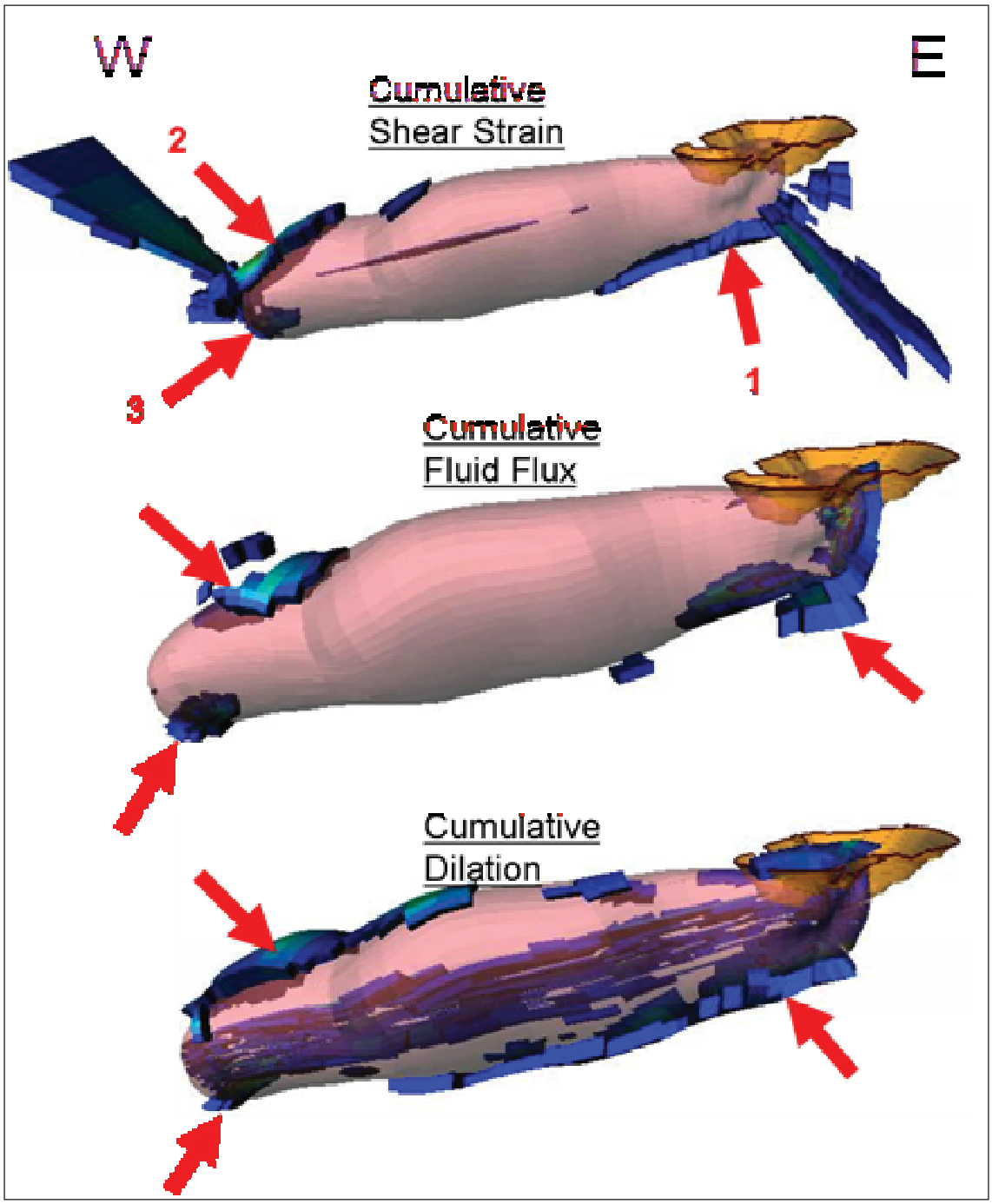

Figure 4. New targets identified on the margin of the Tarmoola Granodiorite. Anomalies 1 and 2 are predicted to be shear vein and/or disseminated shear zone hosted anomalies associated with low angle thrusting along the granodiorite contact. These relatively flat dipping broad distributed shear strain and fluid flux sites should be very easy to test with a limited number of holes. Anomaly 3 is predicted to be a highly localised zone of significant dilation and veining similar to the Tarmoola high grade brittle vein hosted mineralisation, however, anomaly 3 has a significantly higher tenor than the Tarmoola anomaly, and is also significantly more focussed, potentially indicating more intense veining and fluid focussing.